Sensing With Communication Signals: From Information Theory to Signal Processing

Fan Liu, *Senior Member, IEEE*, Ya-Feng Liu, *Senior Member, IEEE*, Yuanhao Cui, *Member, IEEE*, Christos Masouros, *Fellow, IEEE*, Jie Xu, *Fellow, IEEE*, Tony Xiao Han, *Senior Member, IEEE*, Stefano Buzzi, *Senior Member, IEEE*, Yonina C. Eldar, *Fellow, IEEE*, and Shi Jin, *Fellow, IEEE*

***Abstract*—The Integrated Sensing and Communications (ISAC) paradigm is anticipated to be a cornerstone of the upcoming 6G networks. In order to optimize the use of wireless resources, 6G ISAC systems need to harness the communication data payload signals, which are inherently random, for both sensing and communication (S&C) purposes. This tutorial paper provides a comprehensive technical overview of the fundamental theory and signal processing methodologies for ISAC transmission with random communication signals. We begin by introducing the deterministic-random tradeoff (DRT) between S&C from an information-theoretic perspective, emphasizing the need for specialized signal processing techniques tailored to random ISAC signals. Building on this foundation, we review the core signal models and processing pipelines for communication-centric ISAC systems, and analyze the average squared auto-correlation function (ACF) of random ISAC signals, which serves as a fundamental performance metric for multi-target ranging tasks. Drawing insights from these theoretical results, we outline the design principles for the three key components of communication-centric ISAC systems: modulation schemes, constellation design, and pulse shaping filters. The goal is to either enhance sensing performance without compromising communication efficiency or to establish a scalable tradeoff between the two. We then extend our analysis from a single-antenna ISAC system to its multi-antenna counterpart, discussing recent advancements in multi-input multi-output (MIMO) precoding techniques specifically designed for random ISAC signals. We conclude by highlighting several open challenges and future research directions in the field of sensing with communication signals.**

***Index Terms*—Integrated sensing and communications (ISACs), deterministic-random tradeoff, modulation basis, constellation design, pulse shaping, multi-antenna precoding.**

Received 14 February 2025; revised 2 July 2025 and 30 July 2025; accepted 30 July 2025. Date of publication 17 October 2025; date of current version 4 February 2026. This work was supported in part by the National Natural Science Foundation of China (NSFC) under Grant 62522107, Grant 62261160576, Grant 62471424, and Grant 92267202; in part by Guangdong Basic and Applied Basic Research Foundation under Grant 2024A1515011218; in part by Guangdong Provincial Key Laboratory of Future Networks of Intelligence under Grant 2022B1212010001; and in part by Guangdong Major Project of Basic and Applied Basic Research under Grant 2023B0303000001. The work of Ya-Feng Liu was supported by NSFC under Grant 12371314 and Grant 12021001. The work of Christos Masouros was supported in part by the Smart Networks and Services Joint Undertaking (SNS JU) Project 6G-MUSICAL under European Union's Horizon Europe Research and Innovation Program under Agreement 101139176 and in part by the Intelligent speCtrum innOvatioN (ICON) through the Engineering and Physical Sciences Research Council Project under Agreement UKRI859. *(Corresponding authors: Ya-Feng Liu; Shi Jin.)*

Fan Liu and Shi Jin are with the School of Information Science and Engineering, Southeast University, Nanjing 210096, China (e-mail: fan.liu@seu.edu.cn; jinshi@seu.edu.cn).

Ya-Feng Liu is with the Ministry of Education Key Laboratory of Mathematics and Information Networks, School of Mathematical Sciences, Beijing University of Posts and Telecommunications, Beijing 102206, China (e-mail: yafengliu@bupt.edu.cn).

Yuanhao Cui is with the Department of Communication Engineering, Beijing University of Posts and Telecommunications, Beijing 100876, China (e-mail: yuanhao.cui@bupt.edu.cn).

Christos Masouros is with the Department of Electronic and Electrical Engineering, University College London, WC1E 7JE London, U.K. (e-mail: chris.masouros@ieee.org).

Jie Xu is with the School of Science and Engineering, Shenzhen Future Network of Intelligence Institute (FNii-Shenzhen), and Guangdong Provincial Key Laboratory of Future Networks of Intelligence, The Chinese University of Hong Kong (Shenzhen), Shenzhen, Guangdong 518172, China (e-mail: xujie@cuhk.edu.cn).

Tony Xiao Han is with Huawei Technologies Company Ltd., Shenzhen 518129, China (e-mail: tony.hanxiao@huawei.com).

Stefano Buzzi is with the Department of Electrical and Information Engineering, University of Cassino and Southern Lazio, 03043 Cassino, Italy, also with the Department of Electronics, Information and Bioengineering, Politecnico di Milano, 20133 Milan, Italy, and also with the Consorzio Nazionale Interuniversitario per le Telecomunicazioni (CNIT), 43124 Parma, Italy (e-mail: buzzi@unicas.it).

Yonina C. Eldar is with the Faculty of Mathematics and Computer Science, Weizmann Institute of Science, Rehovot 7610001, Israel (e-mail: yonina.eldar@weizmann.ac.il).

Digital Object Identifier 10.1109/JSAC.2025.3614025

I. Introduction

A. Background and Motivation

NEXT-GENERATION wireless networks (5G-Advanced (5G-A) and 6G) are increasingly recognized as a pivotal enabler for a broad spectrum of emerging applications, including the Digital Twin, Metaverse, Smart Cities, Industrial Internet-of-Things (IoT), and the Low-Altitude Economy powered by Unmanned Aerial Vehicles (UAVs) [1], [2]. These applications promise to revolutionize industries and societies by providing advanced digital experiences, real-time environment monitoring, and intelligent automation. In May 2023, the International Telecommunications Union (ITU) successfully completed the Recommendation Framework for IMT-2030, which is commonly referred to as the *global 6G vision* [3]. This achievement marks the formal initiation of the 6G standardization process, laying the foundation for the development of next-generation communication systems. Among the six key usage scenarios identified by the ITU, Integrated Sensing and Communications (ISAC) stands out as a particularly transformative innovation [4], [5]. ISAC is envisioned to offer integrated solutions that combine wireless sensing and communication (S&C) functions in a seamless and efficient manner, thereby enhancing the performance and capabilities

of 6G networks [5], [6]. By incorporating native sensing functionalities directly into the communication infrastructure, ISAC-enabled cellular networks will further unlock distributed sensing of unprecedented scale. In doing so, it will support another one of key 6G usage scenarios, that of integrated artificial intelligence (AI) and communications, by generating the necessary volume of sensory data to build the networked intelligence.

ISAC technologies can be conceptualized in a number of progressive stages [7]. The initial stage focuses on the independent use of spectral resources by S&C systems, ensuring no interference between the two. In the subsequent stage, both S&C functions are consolidated onto a shared RF front-end. In the third stage, namely, fully integrated ISAC systems, S&C functions are performed on a unified hardware platform using a shared waveform within the same frequency band [6]. In such a system, a single radio signal is transmitted to both deliver data information to communication users, as well as to acquire critical sensory information from the returned echoes, e.g., range, angle, velocity, trajectory, size and shape of targets of interest, or even image of the surrounding environment. This integration poses considerable challenges at the physical layer (PHY), where innovative signaling schemes are crucial for supporting higher-layer ISAC applications. Among various design strategies, three primary approaches have garnered significant attention from both academia and industry, as outlined below.

1) Sensing-Centric Design: Sensing-centric design focuses on incorporating communication bits into legacy radar waveforms, which is often referred to as the *information embedding* method [8]. Taking chirp waveforms as an example, this can be achieved by representing communication symbols using inter-pulse modulation, through varying the amplitude, phase, frequency, or even the chirp rate of each chirp pulse [9], [10], [11]. Additionally, for a MIMO radar system, useful information can also be embedded in the spatial domain, through techniques like sidelobe control of the beampattern [12], [13], [14], or via index modulation (IM) [15], [16], [17], [18]. The IM-based sensing-centric ISAC was first introduced in [15], where a set of N_t orthogonal waveforms is transmitted from a radar equipped with N_t antennas. By permuting the assignment of these waveforms to the antennas, information can be readily encoded, with each permutation corresponding to a unique communication symbol. This approach effectively enables data transmission at a bit rate of $f_{\text{PRF}} \cdot \log_2 N_t!$, where f_{PRF} is the pulse repetition frequency (PRF) of the radar. Building on this idea, the multi-carrier agile joint radar communication (MAJoRCom) framework [17], [18] introduces a more dynamic modulation technique based on the carrier-agile phased array radar (CAESAR) platform. In this scheme, the carrier frequency is varied randomly between pulses, and different frequency tones are allocated to individual antenna elements. This dual-domain agility in both spatial and spectral dimensions facilitates the joint execution of radar sensing and data communication tasks. However, since most sensing-centric methods rely on inter-pulse modulation (or slow-time coding) to avoid disrupting the structure of radar waveforms, these approaches typically result in lower data rates, constrained by the PRF [19].

2) Communication-Centric Design: The communication-centric design refers to ISAC signaling strategies that strictly follow the standard communication system processing pipeline. In such systems, the sensing functionality is implemented over standardized communication waveforms and protocols, such as 5G New Radio (NR) [20] and IEEE 802.11ad [21], without altering the fundamental structure of the signal processing chain. As a result, the available design degrees of freedom (DoFs) are limited to tunable parameters within this architecture. Early efforts in communication-centric ISAC date back to the code-division multi-access (CDMA) era, where Oppermann sequences were explored for dual-purpose communication and radar functionalities [22]. A more widely studied example is the orthogonal frequency division multiplexing (OFDM) waveform [23], [24], whose sensing capabilities were first demonstrated in [25]. Building upon this, orthogonal time-frequency space (OTFS) modulation has been proposed as a candidate for 6G ISAC due to its representation in the delay-Doppler domain, aligning well with radar target characterization [26], [27], [28], [29]. However, while OTFS shows resilience to Doppler shifts in communication systems, its sensing performance is generally comparable to that of OFDM, and both waveforms depend largely on the radar receiver's complexity for optimal performance [26], [29]. As will be elaborated in later sections, OFDM achieves the lowest average ranging sidelobe level when carrying independent and identically distributed (i.i.d.) Quadrature Amplitude Modulation (QAM) and Phase Shift Keying (PSK) symbols, making it a strong candidate for ranging applications. Recently, affine frequency division multiplexing (AFDM) has emerged as a novel waveform offering robustness in high-mobility scenarios while supporting both S&C objectives [30], [31]. While in principle, any communication waveform can be repurposed for sensing, this reuse comes with limitations. Since these waveforms are optimized primarily for communication performance, the sensing functionality, which is added as an overlay, may suffer from reduced performance or limited tunability. Nevertheless, the communication-centric approach remains attractive due to its low complexity, backward compatibility, and suitability for real-world deployment.

3) Joint Design: In contrast to communication-centric methods, the joint design strategy offers far greater flexibility by constructing ISAC waveforms from the ground up. This approach does not rely on standard communication or radar signal processing blocks. Instead, it formulates ISAC signaling as a multi-objective optimization problem, allowing for end-to-end waveform design that balances S&C performance. Typical joint design formulations aim to optimize communication metrics, such as inter-user interference, under sensing constraints like MIMO radar beampattern requirements, or radar waveform similarity [32], [33], [34], [35], [36], [37]. Alternatively, one may optimize the sensing-specific objective functions, e.g., radar beamforming gain [38], [39] or Cramér-Rao Bound (CRB) [40], subject to communication signal-to-interference-plus-noise ratio (SINR) constraints. Beyond conventional optimization-based approaches, joint design may also be

realized through learning based techniques [41], [42]. Recent advances further consider practical implementation challenges, including hardware impairments and front-end non-idealities [43], [44], [45], [46]. Unlike communication-centric designs, joint designs are not constrained to standard waveforms and may employ novel signal structures, such as intra-pulse modulated chirps [32] or other suitable constant-modulus analog waveforms, that optimize sensing metrics while still carrying massive communication data. However, this flexibility comes at the cost of increased computational complexity and lack of compatibility with existing infrastructure, making joint design less viable for near-term standardized deployment.

Among the three design philosophies, the communication-centric ISAC design holds more promise for practical deployment in 5G-A and 6G networks, primarily due to its low implementation costs and full compatibility with existing cellular infrastructure [20]. Indeed, ISAC standardization is progressing well within the 3rd Generation Partnership Project (3GPP), which builds upon the 5G NR protocols. For instance, a key focus of 3GPP Release 18 (Rel-18) is on improving device positioning [47], crucial for ISAC and wireless sensing in 5G-A. As a further step, a Technical Report TR 22.837 was introduced towards Rel-19 in April 2022, identifying 32 ISAC use cases [48]. In August 2023, the Technical Specification TS 22.137 outlined the service requirements for wireless sensing, detailing eight key performance indicators (KPIs) [49]. These include positioning accuracy, velocity estimation accuracy, confidence levels, sensing resolution, miss detection probability, false-alarm probability, sensing service latency, and refresh rates. Additionally, in December 2023, a study on channel modeling for ISAC was approved [50]. More recently, the 3GPP defined the scope of 6G research in the 6G Study Item Description (6G SID, RP-251809) towards Rel-20 [51], where "sensing" was identified as one of the nine key objectives. Complementary work is also underway in the European Telecommunications Standards Institute (ETSI), focusing on ISAC-specific use cases and security. Meanwhile, IEEE 802.11bf aims to enhance WLAN standards for sensing [52]. On top of that, air interface technologies for ISAC are expected to be finalized in the first set of 3GPP 6G technical specifications under Rel-21 [53]. As part of this evolution, research on PHY signaling and processing techniques for communication-centric ISAC will become increasingly crucial.

B. Sensing With Communication Data Payload Signals

The current 5G NR and Wi-Fi-based communication-centric ISAC signaling frameworks primarily rely on reference signals, commonly referred to as "pilots", that are embedded within standardized communication frame structures. For instance, in 3GPP Rel-18, Reduced-Capability (RedCap) devices utilize positioning reference signals (PRS) for downlink positioning and sounding reference signals (SRS) for uplink localization [47], [54]. Other PHY reference signals, such as channel state information reference signals (CSI-RS), demodulation reference signals (DMRS), and synchronization signals, have also been leveraged for sensing applications [55], [56], [57]. A representative early implementation of this pilot-based ISAC philosophy is the IEEE 802.11ad-based system developed for vehicular networks [21]. In this framework, radar sensing is performed using only the preamble of each Single-Carrier (SC) PHY frame, namely, the Short Training Field (STF) and Channel Estimation Field (CEF). This time-division design cleanly separates the S&C functions and has demonstrated practical feasibility and low implementation complexity.

Despite their favorable correlation properties (e.g., Zadoff-Chu sequences, m-sequences, and Golay sequences) and ease of implementation, such reference signals occupy only a limited portion of time-frequency resources, typically around 10–15% in 5G NR and 1-2% in IEEE 802.11ad. For example, in a typical 802.11ad SC PHY frame containing 511 data blocks with a chip rate of 1.76 GHz, the preamble (comprising 7552 samples) accounts for only about 2.2% of the frame duration. In long-frame configurations, this ratio drops to as low as 0.36% [58]. Consequently, the achievable sensing resolution and SINR is fundamentally constrained by the restricted resources allocated to the reference signals. Scaling up performance in such designs often requires accumulating information across multiple frames, introducing additional latency and system complexity. To overcome these limitations, a promising direction is to repurpose the communication data payload, which occupies 85% to 98% of the total time-frequency resources, for both S&C tasks. By fully exploiting the entire bandwidth and time duration of communication signals, this approach offers substantial improvements in range-Doppler resolution, target detection probability, and parameter estimation accuracy, which aligns closely with the long-term vision of integrating pervasive, seamless sensing capabilities into future 6G networks.

While leveraging data payload signals for ISAC offers significant performance gains over conventional pilot-only schemes, these signals are not inherently designed for sensing applications, leading to critical challenges in implementing communication-centric ISAC systems. First, unlike pseudo-random sequences discussed earlier, data payload signals are *random signals* that carry useful information [59]. These signals are generated randomly from specific codebooks, with their structure determined by the distribution of information sources. Recent advancements in ISAC information theory have underscored a key distinction between the requirements for S&C. That is, communication systems rely on random signals to efficiently convey information, while radar sensing systems demand deterministic signals with favorable ambiguity properties. Consequently, the randomness embedded in ISAC signals improves the communication rate but deteriorates sensing performance, giving rise to the deterministic-random tradeoff (DRT) between S&C [60], [61], [62], [63]. This tradeoff, particularly concerning the input distribution of ISAC signals [64], poses a significant challenge in characterizing the Pareto performance boundary for S&C. In this context, the work in [61] examined a basic point-to-point (P2P) ISAC system operating over vector Gaussian channels, and evaluated the achievable S&C performance at communication- and sensing-optimal operating points, respectively, providing valuable theoretical insights into the design of more sophisticated ISAC systems by leveraging the DRT.

Second, beyond the foundational nature of the theoretical findings derived from ISAC information theory [60], [61], [62], [63], it is of practical importance to further evaluate and optimize the achievable sensing performance under real-world communication signals. Conceived primarily for data delivery, communication signals have a format fundamentally different from conventional radar signals. At its most basic level, a practical communication signal can be decomposed into the following key components [65]:

- **Channel Codes** that encode information sources into coded bit sequences to improve transmission reliability.
- **Constellation Symbols** mapped from bit sequences that carry information.
- **Orthonormal Modulation Basis** that conveys these symbols by formulating discrete-time signals.
- **Pulse Shaping Filter** that converts discrete time-domain samples into continuous-time signals.
- **MIMO Precoder** required in multi-antenna systems to enable multi-stream or multi-layer transmission.

Each of these components significantly influences the resulting sensing performance, yet their impacts remain largely unexplored. To effectively guide the development of communication-centric ISAC systems for future 6G networks, a deeper understanding of how these core elements of communication systems influence the sensing performance is essential. This understanding serves as the basic motivation of the study in this tutorial paper.

C. Organization of This Paper

In this tutorial paper, we present a comprehensive technical overview of recent advances in the fundamental theory and signal processing methodologies for P2P ISAC systems that leverage random data payload signals [60], [61], [62], [63], [66], [67], [68], [69], [70]. We begin by introducing the DRT between S&C from an information-theoretic standpoint in Sec. II, underscoring the importance of developing tailored signal processing approaches specifically for random ISAC signals [60], [61], [62], [63], [71], [72], [73]. In particular, we review the capacity-distortion (C-D) theory for state-dependent memoryless ISAC channels [63], depicting the impact of input distribution for both S&C. We then generalize our analysis to vector Gaussian channels by examining the CRB-rate tradeoff for ISAC [61], which reveals the optimal distribution and structure of ISAC signal matrix at sensing- and communication-optimal points, and characterizes the achievable S&C performance, respectively.

Expanding on this theoretical foundation, we proceed to review the core signal models and processing pipelines for communication-centric ISAC systems in Sec. III. A key focus is on the auto-correlation function (ACF) of random ISAC signals, which serves as a critical metric for assessing the sensing performance in multi-target ranging applications [66]. Due to the inherent randomness of data payloads, analyzing the statistical property of ACF becomes essential, instead of relying on specific instances. Recent research has focused on deriving a closed-form expression for the expected squared ACF [66], taking into account arbitrary modulation techniques and constellation mappings within the Nyquist pulse shaping framework. This expression is metaphorically described as an "iceberg-in-the-sea" structure, where the "iceberg" represents the squared mean of the ACF of random ISAC signals, determined by the pulse shaping filter, and the "sea level" corresponds to the variance, which reflects the variability introduced by the data randomness.

Drawing insights from these results, we further overview the design principles for the three key components of communication-centric ISAC systems in Sec. IV, including modulation schemes [67], constellation designs [68], and pulse shaping filters [66], [69]. The objective is either to improve sensing performance without sacrificing communication efficiency, or, alternatively, to establish a scalable tradeoff between the two. This balance is crucial for enabling the seamless integration of S&C functionalities within the same system. Notably, we show that among all orthogonal linear modulation schemes, OFDM attains the lowest average ranging sidelobe level for i.i.d. QAM/PSK symbols [67]. We then review a probabilistic constellation shaping method to maximize the communication rate while further reducing the sidelobe level for OFDM signaling [68], followed by a Nyquist pulse design approach to reshape the ACF of ISAC signals [66], [69]. Furthermore, we extend the discussion to more complex MIMO settings in Sec. V, elaborating on the latest advancements in data-dependent and data-independent MIMO precoding techniques specifically designed for random ISAC signals [70].

Finally, we conclude with a discussion of several open challenges and promising future research directions in sensing with random communication signals. We hope that this work would provide reference value to the ongoing efforts for implementing ISAC in the forthcoming 6G networks.

D. Notations

Throughout this paper, a, $\mathbf{a}$, and $\mathbf{A}$ represent random scalars, random vectors, and random matrices, respectively. Their corresponding deterministic quantities are denoted by a, $\boldsymbol{a}$, and $\boldsymbol{A}$, respectively. The size-N identity matrix is denoted by $\boldsymbol{I}_N$. The size-N discrete Fourier transform (DFT) matrix is denoted as $\boldsymbol{F}_N$, with its (m,n)-th entry being defined as $\frac{1}{\sqrt{N}}e^{-\frac{j2\pi(m-1)(n-1)}{N}}$ with j denoting the imaginary unit. The Kronecker product and Hadarmard product between matrices $\boldsymbol{A}$ and $\boldsymbol{B}$ are denoted by $\boldsymbol{A}\otimes\boldsymbol{B}$ and $\boldsymbol{A}\odot\boldsymbol{B}$, respectively. $\|\boldsymbol{x}\|_p$ denotes the ℓ_p norm, which represents the ℓ_2 norm by default when the subscript is omitted. The notations $\mathbb{E}(\cdot)$ and $\mathrm{var}(\cdot)$ denote the expectation and variance of the input argument, respectively. $(\cdot)^*$, $(\cdot)^T$, and $(\cdot)^H$ represent the complex conjugate, transpose, and Hermitian transpose of their arguments, respectively. $\boldsymbol{a}_n$ denotes the n-th column of $\boldsymbol{A}$. The notation $\mathrm{Diag}(\cdot)$ denotes the matrix obtained by placing its arguments on the main diagonal of a square matrix. $\mathrm{Tr}(\cdot)$ stands for the trace of a square matrix, and $\mathrm{rank}(\cdot)$ stands for the rank of a matrix. The subscripts in the aforementioned notations may be omitted when they are clear from the context.

II. Deterministic-Random Tradeoff in ISAC Systems: An Information-Theoretic Perspective

In this section, we introduce the fundamental DRT between S&C, highlighting the need for developing dedicated signal

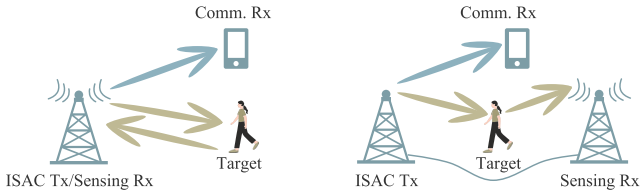

Fig. 1. The P2P ISAC model: An ISAC Tx transmits a unified signal to sense targets while communicating with a communication Rx. A dedicated sensing Rx is either collocated with the ISAC Tx (monostatic mode), or placed separately but connected with the ISAC Tx through a wired link (cooperative bistatic mode).

processing techniques towards random ISAC signals. We first review the C-D theory for the state-dependent memoryless ISAC channel, framing the S&C tradeoff as a functional optimization problem from an information-theoretic perspective. Building on this foundation, we generalize the DRT to vector Gaussian ISAC channels by depicting the CRB-rate region.

A. System Model

We consider a P2P ISAC system, as shown in Fig. 1, where the ISAC transmitter (Tx) emits a unified signal to both sense targets and transmit information to a communication receiver (Rx). Simultaneously, a dedicated sensing receiver (Rx) is either collocated with the ISAC Tx (monostatic mode) or placed separately and connected to the Tx via a wired link (cooperative bistatic mode). In both scenarios, the sensing Rx has full knowledge of the transmitted ISAC signal, while the communication Rx does not, as the ISAC signal carries information intended for the communication user. Specifically, the primary objectives of S&C subsystems are:

- **Sensing**: Detecting the presence of targets and accurately estimating key parameters such as delay, Doppler, and angle by processing echo signals reflected from targets.
- **Communication:** Decoding information bits transmitted by the ISAC Tx via processing the received signal output from the communication channel.

In this model, communication performance is typically measured by the achievable rate or channel capacity, which is omitted here for brevity. The sensing performance, on the other hand, critically depends on the specific sensing task. Broadly, sensing tasks can be categorized into estimation and detection, defined as follows [74] and [75]:

- **Estimation**: Extracting target parameters, such as delay, Doppler frequency, and angle, from noisy or interfered observations.
- **Detection**: Determining the state of a target (e.g., presence/absence or multiple hypotheses) based on observed echo signals.

Accordingly, estimation performance is typically quantified by the MSE, while detection performance is evaluated using metrics like detection and false-alarm probabilities. These metrics are explained in further detail below.

- **Estimation Metrics**: Estimation accuracy can be evaluated by the difference between the ground truth and estimated value. Let h be the ground truth of sensing parameters, such as delay, Doppler, or angle, with $\hat{\mathsf{h}}$ denoting their estimates. The estimation error is quantified by the MSE ϵ, defined as

$$\epsilon := \mathbb{E}\left(\left|\mathsf{h}-\hat{\mathsf{h}}\right|^2\right), \tag{1}$$

  where the expectation is taken over both h and $\hat{\mathsf{h}}$, given their potential randomness.
- **Detection Metrics**: The detection problem, in its simplest form, is commonly framed as a binary hypothesis testing problem, where $\mathcal{H}_0$ hypothesis stands for the case that the sensing Rx detects only the noise, and $\mathcal{H}_1$ hypothesis signifies the situation that the sensing Rx receives target return plus noise. Accordingly, the detection probability $P_{\rm D}$ is the probability that, when the target is present, the sensing Rx correctly chooses $\mathcal{H}_1$. The false alarm probability, on the other hand, is the probability that the sensing Rx erroneously selects $\mathcal{H}_1$ when the target is absent. These probabilities can be expressed as:

$$P_{\rm D} = \Pr\left(\mathcal{H}_1|\mathcal{H}_1\right), \quad P_{\rm FA} = \Pr\left(\mathcal{H}_1|\mathcal{H}_0\right). \tag{2}$$

Notably, both detection and estimation metrics may be unified as a generic *distortion measure* in the context of information theory, which is defined by a bounded distance function $d(\mathsf{h},\hat{\mathsf{h}})$. For estimation tasks, a common distortion function is the Euclidean distance, $d(\mathsf{h},\hat{\mathsf{h}}) = |\mathsf{h}-\hat{\mathsf{h}}|^2$, which induces the MSE in (1). For detection tasks, one may define $\mathsf{h} \in \{0,1\}$ as a binary variable indicating the presence or absence of a target, and use the Hamming distance $d(\mathsf{h},\hat{\mathsf{h}}) = \mathsf{h} \oplus \hat{\mathsf{h}}$ as the distortion metric. Accordingly, the expected distortion in this case can be written as [60]:

$$\begin{aligned}
&\mathbb{E}\left\{\mathsf{h}\oplus\hat{\mathsf{h}}\right\} \\
&= (1\oplus 1)\Pr\left(\hat{\mathsf{h}}=1\,|\mathsf{h}=1\right) + (0\oplus 0)\Pr\left(\hat{\mathsf{h}}=0\,|\mathsf{h}=0\right) \\
&\quad + (1\oplus 0)\Pr\left(\hat{\mathsf{h}}=1\,|\mathsf{h}=0\right) + (0\oplus 1)\Pr\left(\hat{\mathsf{h}}=0\,|\mathsf{h}=1\right) \\
&= 1 - P_{\rm D} + P_{\rm FA},
\end{aligned} \tag{3}$$

Under the Neyman-Pearson criterion [75], where $P_{\rm FA}$ is fixed, minimizing the average Hamming distortion in (3) leads to the maximization of the detection probability.

Next, we review the C-D framework, which has emerged as a powerful tool for analyzing the tradeoff between S&C performance in ISAC systems. In this context, a generic distortion metric is used as a universal KPI for sensing, without committing to a specific task such as parameter estimation or target detection. Rather than being derived from a particular implementation, the C-D theory serves as an information-theoretic abstraction of practical ISAC transmission models, such as those illustrated in Fig. 1, with the goal of characterizing the fundamental performance boundaries that jointly govern both S&C under generic ISAC channel models.

B. Capacity-Distortion Theory

1) Information-Theoretic Model for Monostatic ISAC: The shared use of resources in ISAC systems inherently couples the performance of S&C, leading to a fundamental

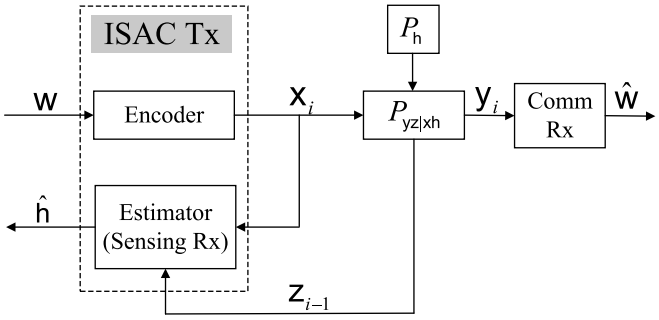

Fig. 2. An information-theoretic model for the P2P monostatic ISAC system.

tradeoff between the two functionalities. The C-D framework, originally formulated in recent works such as [63], offers a unified information-theoretic perspective on this tradeoff [76]. In contrast to the classical rate-distortion theory developed for the lossy source coding [59], in which both rate and distortion metrics pertain to communication fidelity, the C-D framework re-interprets these metrics for the ISAC paradigm: The achievable rate quantifies the communication throughput in the Shannon-theoretic sense, while the distortion serves as a task-agnostic measure of sensing reliability, abstracting over task-specific objectives. To elaborate, consider the P2P monostatic ISAC system as an example,[1] where the ISAC channel is modeled as a memoryless state-dependent delayed-feedback channel [63], [71], [72], [73], subject to a channel law, defined as a conditional distribution $P_{\mathsf{yz|xh}}$, where:

- $\mathsf{x} \in \mathcal{X}$ is the ISAC transmitted signal;
- $\mathsf{h} \in \mathcal{H}$ denotes the sensing channel state, representing the target parameter of interest (e.g., delay, Doppler, angle, or a binary detection variable;
- $\mathsf{y} \in \mathcal{Y}$ represents the received signal at the communication Rx;
- $\mathsf{z} \in \mathcal{Z}$ denotes the reflected echo signal used for sensing (delayed feedback to the Tx).

As shown in the information-theoretic model in Fig. 2, the ISAC Tx consists of two components:

- An enconder for delivering a message $\mathsf{w} \in \mathcal{W}$;
- An estimator (collocated sensing Rx) for inferring the unknown target parameter h by analyzing the received echoes.

At each time slot $i \in \{1, 2, \ldots, n\}$, the system evolves as follows:

- The state realization $\mathsf{h}_i \sim P_{\mathsf{h}}$ is drawn independently from a known distribution;
- The encoder generates the ISAC signal $\mathsf{x}_i = \Phi_i\left(\mathsf{w}, \mathsf{z}^{i-1}\right)$, where $\mathsf{z}^{i-1} = \{\mathsf{z}_1, \mathsf{z}_2, \ldots, \mathsf{z}_{i-1}\}$ denotes the sequence of the prior echoes;
- The channel produces outputs y_i and z_i according to $P_{\mathsf{yz|xh}}(y_i, z_i|x_i, h_i)$.

Upon relying on the above model, a $\left(2^{nR}, n\right)$ ISAC coding scheme consists of [63]:

- **Message Set** $\mathcal{W}$: containing at least 2^{nR} messages for transmission;
- **Encoding Functions** $\Phi_i : \mathcal{W} \times \mathcal{Z}^{i-1} \to \mathcal{X}$: one per time index i, generating each channel input x_i as a function of the message w and previously received echoes z^{i-1};
- **Decoding Function** $\psi : \mathcal{H}^n \times \mathcal{Y}^n \to \mathcal{W}$: designed to recover the transmitted message using both the sequence of communication outputs y and the sensing channel state h. The decoded message may be expressed as $\hat{\mathsf{w}} = \psi\left(\mathsf{h}^n, \mathsf{y}^n\right)$;
- **State Estimator** $\hat{h} : \mathcal{X}^n \times \mathcal{Z}^n \to \hat{\mathcal{H}}^n$: adopted by the sensing Rx to estimate the state sequence $\hat{\mathsf{h}}^n = \hat{h}\left(\mathsf{x}^n, \mathsf{z}^n\right)$, where $\hat{\mathcal{H}}^n$ denotes the finite set of reconstructed state values.

2) S&C Performance Evaluation: To evaluate the sensing performance of the presented ISAC system, we use the average per-block distortion by relying on a certain distortion function $d(\mathsf{h}, \hat{\mathsf{h}})$, e.g., Euclidean distance for estimation or Hamming distance for detection. This is defined as:

$$\Delta^{(n)} := \mathbb{E}\left\{d(\mathsf{h}^n, \hat{\mathsf{h}}^n)\right\} = \frac{1}{n}\sum_{i=1}^{n}\mathbb{E}\left\{d(\mathsf{h}_i, \hat{\mathsf{h}}_i)\right\}. \tag{4}$$

Thanks to the memoryless nature of the ISAC channel, it is provable that the optimal estimator $\hat{h}^\star$ is single-letterized, which minimizes the expected posterior distortion, given by

$$\hat{h}^\star(x, z) := \arg\min_{h' \in \hat{\mathcal{H}}} \sum_{h \in \mathcal{H}} P_{\mathsf{h|xz}}(h|x, z) d(h, h'). \tag{5}$$

This yields an estimation error:

$$e(x) = \mathbb{E}\left\{d[\mathsf{h}, \hat{h}^\star(\mathsf{x}, \mathsf{z})]|\mathsf{x} = x\right\}, \tag{6}$$

which acts as the sensing cost function for a given instance of ISAC signal x. For communication performance, on the other hand, we consider the average error probability of the transmitted message:

$$P_e^{(n)} := \frac{1}{2^{nR}}\sum_{i=1}^{2^{nR}} \Pr(\hat{\mathsf{w}} \neq i|\mathsf{w} = i). \tag{7}$$

To model the constraint on wireless resources (e.g., transmission power or bandwidth), we introduce a cost function $b(\cdot)$ for the ISAC signal x, defined by

$$\mathbb{E}\left\{b(\mathsf{x}^n)\right\} = \frac{1}{n}\sum_{i=1}^{n}\mathbb{E}\left\{b(\mathsf{x}_i)\right\}. \tag{8}$$

Given a resource budget B, a rate-distortion-cost tuple $\{R, D, B\}$ is deemed achievable if there exists a $\left(2^{nR}, n\right)$ ISAC coding scheme, such that [63]

$$\lim_{n\to\infty} P_e^{(n)} = 0, \tag{9a}$$

$$\lim_{n\to\infty} \Delta^{(n)} \leq D, \tag{9b}$$

$$\lim_{n\to\infty} \mathbb{E}\left\{b(\mathsf{x}^n)\right\} \leq B. \tag{9c}$$

Under the above framework, the C-D tradeoff of an ISAC system is defined as

$$C_B(D) = \sup\left\{R|\left\{R, D, B\right\} \text{is achievable}\right\}. \tag{10}$$

Although the above definition clarifies the operational meaning of the C-D tradeoff, it is often challenging to directly

[1]While we focus on the P2P case, the C-D framework has been extended to multi-user settings, such as two-user memoryless broadcast and multi-access ISAC channels [72], [73].

compute $C_B(D)$ in a tractable manner. To that end, the following information-theoretic C-D function, which maximizes the conditional mutual information (MI) over the ISAC signal distribution $P_{\mathsf{x}}(x)$, was proved to be equivalent to (10) [63]:

$$C_B(D) = \arg\max_{P_{\mathsf{x}}(x)} I(\mathsf{x};\mathsf{y}|\mathsf{h}) \tag{11a}$$

$$\text{s.t.} \quad \sum_{x\in\mathcal{X}} P_{\mathsf{x}}(x)e(x) \le D, \tag{11b}$$

$$\sum_{x\in\mathcal{X}} P_{\mathsf{x}}(x)b(x) \le B, \tag{11c}$$

where $I(\mathsf{x};\mathsf{y}|\mathsf{h})$ stands for the conditional MI between the input x and output y conditioned on the channel h, and (11b) and (11c) represent the constraints on the average sensing distortion and resource cost, respectively. For a given channel law $P_{\mathsf{yz}|\mathsf{xh}}$, the functional optimization problem (11) may be solved in an iterative manner via the celebrated Blahut-Arimoto (BA) algorithm [77], [78].

3) Example of the C-D Tradeoff in the Linear Gaussian Channel: We consider a scalar linear Gaussian channel $P_{\mathsf{yz}|\mathsf{xh}}$, with the following input-output relationship [71]:

$$\mathsf{y} = \mathsf{h}\mathsf{x} + \mathsf{n}, \quad \mathsf{z} = \mathsf{y}, \tag{12}$$

where the channel coefficient $\mathsf{h} \in \mathbb{R}$, obeying the Gaussian distribution, is the parameter to be estimated by the ISAC signal $\mathsf{x} \in \mathbb{R}$, and $\mathsf{n} \in \mathbb{R}$ is the additive white Gaussian noise (AWGN) with zero mean and unit variance. The resource budget is the transmit power, which is set as $\mathbb{E}(|\mathsf{x}|^2) \le B = 10$. Here, the communication Rx wishes to recover x upon receiving y, whereas the sensing Rx wishes to estimate h by observing the echo signal z with a minimum MSE (MMSE) estimator. We note here that the model (12) assumes perfect feedback. This is a toy model simply to illustrate the C-D tradeoff, which may not fully align with the realistic ISAC transmission scenario elaborated in later sections.

Fig. 3 portrays the C-D tradeoff result as well as corresponding optimal ISAC signal distributions under the above model, through numerically solving problem (11). It is observed that at points ① and ④, the optimal input distributions of x are the Gaussian and BPSK constellations, respectively, corresponding to the communication-optimal and sensing-optimal performance. Along the C-D tradeoff curve, $P_{\mathsf{x}}(x)$ smoothly evolves from Gaussian to BPSK, indicating a gradual reduction in the randomness of the ISAC signal [71].

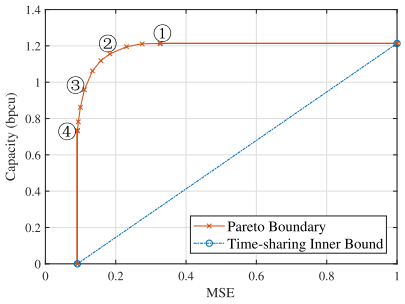

(a) The capacity-distortion boundary.

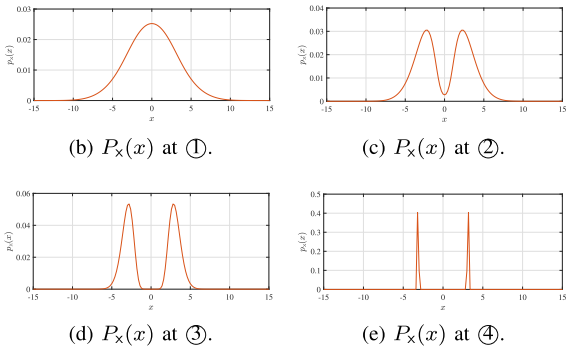

(b) $P_{\mathsf{x}}(x)$ at ①. (c) $P_{\mathsf{x}}(x)$ at ②.

(d) $P_{\mathsf{x}}(x)$ at ③. (e) $P_{\mathsf{x}}(x)$ at ④.

Fig. 3. The C-D tradeoff boundary of the real-valued scalar Gaussian channel scenario with $B = 10$, as well as the Pareto-optimal input distributions $P_{\mathsf{x}}(x)$ along the boundary.

C. CRB-Rate Region for Vector Gaussian ISAC Channels

1) Generic Framework: The C-D theory presented above provides clear evidence of the DRT between S&C in terms of the input distribution of the ISAC channel. A natural question arises as to whether this tradeoff holds in more complex scenarios, such as MIMO or OFDM systems with multiple sensing parameters. To explore this, the study in [61] examined the CRB-rate tradeoff between S&C in the context of the following P2P vector Gaussian ISAC channel model:

$$\mathbf{Y}_s = \mathbf{H}_s(\boldsymbol{\eta})\mathbf{X} + \mathbf{Z}_s \tag{13a}$$

$$\mathbf{Y}_c = \mathbf{H}_c\mathbf{X} + \mathbf{Z}_c, \tag{13b}$$

where $\mathbf{X} \in \mathbb{C}^{N_t\times N}$ denotes the dual-functional ISAC waveform emitted from the ISAC Tx, $\mathbf{Y}_s \in \mathbb{C}^{N_s\times N}$ and $\mathbf{Y}_c \in \mathbb{C}^{N_c\times N}$ are signal matrices received at the S&C Rxs, $\mathbf{H}_s \in \mathbb{C}^{N_s\times N_t}$ and $\mathbf{H}_c \in \mathbb{C}^{N_c\times N_t}$ represent the S&C channel matrices, while $\mathbf{Z}_s \in \mathbb{C}^{N_s\times N}$ and $\mathbf{Z}_c \in \mathbb{C}^{N_c\times N}$ are white Gaussian noise matrices, with each entry being i.i.d. and following $\mathcal{CN}\left(0,\sigma_s^2\right)$ and $\mathcal{CN}\left(0,\sigma_c^2\right)$, respectively. Moreover, the sensing channel $\mathbf{H}_s$ is assumed to be a function of the sensing parameter vector $\boldsymbol{\eta} \in \mathbb{R}^K$, which has a prior distribution $P_{\boldsymbol{\eta}}$ and may include delay, Doppler, and angle parameters of one or more targets. The two channels may be correlated with each other to a certain degree, depending on the specific ISAC scenarios.

While the focus of this tutorial is on the P2P ISAC channel in (13), which corresponds to a single-user communication and multi-target sensing scenario, this framework can be readily extended to a multi-user (MU) scenario by treating $\mathbf{H}_c$ as the MU-MIMO communication channel matrix. However, due to the complex coupling between users and targets, the tradeoff between target sensing and multi-user communication remains largely unexplored in the existing literature. Even in communication-only scenarios, such as MIMO broadcast channels, the capacity region is still an open problem in information theory. The inclusion of multiple sensing targets adds additional complexity to this challenge. This highlights the need for foundational research before scaling to multi-user systems, which is identified as a key direction for future work.

The sensing channel matrix $\mathbf{H}_s$ may have different forms depending on the specific sensing scenarios and adopted target models. Below, we discuss two typical cases.

- **Multi-Target Angle Estimation**: Consider estimating the angles of Q point-like targets within a single delay-Doppler bin, using a MIMO-ISAC system. Here, the sensing channel is defined in the spatial domain as:

$$\mathbf{H}_s = \sum_{q=1}^{Q} \beta_q \mathbf{b}(\theta_q)\mathbf{a}^T(\phi_q), \tag{14}$$

where β_q, θ_q, and ϕ_q denote the complex amplitude, angle of arrival (AoA), and angle of departure (AoD) of the q-th target,[2] respectively, with $\mathbf{a}(\phi)$ and $\mathbf{b}(\theta)$ being the steering vectors of transmit and receive antenna arrays, determined by the array geometry. Specifically, for uniform linear arrays (ULAs) with half-wavelength spacing, the steering vectors may be modeled as

$$\begin{aligned}\mathbf{a}(\phi) &= \left[1, e^{j\pi\sin\phi}, \ldots, e^{j\pi(N_t-1)\sin\phi}\right]^T,\\ \mathbf{b}(\theta) &= \left[1, e^{j\pi\sin\theta}, \ldots, e^{j\pi(N_s-1)\sin\theta}\right]^T,\end{aligned} \tag{15}$$

where N_t, N_s, and N_c stand for the antenna number at ISAC Tx, sensing Rx, and communication Rx, respectively, and N is the number of time-domian snapshots. Accordingly, the target parameter vector $\boldsymbol{\eta}$ is a size-$4Q$ vector containing AoA, AoD and real/imaginary parts of β_q for each target.

- **Multi-Target Ranging with OFDM**: Consider estimating the ranges of Q static targets under OFDM signaling with N_t subcarriers. Assume that each target has a delay τ_q and a complex amplitude β_q. After removing the cyclic prefix (CP), the sensing channel becomes a circulant matrix, decomposable as:

$$\mathbf{H}_s = \boldsymbol{F}_{N_t}^H \mathrm{Diag}\left\{\sum_{q=1}^{Q}\beta_q \mathbf{c}(\tau_q)\right\}\boldsymbol{F}_{N_t}, \tag{16}$$

where $\boldsymbol{F}_N$ is the N-dimensional discrete Fourier transform (DFT) matrix, and $\mathbf{c}(\tau)$ is the frequency-domain steering vector defined over subcarriers, which is

$$\mathbf{c}(\tau) = \left[1, e^{-j2\pi\Delta f\tau}, \ldots, e^{-j2\pi(N_t-1)\Delta f\tau}\right]^T, \tag{17}$$

with Δf being the subcarrier spacing. In such a case, $N_t = N_c = N_s$ represent the number of subcarriers, and N is the number of OFDM symbols. As a consequence, $\boldsymbol{\eta}$ is a size-$3Q$ vector comprising τ_q and the real/imaginary parts of β_q for each target.

Beyond these examples, the generic model in (13) is widely applicable to more complex sensing scenarios, which are omitted here for brevity.

We now examine the CRB-rate tradeoff using the MIMO-ISAC system as an example. As illustrated in Fig. 1, an ISAC Tx equipped with N_t antennas emits a dual-functional ISAC signal $\mathbf{X}$ over N consecutive time slots, enabling communication with an N_c-antenna communication Rx, while simultaneously estimating the parameter vector $\boldsymbol{\eta}$ by observing the echo signal $\mathbf{Y}_s$ at an N_s-antenna sensing Rx. We therefore model $\mathbf{X}$ as a random matrix governed by a distribution $P_{\mathbf{X}}(\boldsymbol{X})$, with its realization fully known to the sensing Rx but unknown to the communication Rx. Under such a setup:

- The communication performance is quantified by the achievable rate, characterized by the input-output MI conditioned on the channel $\mathbf{H}_c$, i.e., $I(\mathbf{X};\mathbf{Y}|\mathbf{H}_c)$.
- The sensing performance is evaluated using the CRB, which serves as the lower bound for the MSE of any weakly unbiased estimator of the target parameter $\boldsymbol{\eta}$.

Since the unified ISAC signal $\mathbf{X}$ serves both S&C functions, the ISAC system cannot simultaneously achieve sensing-optimal and communication-optimal performance, leading to a fundamental tradeoff between CRB and communication rate. A rigorous analytical characterization of this tradeoff would provide valuable insights for system design and ISAC signal optimization.

Unlike conventional radar systems, the sensing CRB of the considered ISAC system is not straightforwardly characterizable due to the randomness in the probing waveform $\mathbf{X}$. To address this issue, one may treat $\mathbf{X}$ as a *random but known* nuisance parameter, and resort to the Miller-Chang bound (MCB) as a potential solution [79]. In particular, the MCB is obtained by computing the CRB for a given instance of $\mathbf{X}$, and then taking the expectation over $\mathbf{X}$. For any weakly unbiased estimate $\hat{\boldsymbol{\eta}}$, the resulting MSE is lower-bounded by the Bayesian MCB as follows:

$$\varepsilon := \mathbb{E}\left\{\|\hat{\boldsymbol{\eta}} - \boldsymbol{\eta}\|^2\right\} \geq \mathbb{E}_{\mathbf{X}}\left\{\mathrm{Tr}\left(\mathbf{M}_{\boldsymbol{\eta}|\mathbf{X}}^{-1}\right)\right\}, \tag{18}$$

where $\mathbf{M}_{\boldsymbol{\eta}|\mathbf{X}} \in \mathbb{C}^{K\times K}$ is the Bayesian Fisher Information matrix (BFIM) of $\boldsymbol{\eta}$ [80], which can be equivalently expressed as an affine map of the sample covariance matrix $\mathbf{R}_{\mathbf{X}} := N^{-1}\mathbf{X}\mathbf{X}^H$ in the following form [61]:

$$\begin{aligned}\mathbf{M}_{\boldsymbol{\eta}|\mathbf{X}} &= \boldsymbol{\Phi}(\mathbf{R}_{\mathbf{X}})\\ &:= \frac{N}{\sigma_s^2}\left(\sum_{n=1}^{r_1}\boldsymbol{B}_{1,n}\mathbf{R}_{\mathbf{X}}^T\boldsymbol{B}_{1,n}^H + \sum_{m=1}^{r_2}\boldsymbol{B}_{2,m}\mathbf{R}_{\mathbf{X}}\boldsymbol{B}_{2,m}^H + \boldsymbol{M}_P\right),\end{aligned} \tag{19}$$

with the term $\boldsymbol{M}_P$ representing the prior FIM contributed by $P_{\boldsymbol{\eta}}$. Additionally, the matrices $\boldsymbol{B}_{1,n}$ and $\boldsymbol{B}_{2,m}$ are partitioned from the Jacobian matrix $\frac{\partial \mathrm{vec}(\mathbf{H}_s^*)}{\partial \boldsymbol{\eta}}$.

The Bayesian MCB in (18) may be achieved by the *maximum a posterior (MAP)* estimator at the high SNR regime [80]. By comparing (18) and (11b), it becomes evident that the MCB serves as an equivalent average sensing cost function of the random ISAC signal $\mathbf{X}$, even though it is not a traditional "distortion" metric. Consequently, the CRB-rate tradeoff in the ISAC system can be framed as the following Pareto optimization problem:

$$\min_{P_{\mathbf{X}}(\boldsymbol{X})} \rho\mathbb{E}\left\{\mathrm{Tr}\left[\left(\boldsymbol{\Phi}(\mathbf{R}_{\mathbf{X}})\right)^{-1}\right]\right\} - (1-\rho)I(\mathbf{X};\mathbf{Y}_c|\mathbf{H}_c) \tag{20a}$$

$$\text{s.t. } \mathbb{E}\{\mathrm{Tr}(\mathbf{R}_{\mathbf{X}})\} = P_T, \tag{20b}$$

where P_T stands for the average transmit power budget, and $\rho \in [0,1]$ is a parameter that balances the tradeoff between S&C objectives. As illustrated in Fig. 4, adjusting ρ from 0 to 1 traces out the Pareto boundary of the two objectives,

[2]Note that under the monostatic mode we have $\phi_q = \theta_q, \ \forall q$.

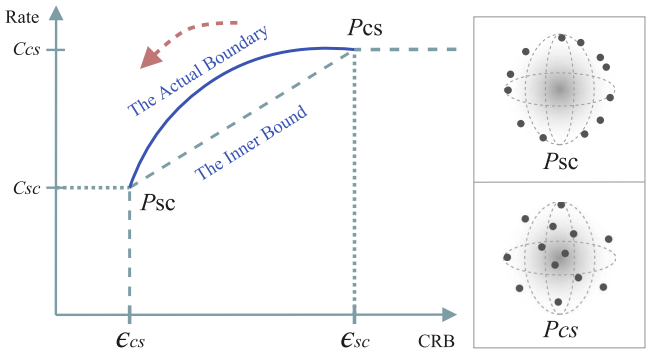

Fig. 4. CRB-Rate tradeoff for a P2P monostatic ISAC system.

capturing the achievable CRB-rate pairs and thus defining the CRB-rate region of the ISAC system.

Despite the convexity of (20) with respect to $P_{\mathbf{X}}$, obtaining the complete CRB-rate boundary is computationally challenging due to the infinite dimensionality of $P_{\mathbf{X}}$. Therefore, our focus shifts to the two extreme points $P_{\rm CS}$ and $P_{\rm SC}$, representing the optimal ISAC signal distributions for communication and sensing, respectively. Notably, the line segment connecting these two points forms a time-sharing inner bound for the CRB-rate region.

2) S&C Performance at $P_{\rm CS}$: Given the linear Gaussian model in (13b), the communication rate at $P_{\rm CS}$ is maximized by a Gaussian input distribution, where each column of $\mathbf{X}$ is independently drawn from $\mathcal{CN}(\mathbf{0}, \widetilde{\mathbf{R}}_{\mathbf{X}}^{\rm SC})$, with a statistical covariance matrix defined by

$$\widetilde{\mathbf{R}}_{\mathbf{X}}^{\rm CS} = \boldsymbol{U}_c \boldsymbol{\Lambda}_{\rm CS} \boldsymbol{U}_c^H, \tag{21}$$

where $\boldsymbol{U}_c$ contains the right singular vectors of $\mathbf{H}_c$, and $\boldsymbol{\Lambda}_{\rm CS}$ is a diagonal matrix with eigenvalues determined by the water-filling power allocation approach. Consequently, the optimal ISAC signal structure at $P_{\rm CS}$ is given by

$$\mathbf{X}^{\rm CS} = \boldsymbol{U}_c \boldsymbol{\Lambda}_{\rm CS}^{1/2} \mathbf{D}, \tag{22}$$

where $\mathbf{D}$ is an information-bearing random matrix containing i.i.d. entries following $\mathcal{CN}(0,1)$. The resulting achievable rate at $P_{\rm CS}$ can then be expressed by the renowned Shannon capacity formula as

$$C_{\rm CS} = \mathbb{E}\left\{\log\det\left(\boldsymbol{I} + \sigma_c^{-2}\mathbf{H}_c \widetilde{\mathbf{R}}_{\mathbf{X}}^{\rm CS} \mathbf{H}_c^H\right)\right\}. \tag{23}$$

In contrast to the communication rate that depends on the statistical covariance matrix of $\mathbf{X}$, the sensing CRB is determined by the sample covariance matrix $\mathbf{R}_{\mathbf{X}}$. The latter follows a complex Wishart distribution due to the Gaussian-distributed $\mathbf{X}^{\rm CS}$ at $P_{\rm CS}$. Unfortunately, the CRB at $P_{\rm CS}$, which involves calculating the expectation of a highly nonlinear function of $\mathbf{R}_{\mathbf{X}}$, is unlikely to be expressed in a closed form. To that end, one may resort to establishing the lower- and upper-bounds of the sensing CRB $\epsilon_{\rm CS}$ as follows [61]:

$$\mathrm{Tr}\left\{\left[\boldsymbol{\Phi}(\widetilde{\mathbf{R}}_{\mathbf{X}}^{\rm CS})\right]^{-1}\right\} \le \epsilon_{\rm CS} \le \frac{N\cdot\mathrm{Tr}\left\{\left[\boldsymbol{\Phi}(\widetilde{\mathbf{R}}_{\mathbf{X}}^{\rm CS})\right]^{-1}\right\}}{N - \min\left\{K, \mathrm{rank}(\widetilde{\mathbf{R}}_{\mathbf{X}}^{\rm CS})\right\}}. \tag{24}$$

Observe that the two bounds become identical when $N \to \infty$.

3) S&C Performance at $P_{\rm SC}$: Evaluating S&C performance at point $P_{\rm SC}$ is generally more challenging than at $P_{\rm CS}$, as neither the optimal ISAC signal distribution nor the achievable communication rate is explicitly determined at this stage. Denoting the CRB at $P_{\rm SC}$ as $\epsilon_{\rm SC}$, we can characterize it using the Jensen's inequality:

$$\begin{aligned}\mathbb{E}\left\{\mathrm{Tr}\left[\left(\boldsymbol{\Phi}(\mathbf{R}_{\mathbf{X}})\right)^{-1}\right]\right\} &\ge \mathrm{Tr}\left\{\left(\boldsymbol{\Phi}\left[\mathbb{E}\left(\mathbf{R}_{\mathbf{X}}\right)\right]\right)^{-1}\right\}\\ &\ge \mathrm{Tr}\left\{\left[\boldsymbol{\Phi}\left(\widetilde{\mathbf{R}}_{\mathbf{X}}^{\rm SC}\right)\right]^{-1}\right\} := \epsilon_{\rm SC},\end{aligned} \tag{25}$$

where $\widetilde{\mathbf{R}}_{\mathbf{X}}^{\rm SC}$ is the optimal covariance matrix at $P_{\rm SC}$, attained by solving the deterministic CRB minimization problem:

$$\widetilde{\mathbf{R}}_{\mathbf{X}}^{\rm SC} = \underset{\widetilde{\boldsymbol{R}}\succeq\mathbf{0},\, \widetilde{\boldsymbol{R}}=\widetilde{\boldsymbol{R}}^H}{\arg\min}\ \mathrm{Tr}\left\{\left[\boldsymbol{\Phi}(\widetilde{\boldsymbol{R}})\right]^{-1}\right\}\ \text{s.t. } \mathrm{Tr}(\widetilde{\boldsymbol{R}}) \le P_T. \tag{26}$$

The equality in (25) holds if and only if

$$\frac{1}{N}\mathbf{X}\mathbf{X}^H = \mathbf{R}_{\mathbf{X}} = \mathbb{E}\left(\mathbf{R}_{\mathbf{X}}\right) = \widetilde{\mathbf{R}}_{\mathbf{X}}^{\rm SC}, \tag{27}$$

indicating that $\mathbf{R}_{\mathbf{X}}$ becomes deterministic at $P_{\rm SC}$.[3] This suggests the optimal ISAC signal structure at $P_{\rm SC}$ as follows:

$$\mathbf{X}^{\rm SC} = \sqrt{N}(\widetilde{\mathbf{R}}_{\mathbf{X}}^{\rm SC})^{1/2}\mathbf{Q} = \sqrt{N}\boldsymbol{U}_s\boldsymbol{\Lambda}_{\rm SC}^{1/2}\mathbf{Q}, \tag{28}$$

where $\boldsymbol{U}_s$ and $\boldsymbol{\Lambda}_{\rm SC}$ are the eigenvectors and eigenvalues of $\widetilde{\mathbf{R}}_{\mathbf{X}}^{\rm SC}$, and $\mathbf{Q} \in \mathbb{C}^{\mathrm{rank}(\boldsymbol{\Lambda}_{\rm SC})\times N}$ is a semi-unitary matrix (i.e., $\mathbf{Q}\mathbf{Q}^H = \boldsymbol{I}$) that carries communication data, which belongs to the Stiefel manifold. The communication degrees of freedom (DoFs) are constrained to $\mathbf{Q}$ due to the deterministic nature of $\widetilde{\mathbf{R}}_{\mathbf{X}}^{\rm SC}$. Under this configuration, the achievable communication rate can be expressed as

$$C_{\rm SC} = \max_{P_{\mathbf{Q}}(\boldsymbol{Q})}\ I\left(\mathbf{Q};\mathbf{Y}_c|\mathbf{H}_c\right)\ \text{s.t. } \mathbf{Q}\mathbf{Q}^H = \boldsymbol{I}. \tag{29}$$

Deriving an explicit form of $C_{\rm SC}$ is challenging; however, as shown in [61], the asymptotic rate at $P_{\rm SC}$ in the high SNR regime is given by:

$$\begin{aligned}C_{\rm SC} = \mathbb{E}\left\{\left(1 - \frac{\mathrm{rank}(\boldsymbol{\Lambda}_{\rm SC})}{2N}\right)\log\det(\sigma_c^{-2}\mathbf{H}_c\widetilde{\mathbf{R}}_{\mathbf{X}}^{\rm SC}\mathbf{H}_c^H) + c_0\right\}\\ + O(\sigma_c^2),\end{aligned} \tag{30}$$

where c_0 is irrelevant to the SNR and approaches zero as $N \to \infty$. The rate in (30) may be achieved asymptotically by a uniformly distributed $\mathbf{Q}$ over the Stiefel manifold.

[3]It is worth mentioning a special case when $N \to \infty$, in which $\mathbf{R}_{\mathbf{X}}$ becomes deterministic at $P_{\rm SC}$, such that the equality in (25) and (27) both hold. In this case, due to the deterministic property of $\mathbf{R}_{\mathbf{X}}$, the Gaussian signaling becomes optimal for both S&C functions, and we can optimize the covariance matrix $\mathbf{R}_{\mathbf{X}}$ to characterize the complete Pareto boundary between $P_{\rm SC}$ and $P_{\rm SC}$; see, e.g., [36], [37] for examples when $\mathbf{H}_s(\boldsymbol{\eta})$ and $\mathbf{H}_c$ are deterministic (instead of random in our context). This, however, only serves as an S&C performance upper bound for the general case with N being finite in general.

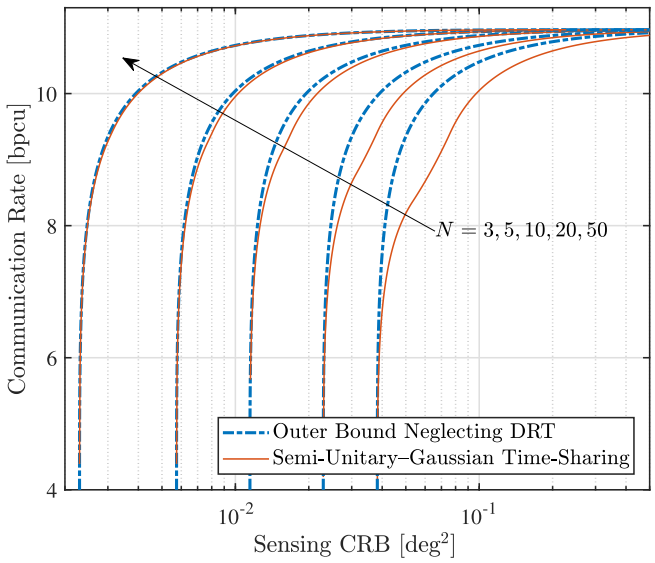

Fig. 5. The outer bound and the semi-unitary-Gaussian time-sharing inner bound of the CRB-rate region for the task of simultaneous target angle estimation and single-user MIMO communication, with various values of snapshot number N.

4) DRT in Vector Gaussian ISAC Channels: We now turn to the discussion of the DRT for the vector Gaussian ISAC model in (13), by examining the S&C performance at two corner points. First, it is clear from the structures of (22) and (28) that the randomness level of ISAC signals decreases as the system shifts from the communication-optimal point to the sensing-optimal point. This occurs because the communication codewords transition from the i.i.d. Gaussian matrix $\mathbf{D}$ to the uniformly distributed semi-unitary matrix $\mathbf{Q}$. This tradeoff in the optimal input distribution of ISAC signals can be seen as a generalized form of the Gaussian-BPSK tradeoff in the scalar Gaussian channel, discussed earlier in the C-D theory.

Additionally, the DRT is evident in the achievable rate (29) at P_{SC}, where a reduction in communication DoFs leads to a rate loss compared to the Gaussian capacity C_{SC}. Conversely, greater randomness in the ISAC signal can impair the sensing performance, as seen in the CRB. Specifically, (24) indicates that a Gaussian-distributed ISAC signal could inflate the CRB by a factor greater than 1, in contrast to the minimum CRB achievable at P_{SC} by signals with deterministic sample covariance matrices.

5) Example of Simultaneous Target Angle Estimation and Single-User MIMO Communication: To validate the effectiveness of the above theoretical framework, we consider a simple monostatic MIMO-ISAC system equipped with ULA antennas for simultaneous target angle estimation and communication in a single-target, single-user scenario. In this configuration, the sensing channel matrix adopts the following structure:

$$\mathbf{H}_s = \beta \mathbf{b}(\theta)\mathbf{a}^T(\theta), \tag{31}$$

where β and θ represent the target's complex amplitude and AoA, respectively. The parameter vector is then given by:

$$\boldsymbol{\eta} = [\theta, \mathrm{Re}(\beta), \mathrm{Im}(\beta)]^T. \tag{32}$$

We assume that β follows a circularly symmetric Gaussian distribution with unit variance, while θ follows a von Mises distribution with a mean of 30° and standard deviation of 5°. The system employs $N_t = N_s = 10$ antennas at the ISAC Tx and sensing Rx, respectively, and $N_c = 1$ antenna at the communication Rx, which is positioned at $\theta_c = 50°$. In Fig. 5, we examine the tradeoff between the CRB of AoA estimation and the achievable communication rate, illustrating both inner and outer bounds for varying snapshot number N. The inner bound is achieved through a semi-unitary-Gaussian time-sharing strategy, which combines optimal signaling schemes at P_{SC} and P_{CS} in a time-division manner. The outer bound, on the other hand, is derived by neglecting ISAC signal randomness in the weighted optimization problem (20), which reduces to solving the following deterministic convex optimization problem by varying ρ from 0 to 1:

$$\begin{aligned} \min_{\boldsymbol{R}_{\mathbf{X}} \succeq \mathbf{0}} \quad & \rho \mathrm{Tr}\left[\left(\boldsymbol{\Phi}(\boldsymbol{R}_{\mathbf{X}})\right)^{-1}\right] \\ & - (1-\rho)\log\det\left(\boldsymbol{I} + \sigma_c^{-2}\mathbf{H}_c \boldsymbol{R}_{\mathbf{X}} \mathbf{H}_c^H\right) \\ \text{s.t.} \quad & \mathrm{Tr}\left(\boldsymbol{R}_{\mathbf{X}}\right) = P_T. \end{aligned} \tag{33}$$

It can be seen that there is a noticeable performance gap between the inner and outer bounds due to the DRT between S&C. However, as N increases from 3 to 50, this gap diminishes, indicating that the DRT becomes less significant with more independent observations.

D. From DRT Theory to Random ISAC Signal Processing

The information-theoretic insights presented in the previous section reveal a fundamental tradeoff between S&C, rooted in the statistical structure of the transmit signal $\mathbf{X}$. This tradeoff, termed the DRT, identifies the input distribution as a critical design DoF in ISAC systems. Unlike traditional radar systems that rely on deterministic or structured pseudo-random signals (e.g., m-sequences, Gold codes), future 6G ISAC systems must extract sensing information directly from communication signals, which are inherently random due to their data-carrying nature. This shift brings both opportunities and challenges. On one hand, the randomness enhances communication throughput by maximizing entropy and mutual information. On the other hand, it induces stochastic fluctuations in the received echo signals, potentially degrading sensing performance in terms of resolution, estimation accuracy, and detection probability. As a result, it becomes necessary to develop new performance metrics and processing methods tailored to sensing with random communication signals.

To connect the theoretical underpinnings with practical implementation, the following sections transition from capacity-distortion theory to the physical-layer design and processing strategies for communication-centric ISAC systems. We begin by analyzing the sensing performance of standard communication waveform, examining their autocorrelation characteristics and matched filtering behavior. We then explore how to systematically design key building blocks, such as modulation schemes, constellation mapping, pulse shaping filters, and precoding strategies, to enable joint S&C operation with tunable tradeoffs. Due to space constraints,

other system components such as source/channel coding and quantization are left for future investigation. The subsequent sections are organized as follows: Sec. III and Sec. IV focus on single-antenna ISAC transmission with random communication signals, while Sec. V extends the discussion to MIMO-based ISAC systems.

III. Communication-Centric ISAC Transmission

We now turn to concrete signal processing techniques for the point-to-point ISAC model introduced in Fig. 1, beginning with the single-antenna case. Specifically, we consider an ISAC system composed of a single ISAC Tx, a communication Rx, and a sensing Rx. The ISAC Tx emits a random data-bearing signal intended for the communication Rx. Simultaneously, the sensing Rx captures the echo of this signal reflected from multiple targets, and subsequently estimates the targets' delay parameters. Consistent with the system setting and assumptions in Sec. II-C, the information symbol vector $\mathbf{s}$ is unknown to the communication Rx, but is fully known to the sensing Rx.

A. Communication-Centric ISAC Signal Model

Let us consider the following generic baseband ISAC signal:

$$\widetilde{\mathsf{x}}(t) = \sum_{n=0}^{N-1} \mathsf{x}_n p(t - nT), \tag{34}$$

where T stands for the symbol duration, $p(t)$ is the impulse response of a *pulse shaping filter*, and $\mathbf{x} = [\mathsf{x}_0, \mathsf{x}_1, \ldots, \mathsf{x}_{N-1}]^T \in \mathbb{C}^{N\times 1}$ represents N discrete time-domain samples, generated from

$$\mathbf{x} = \boldsymbol{U}\mathbf{s} = \sum_{n=0}^{N-1} \mathsf{s}_n \boldsymbol{u}_n, \tag{35}$$

where $\mathbf{s} = [\mathsf{s}_0, \mathsf{s}_1, \ldots, \mathsf{s}_{N-1}]^T \in \mathbb{C}^{N\times 1}$ denotes N data symbols that are independently drawn from a *constellation* $\mathcal{S}$, and $\boldsymbol{U} = [\boldsymbol{u}_0, \boldsymbol{u}_1, \ldots, \boldsymbol{u}_{N-1}] \in \mathbb{U}(N)$ is an N-dimensional unitary matrix representing the orthonormal *modulation basis* in the time domain. Note that signal model (34) serves as a practical realization of the information-theoretic model in Sec. II-B. The assumptions for these three components are elaborated as follows:

1) Constellation: Throughout the paper, we adopt a rotationally invariant constellation $\mathcal{S}$ with zero mean, zero pseudo-variance, and unit power, defined as:

$$\mathbb{E}(\mathsf{s}) = 0, \quad \mathbb{E}(\mathsf{s}^2) = 0, \quad \mathbb{E}(|\mathsf{s}|^2) = 1, \quad \forall\ \mathsf{s} \in \mathcal{S}. \tag{36}$$

We remark that most commonly employed constellations, such as PSK, QAM, and Amplitude and Phase Shift Keying (APSK), satisfy these criteria. The two exceptions are BPSK and 8-QAM, which are seldom used in modern cellular wireless networks. Additionally, the constellation needs not to be uniformly distributed; each point may be transmitted with distinct probabilities if the probabilistic constellation shaping (PCS) technique is applied, as will be discussed later.

2) Modulation Basis: The modulation basis $\boldsymbol{U} \in \mathbb{U}(N)$, which carries information symbols, is often referred to as a "waveform" in a broader context, with $\mathbb{U}(N)$ denoting the size-N unitary group. For clarity, we list several typical examples below:

- **SC Modulation:** $\boldsymbol{U} = \boldsymbol{I}_N$. In this case, the signaling basis consists solely of N time-domain Kronecker-Delta functions, forming an SC signal.
- **OFDM Modulation:** $\boldsymbol{U} = \boldsymbol{F}_N^H$, where we recall that $\boldsymbol{F}_N \in \mathbb{C}^{N\times N}$ represents the N-dimensional DFT matrix. Here, the signaling basis is constructed using N orthogonal sinusoidal functions, which are also Kronecker-Delta functions in the frequency domain.
- **CDMA Modulation:** $\boldsymbol{U} = \boldsymbol{C}_N$, where $\boldsymbol{C}_N \in \mathbb{C}^{N\times N}$ denotes the N-dimensional Hadamard matrix, corresponding to Walsh codes widely used in CDMA2000 [81].
- **AFDM Modulation:** $\boldsymbol{U} = \boldsymbol{\Lambda}_{c_1}^H \boldsymbol{F}_N^H \boldsymbol{\Lambda}_{c_2}^H$, where $\Lambda_c = \mathrm{Diag}(1, e^{-j2\pi c 1^2}, \ldots, e^{-j2\pi c(N-1)^2})$. This configuration makes $\boldsymbol{U}$ an inverse discrete affine Fourier transform (IDAFT) matrix with tunable parameters c_1 and c_2, with symbols placed in the affine Fourier transform (AFT) domain [23].
- **OTFS Modulation:** $\boldsymbol{U} = \boldsymbol{F}_{N_1}^H \otimes \boldsymbol{I}_{N_2}$. In this case, the symbols are mapped to the delay-Doppler (DD) domain, where N_1 and $N_2 = \frac{N}{N_1}$ represent the number of occupied time slots and subcarriers, respectively. Note that OTFS is a 2-dimensional modulation scheme by its definition [82].

To facilitate efficient signal processing in the frequency domain, we assume that a cyclic prefix (CP) is added to the signal $\mathbf{x}$, which is longer than the maximum delay of the target or communication path.

3) Pulse Shaping Filter: The pulse shaping filter plays a crucial role in modern wireless communication systems by eliminating inter-symbol interference (ISI) while limiting the signaling bandwidth. Here, we employ a band-limited Nyquist prototype pulse with a one-sided bandwidth B and a roll-off factor α, resulting in a symbol duration of $T = \frac{1+\alpha}{2B}$. The Nyquist pulse ensures zero ISI among symbols, which can be expressed as the following condition:

$$\widetilde{p}\,(nT) = \begin{cases} 1, & n = 0 \\ 0, & n \neq 0 \end{cases}, \quad \forall\ n \in \mathbb{Z}, \tag{37}$$

where $\widetilde{p}\,(\tau) = \int p\,(t)\, p^*\,(t-\tau)\, dt$ is the ACF of $p\,(t)$. This translates to an equivalent frequency-domain condition, known as the *folded-spectrum criterion*, given by [65]

$$\sum_{m=-\infty}^{\infty} g\left(f + \frac{m}{T}\right) = T, \tag{38}$$

where $g(f)$ is the Fourier transform of $\widetilde{p}\,(\tau)$, which is also the squared frequency spectrum of the pulse $p(t)$.

B. Signal Processing for Communication and Sensing

In this subsection, we elaborate on the signal processing pipeline for both S&C, which is also illustrated in Fig. 6.

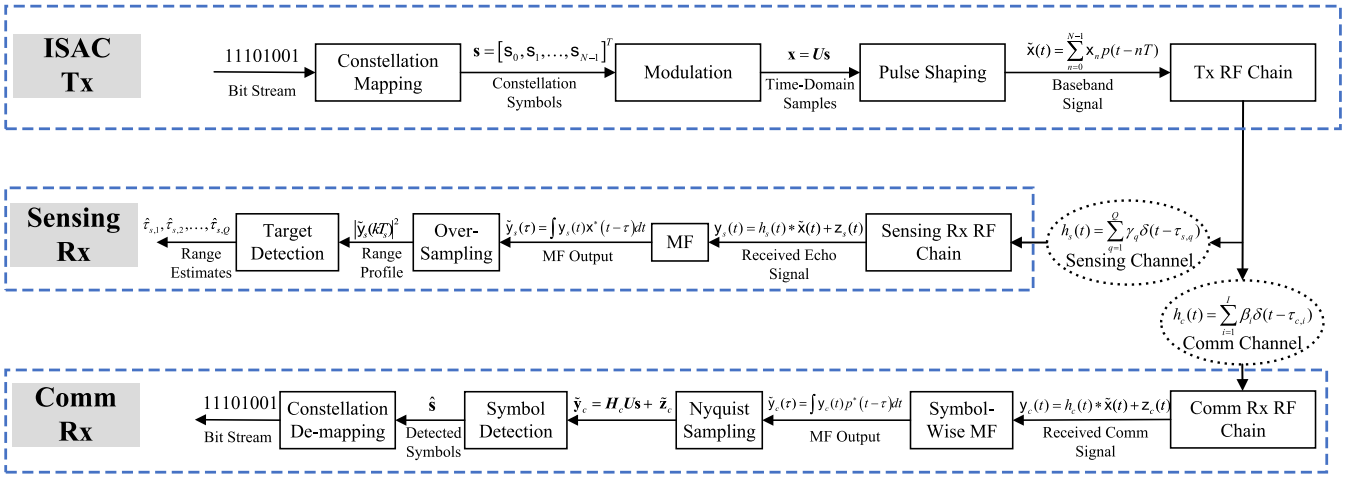

Fig. 6. A signal processing pipeline for P2P ISAC model in Fig. 1. The communication Rx aims to correctly detect symbols in the presence of multi-path interference, whereas the sensing Rx aims at extracting range parameters of multiple targets.

Without loss of generality, we model both communication and sensing channels as linear time-invariant (LTI) multi-path channels containing I paths and Q targets, respectively. Their time-domain impulse responses can be expressed as

$$h_c(t) = \sum_{i=1}^{I} \beta_i \delta(t - \tau_{c,i}), \quad h_s(t) = \sum_{q=1}^{Q} \gamma_q \delta(t - \tau_{s,q}), \quad (39)$$

where $\delta(t)$ is the Dirac-Delta function, β_i and γ_q denote the complex amplitudes of the i-th communication path and the q-th sensing target, respectively, with $\tau_{c,i}$ and $\tau_{s,q}$ representing the corresponding delays. For simplicity, we omit the impact of Doppler phase shifts on the two channels here, reserving those effects for future discussions. Note that $h_c(t)$ and $h_s(t)$ may exhibit certain correlations depending on the geometric environment, indicating that communication paths and sensing targets might partially overlap. This overlap gives rise to another fundamental tradeoff in S&C, known as the subspace tradeoff (ST). Due to space constraints, we will not delve into the details of the ST here and instead refer interested readers to [62] for further information.

1) Receive Signal Model: By transmitting the ISAC signal $\widetilde{\mathsf{x}}(t)$, the received signals at the communication and sensing Rxs are expressed as

$$\begin{aligned} \mathsf{y}_c(t) &= h_c(t) * \widetilde{\mathsf{x}}(t) + \mathsf{z}_c(t) \\ &= \sum_{i=1}^{I} \beta_i \sum_{n=0}^{N-1} \mathsf{x}_n p(t - nT - \tau_{c,i}) + \mathsf{z}_c(t), \quad (40a) \\ \mathsf{y}_s(t) &= h_s(t) * \widetilde{\mathsf{x}}(t) + \mathsf{z}_s(t) \\ &= \sum_{q=1}^{Q} \gamma_q \sum_{n=0}^{N-1} \mathsf{x}_n p(t - nT - \tau_{s,q}) + \mathsf{z}_s(t), \quad (40b) \end{aligned}$$

where $\mathsf{z}_s(t)$ and $\mathsf{z}_s(t)$ stand for the zero-mean white Gaussian noise with variances σ_c^2 and σ_s^2, respectively. For the communication Rx, the objective is to detect the information symbols $\mathbf{s}$ embedded in $\widetilde{\mathsf{x}}(t)$ from (40a), using an estimate of the channel $h_c(t)$. In contrast, the sensing Rx aims to detect the Q targets and extract corresponding delay parameters $\{\tau_{s,q}\}$ by the observation in (40b), with prior knowledge of $\widetilde{\mathsf{x}}(t)$.

2) Signal Processing for Communication: Let us first discuss the signal processing procedure at the communication Rx's side. Upon receiving $\mathsf{y}_c(t)$, the communication Rx performs a symbol-wise matched-filtering (MF) by using the pulse shaping filter, leading to the following output signal [65]:

$$\widetilde{\mathsf{y}}_c(\tau) = \int \mathsf{y}_c(t) p^*(t - \tau) dt. \quad (41)$$

Sampling at $\tau = \ell T$, where $\ell \in \mathbb{Z}$, yields

$$\widetilde{\mathsf{y}}_c(\ell T) = \sum_{i=1}^{I} \beta_i \sum_{n=0}^{N-1} \mathsf{x}_n \widetilde{p}_{\ell - n, \tau_{c,i}} + \widetilde{\mathsf{z}}_{c,\ell}, \quad (42)$$

where $\widetilde{p}_{k,\tau} := \widetilde{p}(kT - \tau)$, and $\widetilde{\mathsf{z}}_{c,l} = \int \mathsf{z}_c(t) p^*(t - \ell T) dt$ represents the output noise, which remains Gaussian distributed. By defining $\widetilde{\mathbf{y}}_c$ as the discrete MF output vector, where its $(\ell+1)$-th entry corresponds to $\widetilde{\mathsf{y}}_c(\ell T)$, we obtain:

$$\widetilde{\mathbf{y}}_c = \sum_{i=1}^{I} \beta_i \widetilde{\boldsymbol{P}}_i \mathbf{x} + \widetilde{\mathbf{z}}_c := \boldsymbol{H}_c \boldsymbol{U} \mathbf{s} + \widetilde{\mathbf{z}}_c, \quad (43)$$

where $\widetilde{\mathbf{z}}_c = \left[\widetilde{\mathsf{z}}_{c,0}, \widetilde{\mathsf{z}}_{c,1}, \ldots, \widetilde{\mathsf{z}}_{c,N-1}\right]^T$, and

$$\widetilde{\boldsymbol{P}}_i = \begin{bmatrix} \widetilde{p}_{0,\tau_{c,i}} & \widetilde{p}_{-1,\tau_{c,i}} & \cdots & \widetilde{p}_{-N+1,\tau_{c,i}} \\ \widetilde{p}_{1,\tau_{c,i}} & \widetilde{p}_{0,\tau_{c,i}} & \cdots & \widetilde{p}_{-N+2,\tau_{c,i}} \\ \vdots & \vdots & \ddots & \vdots \\ \widetilde{p}_{N-1,\tau_{c,i}} & \widetilde{p}_{N-2,\tau_{c,i}} & \cdots & \widetilde{p}_{0,\tau_{c,i}} \end{bmatrix} \quad (44)$$

is a Toeplitz matrix, making the equivalent channel matrix $\boldsymbol{H}_c$ also Toeplitz. If a CP is added to the time-domain sequence $\mathbf{x}$, then $\boldsymbol{H}_c$ becomes approximately circulant after the CP is removed from the received signal. It can be observed that ISI exists among the entries of $\mathbf{s}$ since $\boldsymbol{H}_c \boldsymbol{U}$ is not a diagonal matrix. To recover the information symbols, the ISI needs to be eliminated through channel equalization. This is typically achieved by first estimating $\boldsymbol{H}_c$ using known pilot symbols, followed by implementing an equalizer based on the estimate.

To reduce signal processing complexity, one may employ OFDM modulation by setting $\boldsymbol{U} = \boldsymbol{F}_N^H$, which yields:

$$\begin{aligned}\widetilde{\mathbf{y}}_c^{\text{OFDM}} &= \boldsymbol{H}_c \boldsymbol{F}_N^H \mathbf{s} + \widetilde{\mathbf{z}}_c \\ &= \sqrt{N}\boldsymbol{F}_N^H \text{Diag}\left(\boldsymbol{F}_N \boldsymbol{h}_c\right) \boldsymbol{F}_N \boldsymbol{F}_N^H \mathbf{s} + \widetilde{\mathbf{z}}_c \\ &= \sqrt{N}\boldsymbol{F}_N^H \text{Diag}\left(\boldsymbol{F}_N \boldsymbol{h}_c\right) \mathbf{s} + \widetilde{\mathbf{z}}_c, \end{aligned} \tag{45}$$

where we utilize the property that a circulant matrix can be diagonalized by the DFT matrix [83], with $\boldsymbol{h}_c$ denoting the first column of $\boldsymbol{H}_c$. Accordingly, the ISI can be removed by simply performing a DFT on (45), resulting in:

$$\boldsymbol{F}_N \widetilde{\mathbf{y}}_c^{\text{OFDM}} = \sqrt{N}\text{Diag}\left(\boldsymbol{F}_N \boldsymbol{h}_c\right) \mathbf{s} + \boldsymbol{F}_N \widetilde{\mathbf{z}}_c, \tag{46}$$

which can be readily processed as N parallel additive white Gaussian noise (AWGN) channels.

While OFDM minimizes the complexity of symbol detection by diagonalizing the multi-path channels, other modulation schemes such as SC, CDMA, AFDM, and OTFS can also be employed to satisfy specific application requirements, such as ensuring reliable communication in high-mobility channels.

3) Signal Processing for Sensing: We now turn our focus to processing the received sensing signal (40b) to extract the target delay parameters, where the first step is also to perform MF over the observed echo signal $\mathsf{y}_s(t)$. In sharp contrast to its communication counterpart, the matched filter used for sensing is the transmitted baseband signal $\widetilde{\mathsf{x}}(t)$ rather than the pulse shaping filter $p(t)$, leading to the following output [84]:

$$\begin{aligned}&\widetilde{\mathsf{y}}_s(\tau) \\ &= \int \mathsf{y}_s(t)\widetilde{\mathsf{x}}^*\left(t-\tau\right)dt \\ &= \sum_{q=1}^{Q}\gamma_q \int \widetilde{\mathsf{x}}(t-\tau_{s,q})\widetilde{\mathsf{x}}^*\left(t-\tau\right)dt + \int \mathsf{z}_s(t)\widetilde{\mathsf{x}}^*\left(t-\tau\right)dt \\ &= \sum_{q=1}^{Q}\gamma_q \mathsf{R}(\tau-\tau_{s,q}) + \widetilde{\mathsf{z}}_s(\tau), \quad 0 \le \tau \le NT. \end{aligned} \tag{47}$$

where $\mathsf{R}(\tau) = \int \widetilde{\mathsf{x}}(t)\widetilde{\mathsf{x}}^*(t-\tau)dt$ is the ACF of the ISAC signal $\widetilde{\mathsf{x}}(t)$, and $\widetilde{\mathsf{z}}_s(\tau)$ is the output Gaussian noise. It is worthwhile to point out that other methods, such as compressive sensing, may also be adopted to reduce sampling rates and improve resolution [85]. In order to highlight the impact of random data over sensing performance, here we employ the most basic MF approach for ranging, while designating the investigation of more advanced algorithms as our future work.

Notably, $\widetilde{\mathsf{y}}_s(\tau)$ can be interpreted as a linear combination of Q time-shifted versions of $\mathsf{R}(\tau)$, with added noise, often referred to as the *range profile* in radar literature [86]. To detect the targets, one typically identifies Q peaks in the squared MF output $|\widetilde{\mathsf{y}}_s(\tau)|^2$, where an example is portrayed in Fig. 7 for ranging with OFDM signal using 16-PSK constellation and root-raised cosine (RRC) pulse shaping under an SNR = 0 dB, including $Q = 3$ targets with varying amplitudes located at 10m, 20m, and 25m, respectively. The target detection may be achieved using thresholding algorithms such as the constant false-alarm rate (CFAR) detector [86]. In order to improve the sensing performance, it is desirable for $|\widetilde{\mathsf{y}}_s(\tau)|^2$ to exhibit high peaks at $\tau = \tau_q$ while maintaining low sidelobes elsewhere, which benefits both target detection and estimation.

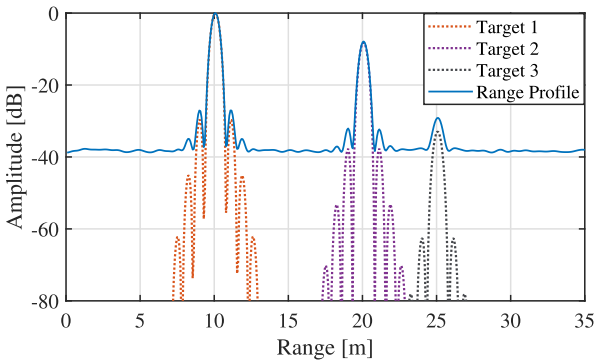

Fig. 7. An example of the range profile for OFDM signal with PSK constellation, including 3 targets located at 10m, 20m, and 25m.

To further enhance the sensing performance, the coherent integration technique can be employed to effectively reduce both sidelobe and noise levels. In this scheme, the ISAC Tx transmits M i.i.d. information symbol sequences, denoted as $\mathbf{s}^{(0)}, \mathbf{s}^{(1)}, \ldots, \mathbf{s}^{(M-1)}$, by emitting M ISAC signals $\widetilde{\mathsf{x}}^{(0)}(t), \widetilde{\mathsf{x}}^{(1)}(t), \ldots, \widetilde{\mathsf{x}}^{(M-1)}(t)$. Assume that the target parameters $\{\gamma_q\}_{q=1}^Q$ and $\{\tau_{s,q}\}_{q=1}^Q$ remain constant over the M transmission slots, such that the sensing Rx can generate M range profiles $\widetilde{\mathsf{y}}_s^{(0)}(\tau), \widetilde{\mathsf{y}}_s^{(1)}(\tau), \ldots, \widetilde{\mathsf{y}}_s^{(M-1)}(\tau)$ through matched-filtering the M received echoes. By coherently integrating these MF outputs, we obtain:

$$\begin{aligned}\frac{1}{M}\sum_{m=0}^{M-1}\widetilde{\mathsf{y}}_s^{(m)}(\tau) &= \frac{1}{M}\sum_{q=1}^{Q}\gamma_q \sum_{m=0}^{M-1}\mathsf{R}^{(m)}(\tau-\tau_{s,q}) \\ &\quad + \frac{1}{M}\sum_{m=0}^{M-1}\widetilde{\mathsf{z}}_s^{(m)}(\tau), \quad 0 \le \tau \le NT. \end{aligned} \tag{48}$$

where $\mathsf{R}^{(m)}(\tau)$ is the ACF of $\widetilde{\mathsf{x}}^{(m)}(t)$, and $\widetilde{\mathsf{z}}_s^{(m)}(\tau)$ represents the output noise from the m-th matched filter.

Observe that the noise term in (48) has been averaged, resulting in a reduction of its variance. Furthermore, the overall target sensing performance now critically depends on the geometry of the coherently integrated ACF, defined as:

$$\overline{\mathsf{R}}(\tau) := \frac{1}{M}\sum_{m=0}^{M-1}\mathsf{R}^{(m)}(\tau), \quad 0 \le \tau \le NT. \tag{49}$$

As will be shown later, the sidelobe levels of $\overline{\mathsf{R}}(\tau)$ are also suppressed thanks to the independence among the M realizations. Due to the randomness of communication symbols carried by the ISAC signal $\widetilde{\mathsf{x}}^{(m)}(t)$, $\overline{\mathsf{R}}(\tau)$ becomes a random function. Therefore, it is more appropriate to analyze its statistical properties rather than focusing on a single realization. In particular, we aim to characterize the expected value of the squared magnitude of $\overline{\mathsf{R}}(\tau)$, given that $\overline{\mathsf{R}}(\tau)$

is a complex-valued function. This expectation is defined as:

$$\mathbb{E}\left(|\overline{\mathsf{R}}(\tau)|^2\right) = \mathbb{E}\left(\left|\frac{1}{M}\sum_{m=0}^{M-1}\int \widetilde{\mathsf{x}}^{(m)}(t)\widetilde{\mathsf{x}}^{(m)*}(t-\tau)dt\right|^2\right). \quad (50)$$

In the following subsections, we review recent research efforts in deriving closed-form expressions for (50) for a generic communication signal, and provide useful insights for designing ISAC signals based on the mathematical structure of (50).

C. Characterization of the ISAC ACF

1) Discretization of the ACF: For ease of analysis, let us commence by discretizing the ISAC signal $\widetilde{\mathsf{x}}(t)$ over a temporal grid of $T_s = \frac{T}{L}$, yielding

$$\widetilde{\mathsf{x}}(kT_s) = \sum_{n=0}^{N-1}\mathsf{x}_n p(kT_s - nT) = \sum_{n=0}^{N-1}\mathsf{x}_n \delta(kT_s - nT) \circledast p(kT_s), \quad (51)$$

where $k = 0, 1, \ldots, LN-1$, and $\circledast$ denotes the cyclic convolution due to the addition of a CP. Note here that $L > 1$ is required to capture the impact of pulse shaping on sensing performance. If $L = 1$, the discretization simplifies to $\mathbf{x} = \boldsymbol{U}\mathbf{s}$ due to the zero-ISI property of the Nyquist pulse. This, however, neglects the contributions of the pulse shaping filter on the mainlobe and sidelobes of the ACF.

Define $p_k := p(kT_s)$, and $\widetilde{\mathsf{x}}_k := \widetilde{\mathsf{x}}(kT_s)$, so that the discrete versions of the pulse and baseband signal can be represented as vectors $\boldsymbol{p} = [p_0, p_1, \ldots, p_{LN-1}]^T$ and $\widetilde{\mathbf{x}} = \left[\widetilde{\mathsf{x}}_0, \widetilde{\mathsf{x}}_1, \ldots, \widetilde{\mathsf{x}}_{LN-1}\right]^T$, with the energy of the pulse being normalized to $\|\boldsymbol{p}\|^2 = 1$. In a practical communication Tx, pulse shaping can be implemented digitally through an up-sampling and interpolation procedure applied to $\mathbf{x}$, recasting (51) into a vector formulation as

$$\widetilde{\mathbf{x}} = \boldsymbol{P}\mathbf{x}_{\text{up}}, \quad (52)$$

where

$$\mathbf{x}_{\text{up}} = \left[\mathsf{x}_0, \mathbf{0}_{L-1}^T, \mathsf{x}_1, \mathbf{0}_{L-1}^T, \ldots, \mathsf{x}_{N-1}, \mathbf{0}_{L-1}^T\right]^T, \quad (53)$$

and $\boldsymbol{P} \in \mathbb{C}^{LN\times LN}$ is a circulant matrix defined as

$$\boldsymbol{P} = \begin{bmatrix} p_0 & p_{LN-1} & \cdots & p_1 \\ p_1 & p_0 & \cdots & p_2 \\ \vdots & \vdots & \ddots & \vdots \\ p_{LN-1} & p_{LN-2} & \cdots & p_0 \end{bmatrix}, \quad (54)$$

which interpolates $\mathbf{x}$ to a higher resolution before transmission. Accordingly, the discrete version of the ACF $\mathsf{R}(\tau)$ is given by

$$\mathsf{R}_k = \widetilde{\mathbf{x}}^H \boldsymbol{J}_k \widetilde{\mathbf{x}} = \mathbf{x}_{\text{up}}^H \boldsymbol{P}^H \boldsymbol{J}_k \boldsymbol{P}\mathbf{x}_{\text{up}}, \quad k = 0, 1, \ldots, LN-1, \quad (55)$$

where $\boldsymbol{J}_k \in \mathbb{C}^{LN\times LN}$ is the k-th periodic time-shift matrix, defined by [87]

$$\boldsymbol{J}_k = \begin{bmatrix} \mathbf{0} & \boldsymbol{I}_{LN-k} \\ \boldsymbol{I}_k & \mathbf{0} \end{bmatrix}, \quad (56)$$

and

$$\boldsymbol{J}_{-k} = \boldsymbol{J}_{LN-k} = \boldsymbol{J}_k^T = \begin{bmatrix} \mathbf{0} & \boldsymbol{I}_k \\ \boldsymbol{I}_{LN-k} & \mathbf{0} \end{bmatrix}. \quad (57)$$

Note that the periodicity in $\boldsymbol{J}_k$ is again due to the addition of the CP. It follows that the discrete version of the coherently integrated ACF (49) becomes

$$\overline{\mathsf{R}}_k = \frac{1}{M}\sum_{m=0}^{M-1}\widetilde{\mathbf{x}}^{(m)H}\boldsymbol{J}_k\widetilde{\mathbf{x}}^{(m)}. \quad (58)$$

2) The "Iceberg in the Sea" Structure of the ACF: To shed light on the communication-centric ISAC transmission under random signaling, the work of [66] derived a closed form of the expectation of $\left|\overline{\mathsf{R}}_k\right|^2$, given by

$$\begin{aligned}\mathbb{E}(|\overline{\mathsf{R}}_k|^2) &= \underbrace{LN\left|\widetilde{\boldsymbol{f}}_{k+1}^H\widetilde{\boldsymbol{g}}_k\right|^2}_{\text{Iceberg}} \\ &\quad + \underbrace{\frac{1}{M}\left\{\|\widetilde{\boldsymbol{g}}_k\|^2 + (\kappa-2)LN\left\|\widetilde{\boldsymbol{V}}^T\left(\widetilde{\boldsymbol{g}}_k \odot \widetilde{\boldsymbol{f}}_{k+1}^*\right)\right\|^2\right\}}_{\text{Sea Level}}, \\ &= \left|\mathbb{E}(\overline{\mathsf{R}}_k)\right|^2 + \text{var}(\overline{\mathsf{R}}_k), \quad k = 0, 1, \ldots, LN-1, \end{aligned} \quad (59)$$

where $\widetilde{\boldsymbol{f}}_{k+1} \in \mathbb{C}^{N\times 1}$ contains the first N entries of the $(k+1)$-th column of the size-LN DFT matrix $\boldsymbol{F}_{LN}$, and $\widetilde{\boldsymbol{V}} \in \mathbb{R}^{N\times N}$ is defined as:

$$\widetilde{\boldsymbol{V}} = (\boldsymbol{F}_N\boldsymbol{U}) \odot (\boldsymbol{F}_N^*\boldsymbol{U}^*), \quad (60)$$

where $\boldsymbol{U}$ is the modulation basis. Since $\widetilde{\boldsymbol{V}}$ is generated by the entry-wise square of an unitary matrix $\boldsymbol{F}_N\boldsymbol{U}$, it becomes a bi-stochastic matrix with nonnegative real entries [88], each of whose rows and columns sums to 1. Moreover, κ denotes the *kurtosis* of the adopted constellation $\mathcal{S}$, defined as [67]:

$$\kappa := \frac{\mathbb{E}\left\{|\mathsf{s} - \mathbb{E}(\mathsf{s})|^4\right\}}{\mathbb{E}\left\{|\mathsf{s} - \mathbb{E}(\mathsf{s})|^2\right\}^2} = \mathbb{E}(|\mathsf{s}|^4), \quad \forall\, \mathsf{s} \in \mathcal{S}, \quad (61)$$

which is the normalized fourth moment of the constellation. Finally, due to the folded spectrum criterion and that the roll-off factor $\alpha \leq 1$, the vector $\widetilde{\boldsymbol{g}}_k \in \mathbb{C}^{N\times 1}$ is determined by the squared spectrum of pulse $\boldsymbol{p}$ in the following manner:

$$\widetilde{\boldsymbol{g}}_k = \boldsymbol{g} + (\mathbf{1}_N - \boldsymbol{g})e^{-\frac{j2\pi k}{L}}, \quad (62)$$

where $\boldsymbol{g} = [g_0, g_1, \ldots, g_{N-1}]^T$ contains the first N samples of the squared spectrum $N(\boldsymbol{F}_{LN}\boldsymbol{p}) \odot (\boldsymbol{F}_{LN}^*\boldsymbol{p}^*) \in \mathbb{C}^{LN\times 1}$. Notably, the impact of all three signaling blocks—modulation basis, constellation, and pulse shaping—on the shape of the ACF is well-captured in (59).

The equation (59) reveals an intriguing "iceberg-in-the-sea" structure. The "iceberg" portion represents the squared mean of $\overline{\mathsf{R}}_k$, which can be rigorously shown to correspond to the squared ACF of the pulse itself [66], expressed as:

$$LN\left|\widetilde{\boldsymbol{f}}_{k+1}^H\widetilde{\boldsymbol{g}}_k\right|^2 = \left|\boldsymbol{p}^H\boldsymbol{J}_k\boldsymbol{p}\right|^2, \quad k = 0, 1, \ldots, LN-1. \quad (63)$$

This "iceberg" component defines the overall shape of (59). Meanwhile, the "sea level" aspect is driven by the variance

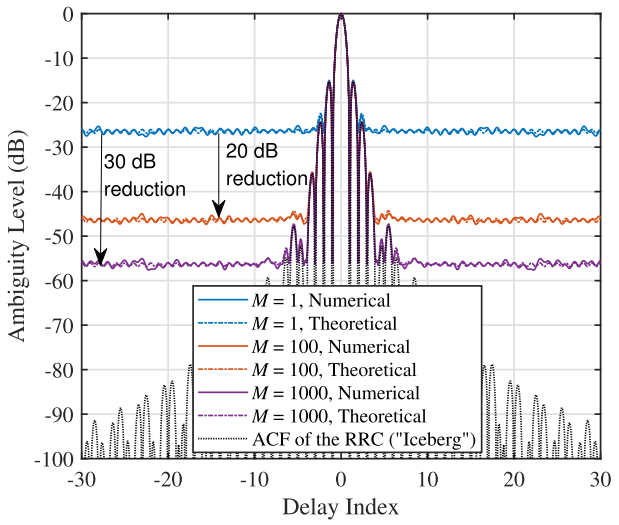

Fig. 8. The average squared ACF and corresponding coherent integration versions of an OFDM signal, with 16-QAM constellation and $\alpha = 0.35$ RRC pulse shaping, $N = 128$, $L = 10$, $M = 1, 100,$ and 1000.

of $\overline{\mathsf{R}}_k$, which arises largely from the randomness of communication symbols. By coherently integrating M MF outputs derived from M i.i.d. ISAC signals, the "sea level" can be significantly reduced by a factor of M.

3) Example on the Average Squared ACF of OFDM Signaling: Fig. 8 demonstrates an example using OFDM signaling with a 16-QAM constellation and $\alpha = 0.35$ RRC pulse shaping, under an $L = 10$ over-sampling ratio. Here, we compare the average squared ACFs for various values of M. Notably, the ACF of the random OFDM signal aligns closely with the pulse's ACF near the mainlobe region, representing the "tip" of the "iceberg". Beyond this region, the sidelobes are dominated by the "sea level" component. By increasing the number of coherent integrations from $M = 1$ to 100 and then to 1000, we observe an obvious reduction in the "sea level" by 20 dB and 30 dB, respectively, thereby revealing more of the "iceberg" component in the average squared ACF.

Building on these observations, we next review recent advances in optimizing modulation basis, constellation design, and pulse shaping for random ISAC signals. These enhancements aim to boost sensing performance while preserving optimal communication quality, or to establish a scalable tradeoff between S&C.

IV. Waveform Design for Random ISAC Signals

In this section, we present design guidelines for three core building blocks in communication-centric ISAC systems, focusing on reshaping the statistical properties of the ACF of random ISAC signals. Specifically, our objective is to minimize the average peak-to-sidelobe level ratio (PSLR) of $\overline{\mathsf{R}}_k$ in (58), thereby enhancing multi-target sensing performance in the range domain within the MF framework. While Doppler effects were not explicitly modeled in this paper, the reviewed ACF shaping framework may be extended to design ambiguity functions with desired delay-Doppler characteristics, thereby enhancing robustness to mobility. Such Doppler-resilient design is particularly relevant in scenarios with high relative velocities. Nevertheless, due to the lack of closed-form expressions for the expected ambiguity surface of random communication signals, such design remains analytically intractable at present. A full characterization of this behavior is thus reserved for future investigation.

TABLE I
Kurtosis Values of Typical Sub-Gaussian Constellations

Constellation	PSK	16-QAM	64-QAM	128-QAM
Kurtosis	1	1.32	1.381	1.3427
Constellation	256-QAM	512-QAM	1024-QAM	2048-QAM
Kurtosis	1.3953	1.3506	1.3988	1.3525

According to [66], [67], the average mainlobe level of the ACF under arbitrary modulation basis, constellation mapping, and pulse shaping filter, can be expressed in closed form as:

$$\mathbb{E}(|\overline{\mathsf{R}}_0|^2) = N^2 + \frac{(\kappa - 1)N}{M}, \tag{64}$$

indicating that the mainlobe level is determined solely by the kurtosis of the constellation. Furthermore, when the coherent integration number M is sufficiently large, the impact of the kurtosis becomes negligible, resulting in an approximately constant average mainlobe level of N^2. Recognizing this, it suffices to optimize only the average sidelobe level, which can be formulated as the following generic optimization problem:

$$\min_{\boldsymbol{U}\in\mathbb{U}(N),\, P_{\mathsf{s}}(s),\, 0\le \boldsymbol{g}\le 1} \mathbb{E}(|\overline{\mathsf{R}}_k|^2), \quad \forall\ k \in \mathcal{K}_{\text{SL}}, \tag{65}$$

where $\boldsymbol{U}$ and $\boldsymbol{g}$ denote the modulation basis and squared spectrum of the pulse, respectively, as defined above, $P_{\mathsf{s}}(s)$ represents the input constellation distribution, and $\mathcal{K}_{\text{SL}}$ refers to the sidelobe region.[4] While seeking for the globally optimal solution of (65) remains a highly challenging task, in what follows, we elaborate on the general design methodology of each component.

A. Modulation Basis Design

From (59), it is evident that the modulation basis influences the sidelobe level solely through the squared norm term $\|\widetilde{\boldsymbol{V}}^T(\widetilde{\boldsymbol{g}}_k \odot \widetilde{\boldsymbol{f}}_{k+1}^*)\|^2$ in the "sea level" part. For a given pair of pulse shaping filter and constellation, (65) simplifies to:

$$\begin{aligned} \min_{\boldsymbol{U}\in\mathbb{U}(N)} \quad & (\kappa - 2)\left\|\widetilde{\boldsymbol{V}}^T\left(\widetilde{\boldsymbol{g}}_k \odot \widetilde{\boldsymbol{f}}_{k+1}^*\right)\right\|^2 \\ \text{s.t.} \quad & \widetilde{\boldsymbol{V}} = (\boldsymbol{F}_N\boldsymbol{U}) \odot (\boldsymbol{F}_N^*\boldsymbol{U}^*). \end{aligned} \tag{66}$$

Clearly, the optimal modulation basis depends on the sign of $(\kappa - 2)$, also referred to as the *excess kurtosis* [89]. Notably, if the constellation follows a standard complex Gaussian distribution, i.e., $\mathsf{s} \sim \mathcal{CN}(0, 1)$, the kurtosis equals 2. In such a case, the average sidelobe level at each lag k remains constant irrespective of the chosen modulation basis, as the standard Gaussian distribution is invariant under unitary

[4] Although clutter effects were not explicitly modeled in this paper, the proposed ACF design framework can be directly applied to target detection in range-spread clutter environments. In such cases, clutter suppression can be interpreted as a weighted sidelobe shaping problem, where the weights reflect the clutter scattering strength at different range bins. For further modeling and design details, we refer readers to [69].

transformations. Inspired by this, we classify constellations into two categories: sub-Gaussian ($\kappa < 2$) and super-Gaussian ($\kappa > 2$). It is worth noting that commonly used constellations, e.g., QAM and PSK, are sub-Gaussian, with their kurtosis values summarized in Table I. Meanwhile, super-Gaussian constellations may be advantageous in scenarios demanding high energy efficiency or where non-coherent communication methods are employed [90], [91], [92]. Typical examples include index modulation and APSK constellations with exponentially growing radii [67].

1) Ranging-Optimal Modulation for Sub-Gaussian Constellations: Let us first discuss the modulation design for sub-Gaussian constellations. In this case, problem (66) reduces to:

$$\begin{aligned} \max_{\boldsymbol{U}\in\mathbb{U}(N)} \quad & \left\| \widetilde{\boldsymbol{V}}^T \left(\widetilde{\boldsymbol{g}}_k \odot \widetilde{\boldsymbol{f}}_{k+1}^* \right) \right\|^2 \\ \text{s.t.} \quad & \widetilde{\boldsymbol{V}} = (\boldsymbol{F}_N \boldsymbol{U}) \odot (\boldsymbol{F}_N^* \boldsymbol{U}^*). \end{aligned} \tag{67}$$

Although problem (67) is generally non-convex, it was proven in [66] that the globally optimal solution exhibits the following structure:

$$\boldsymbol{U}_{\text{sub}}^\star = \boldsymbol{F}_N^H \boldsymbol{\Pi} \text{Diag}(\theta), \tag{68}$$

where $\boldsymbol{\Pi}$ is any size-N permutation matrix, and $\theta \in \mathbb{C}^{N\times 1}$ can be any vector with unit-modulus entries. This corresponds to OFDM modulation, subject to permutation and phase shifts in the subcarriers. Recalling that $\widetilde{\boldsymbol{V}}$ is a bi-stochastic matrix, the optimality of (68) is established by showing that the objective function of (67) is maximized when $\widetilde{\boldsymbol{V}}$ is any real permutation matrix $\boldsymbol{\Pi}$. This result is derived by using the Schur-convexity of the ℓ_2 norm and the concept of majorization [93], [94], [95]. More technical details can be found in [66].

Overall, the result in (68) suggests the following: *For sub-Gaussian constellations (e.g., QAM and PSK), OFDM achieves the lowest average ranging sidelobe at every lag.*

2) Ranging-Optimal Modulation for Super-Gaussian Constellations: Let us now move to the super-Gaussian constellations with $\kappa > 2$. In such a case, problem (66) becomes

$$\begin{aligned} \min_{\boldsymbol{U}\in\mathbb{U}(N)} \quad & \left\| \widetilde{\boldsymbol{V}}^T \left(\widetilde{\boldsymbol{g}}_k \odot \widetilde{\boldsymbol{f}}_{k+1}^* \right) \right\|^2 \\ \text{s.t.} \quad & \widetilde{\boldsymbol{V}} = (\boldsymbol{F}_N \boldsymbol{U}) \odot (\boldsymbol{F}_N^* \boldsymbol{U}^*). \end{aligned} \tag{69}$$

By exploiting again the Schur-convexity of the ℓ_2 norm, and applying a similar argument, one may readily show that the objective is minimized if the bi-stochastic matrix is uniform, namely, $\widetilde{\boldsymbol{V}} = \frac{1}{N}\boldsymbol{1}\boldsymbol{1}^T$. Accordingly, the optimal modulation basis takes the form of

$$\boldsymbol{U}_{\text{super}}^\star = \boldsymbol{\Pi} \text{Diag}(\theta), \tag{70}$$

corresponding to an SC modulation subject to arbitrary permutation and phase shifts of time-domain symbols.

Overall, the result in (70) suggests that: *For super-Gaussian constellations, SC achieves the lowest average ranging sidelobe at every lag.*

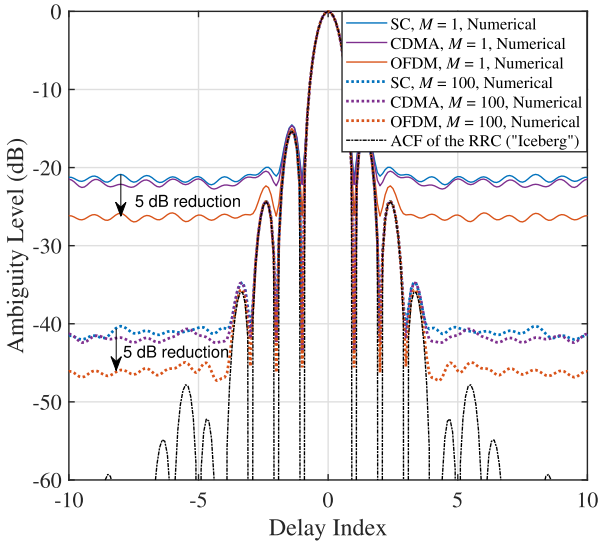

Fig. 9. The average squared ACF and corresponding coherent integration versions of SC, CDMA, and OFDM signals, with 16-QAM constellation and $\alpha = 0.35$ RRC pulse shaping, $N = 128$, $L = 10$, $M = 1$ and 100.

3) Example of the Average Sidelobe Level of Different Modulation Bases: We present an example in Fig. 9 to validate the optimality of OFDM for sub-Gaussian constellations, using the standard 16-QAM alphabet with a kurtosis of 1.32. The average squared ACF is compared across three modulation bases: OFDM, SC, and CDMA2000 (where $\boldsymbol{U}$ is a Hadamard matrix), transmitting $N = 128$ i.i.d. symbols with an $L = 10$ over-sampling ratio, and employing an RRC pulse shaping filter with $\alpha = 0.35$. As predicted by the theoretical results, Fig. 9 demonstrates that OFDM produces the lowest sidelobe at every lag, achieving a 5 dB improvement over both SC and CDMA. Additionally, after coherently integrating i.i.d. MF outputs for $M = 100$ times, a 20 dB reduction in the sidelobe level is observed in the "sea level" region for all signaling schemes.

4) Discussion on the Optimality of OFDM/SC: The aforementioned results provide valuable design insights for the modulation formats of communication-centric ISAC systems. While these findings are mathematically rigorous, a further understanding of the optimality of OFDM/SC requires addressing the following critical question: What is the *physical interpretation* underlying these mathematical results?

To depict the physical insight, we examine the problem through the lens of the Fourier duality and central limit theorem (CLT). Consider a signal with infinite bandwidth, as illustrated in Fig. 10a, which exhibits a perfectly flat amplitude spectrum. According to the Fourier duality, this implies that its ACF is a Dirac-Delta function in the delay domain. This represents the ideal sensing signal for ranging, as it leads to a perfect MF output with no ambiguity. However, as shown in Fig. 10b, the presence of random fluctuations in the communication data payload causes variability in the squared spectrum of the ISAC signal, which, in turn, causes random sidelobes in the ACF of Fig. 10b. Intuitively, this suggests that minimizing the average ranging sidelobe level of an ISAC signal is equivalent to minimizing the fluctuations in

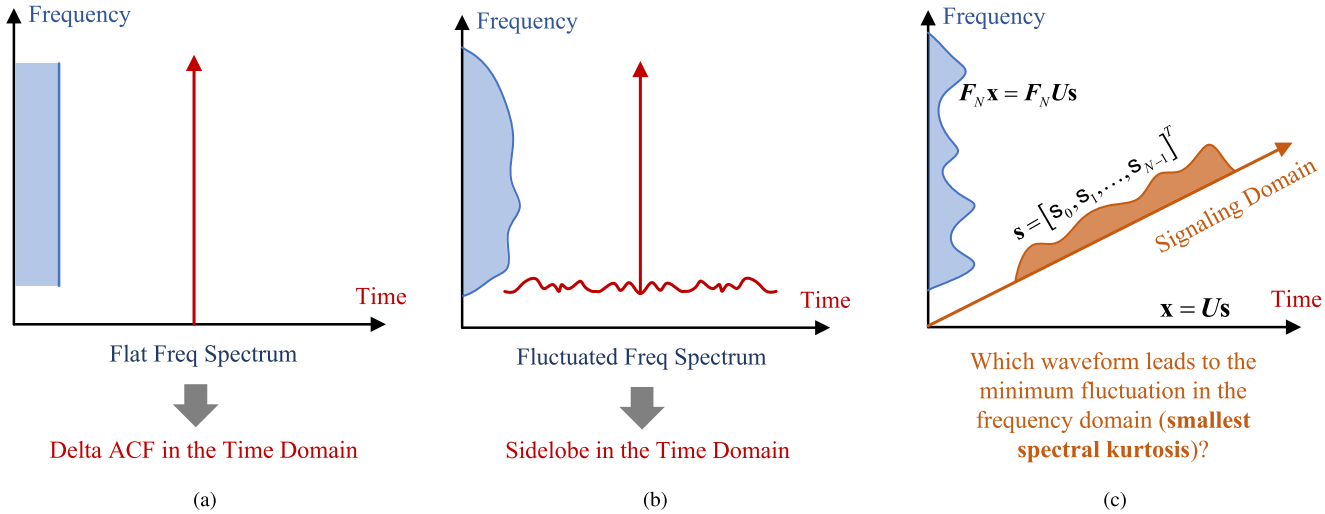

Fig. 10. Physical interpretation of the optimality of OFDM and SC modulation. (a) The ideal case: A completely flat spectrum leads to a Dirac-Delta ACF; (b) Random data payload causes variability in the squared spectrum, introducing random sidelobes in the ACF; (c) The optimal modulation basis minimizes the fluctuation in the squared spectrum, which is measured by the kurtosis of $\boldsymbol{F}_N\boldsymbol{U}\mathbf{s}$, where $\boldsymbol{F}_N\boldsymbol{U}$ is a unitary transform.

its frequency-domain representation, which can be quantified by the variance of the squared spectrum, and is proportional to the frequency-domain kurtosis of the signal. Thus, reducing ranging sidelobes can be achieved by minimizing the signal's frequency-domain kurtosis.

To explore this further, we re-examine the ISAC modulation basis design as presented in Fig. 10c. As outlined in the generic model in (35), a modulation basis can be interpreted as a unitary rotation $\boldsymbol{U}$ applied to the i.i.d. symbol sequence $\mathbf{s}$. Accordingly, the corresponding frequency-domain digital samples are given by $\boldsymbol{F}_N\boldsymbol{U}\mathbf{s}$, where the product $\boldsymbol{F}_N\boldsymbol{U}$ remains unitary. Based on the CLT, a linear transform applied to a random vector with i.i.d. entries results in a distribution that asymptotically approaches a Gaussian form. As a consequence, any unitary transform $\boldsymbol{F}_N\boldsymbol{U}$ increases the kurtosis of i.i.d. sub-Gaussian symbols, while it decreases the kurtosis of i.i.d. super-Gaussian symbols. Therefore, to minimize the kurtosis of the vector $\boldsymbol{F}_N\boldsymbol{U}\mathbf{s}$, where $\mathbf{s}$ is sub-Gaussian (e.g., QAM and PSK), the optimal strategy is to retain its kurtosis, which is achieved by setting $\boldsymbol{F}_N\boldsymbol{U} = \boldsymbol{I}_N$, corresponding to the OFDM modulation. In contrast, if $\mathbf{s}$ is super-Gaussian, since any unitary transform would reduce its kurtosis, the optimal strategy is to maximize the rotation over $\mathbf{s}$. In this case, the appropriate transformation is $\boldsymbol{F}_N\boldsymbol{U} = \boldsymbol{F}_N$, leading to the SC modulation.

B. Constellation Design

Now, we shift our focus from modulation format to constellation design. As noted in (59), $\mathbb{E}(|\overline{\mathsf{R}}_k|^2)$ depends on the constellation solely through its kurtosis. For a given pair of modulation format and pulse shaping filter, the minimum kurtosis (and consequently sidelobes) can be achieved with any PSK constellation, given the fact that $\kappa \geq 1$. However, PSK may result in lower communication rates compared to its QAM counterpart of the same order, highlighting again the DRT in ISAC systems [61].

To balance the achievable rate for communication and ranging sidelobe level for sensing, a practical approach is *constellation shaping* [96], [97], which is originally tailored for improving the spectral and energy efficiencies of digital communication systems. Constellation shaping techniques can be broadly classified into two categories: probabilistic constellation shaping (PCS) and geometric constellation shaping (GCS). PCS modifies the constellation's probability density function (PDF) through a distribution matcher, which maps the bit stream to the desired probability distribution of the constellation. In contrast, GCS directly optimizes the amplitudes and phases of constellation symbols themselves. Both techniques are capable of reshaping the statistical characteristics of the adopted constellation.

1) Probabilistic Constellation Shaping for ISAC: For the ISAC constellation design problem, we focus on the PCS approach, which can be formulated as an optimization problem aimed at maximizing the communication MI under a ranging sidelobe level threshold, with the latter being governed by the constellation's kurtosis. Moreover, the designed constellation This can be expressed as [68]:

$$\begin{aligned} \max_{P_{\mathbf{s}}(s)} \quad & I(\widetilde{\mathbf{y}}_c; \mathbf{s}) \\ \text{s.t.} \quad & \mathbb{E}(|\mathbf{s}|^4) \leq c_0, \ \ \mathbb{E}(|\mathbf{s}|^2) = 1, \\ & \mathbb{E}(\mathbf{s}) = 0, \ \ \mathbb{E}(\mathbf{s}^2) = 0, \ \ \mathbf{s} \in \mathcal{S}, \end{aligned} \tag{71}$$

where $P_{\mathbf{s}}(s)$ stands for the distribution of constellation, $\mathbf{y}_c$ represents the MF output signal at the communication receiver, and $c_0 \geq 1$ is a pre-determined constant that controls the kurtosis of the constellation, ensuring that the average ranging sidelobes remain within acceptable bounds. The alphabet $\mathcal{S}$ denotes the set of discrete constellation points, which must satisfy normalized power and rotational symmetry constraints, as outlined in (36).

Problem (71) is inherently a functional optimization problem, as the optimization variable $P_{\mathbf{s}}(s)$ is a function defined over $\mathcal{S}$. Indeed, problem (71) may be viewed as a specific example of the C-D tradeoff problem in (11), where the kurtosis constraint acts as a sensing cost function. However,

the MI in the objective function does not have a closed-form expression due to the discrete alphabet $\mathcal{S}$. To address this challenge, an optimization-based PCS method was introduced in [68] for M_{s}-ary QAM constellations under OFDM modulation. In this case, the multi-path communication channel is diagonalized into N parallel orthogonal AWGN channels, allowing us to focus on the MI of each single scalar AWGN channel, which is denoted as $I(\mathsf{y}_c;\mathsf{s})$.

Let $\boldsymbol{p}_{\mathsf{s}} = [p_{\mathsf{s},1}, p_{\mathsf{s},2}, \ldots, p_{\mathsf{s},M_{\mathsf{s}}}]^T$ be the probability distribution vector of the considered M_{s}-ary QAM constellation, with s_m being the m-th QAM symbol. The MI, by its definition, can be represented as [98]:

$$\begin{aligned} &I(\mathsf{y}_c;\mathsf{s}) \\ &= \sum_{m=1}^{M_{\mathsf{s}}} p_{\mathsf{s},m} \int p(y_c|s_m) \log \frac{p(y_c|s_m)}{p(y_c)} dy_c \\ &= \max_{q(s_m|y_c)} \underbrace{\sum_{m=1}^{M_{\mathsf{s}}} p_{\mathsf{s},m} \int p(y_c|s_m) \log \frac{q(s_m|y_c)}{p(y_c)} dy_c}_{F(\boldsymbol{p}_{\mathsf{s}}, \boldsymbol{q}_{\mathsf{s}|\mathsf{y}_c})}, \end{aligned} \tag{72}$$

where $q(s_m|y_c)$ is the probability transition function from the received signal set $\mathcal{Y}c$ to the constellation alphabet $\mathcal{S}$, and $\boldsymbol{q}_{\mathsf{s}|\mathsf{y}c}$ is its discretized form. The optimization problem (71) can thus be reformulated as [68]:

$$\begin{aligned} &\max_{\boldsymbol{p}_{\mathsf{s}}} \max_{\boldsymbol{q}_{\mathsf{s}|\mathsf{y}_c}} \quad F(\boldsymbol{p}_{\mathsf{s}}, \boldsymbol{q}_{\mathsf{s}|\mathsf{y}_c}) \\ &\text{s.t.} \quad \sum_{m=1}^{M_{\mathsf{s}}} p_{\mathsf{s},m}|s_m|^4 \le c_0, \quad \sum_{m=1}^{M_{\mathsf{s}}} p_{\mathsf{s},m}|s_m|^2 = 1, \\ &\qquad \sum_{m=1}^{M_{\mathsf{s}}} p_{\mathsf{s},m} s_m = 0, \quad \sum_{m=1}^{M_{\mathsf{s}}} p_{\mathsf{s},m} s_m^2 = 0, \\ &\qquad \sum_{m=1}^{M_{\mathsf{s}}} p_{\mathsf{s},m} = 1, \quad p_{\mathsf{s},m} \ge 0, \ \forall\ m, \end{aligned} \tag{73}$$

where the last two constraints are enforced since $\boldsymbol{p}_{\mathsf{s}}$ is a point on the probability simplex. Here, $F(\boldsymbol{p}_{\mathsf{s}}, \boldsymbol{q}_{\mathsf{s}|\mathsf{y}c})$ is jointly concave in $\boldsymbol{p}_{\mathsf{s}}$ and $\boldsymbol{q}_{\mathsf{s}|\mathsf{y}c}$, and all constraints are linear in the probability vector $\boldsymbol{p}_{\mathsf{s}}$, making it a convex program. By exploiting this fact, a modified Blahut-Arimoto (MBA) algorithm was proposed in [68]. Through constructing the Lagrange multiplier of (73), and iteratively solving for $\boldsymbol{p}_{\mathsf{s}}$ and $\boldsymbol{q}_{\mathsf{s}|\mathsf{y}_c}$ in an alternative manner, the MBA method ensures efficient convergence to the global optimum.

2) Example of Probabilistic Constellation Shaping for ISAC Systems: We present an illustrative example to demonstrate the effectiveness of the PCS approach for ISAC. Fig. 11a shows the optimal PCS results for 16-QAM and 64-QAM constellations at different kurtosis thresholds c_0, with the probability of each point represented by color depth. As the kurtosis threshold decreases, symbols with nearly or exactly unit modulus are transmitted with higher probabilities, while those on larger or smaller circles are less likely to be used. This aligns with the DRT theory, which suggests that sensing favors constellations with constant modulus. Inevitably, this reduces the communication MI and therefore introduces a graceful tradeoff with the communication rates. Note that

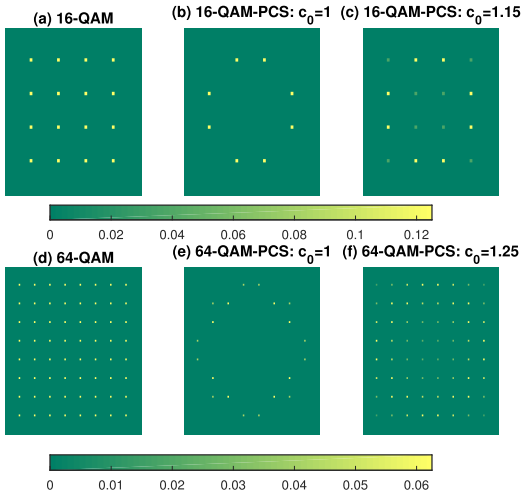

(a) PCS results for 16-QAM and 64-QAM.

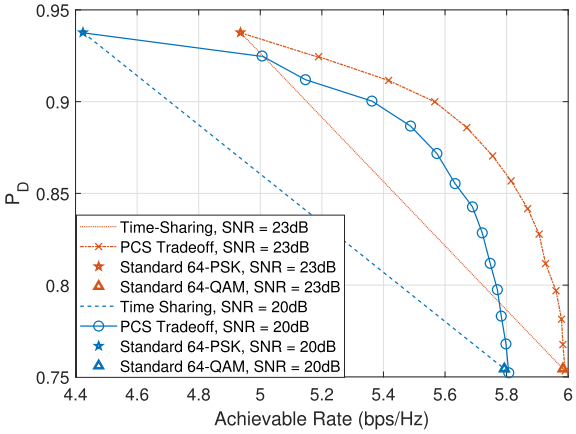

(b) An explicit performance tradeoff between S&C.

Fig. 11. An illustrative example of the PCS technique for random ISAC signals. (a) PCS results for 16-QAM and 64-QAM under varying values of the kurtosis threshold c_0; (b) An explicit performance tradeoff between target detection probability for sensing and achievable rate for communication implemented by adjusting c_0 from 1 to 1.381 (kurtosis of the uniform 64-QAM) in the PCS approach, under OFDM modulation and 64-QAM constellation, with different values of transmit SNR.

reducing the ACF sidelobe level would enhance the weak target detection performance in the range domain, as the sidelobe of strong clutter can significantly interfere with or even mask the mainlobe of weak targets. By realizing this, Fig. 11b illustrates the explicit S&C performance of 64-QAM under OFDM modulation across different transmit SNR values, highlighting the achievable communication rate and the detection probability for sensing a weak target in the presence of strong clutter. By adjusting c_0, the PCS method provides a scalable tradeoff between S&C performance metrics, significantly outperforming the naive time-sharing approach between standard uniformly distributed 64-QAM and 64-PSK constellations.

C. Pulse Shaping Design

We conclude this section by discussing pulse shaping design methodologies for ISAC, given a specific pair of constellation

and modulation bases. A closer examination of (59) reveals that $\mathbb{E}(|\overline{\mathsf{R}}_k|^2)$ is a convex quadratic function of $\widetilde{\boldsymbol{g}}_k$, and thus convex in the squared spectrum of the pulse, namely, the vector $\boldsymbol{g}$. Therefore, one may minimize the sidelobe level within the region $\mathcal{K}_{\rm SL}$ over the feasible set of $\boldsymbol{g}$.

1) Generic Pulse Shaping Design: To proceed, we first discuss the constraints on $\boldsymbol{g}$. It is evident that the folded spectrum criterion (38) is implicitly satisfied in (62), ensuring the Nyquist property of the pulse and consequently eliminating the ISI. This guarantees that the communication performance remains unaffected. Moreover, the pulse has a roll-off factor $\alpha \in [0,1]$, implying that $(1-\alpha)N$ entries of $\boldsymbol{g}$ are either 0 or 1. Upon letting $N_\alpha = \alpha N$, and assuming that $N - N_\alpha$ is even, these constraints can be expressed as

$$g_n = \begin{cases} 0, & \text{if } 0 \le n \le \frac{N-N_\alpha}{2} - 1, \\ 1, & \text{if } \frac{N+N_\alpha}{2} \le n \le N-1. \end{cases} \tag{74}$$

Additionally, to ensure the roll-off part is monotonically increasing, we impose the following constraints:

$$g_{n+1} - g_n \ge 0, \quad \frac{N-N_\alpha}{2} \le n \le \frac{N+N_\alpha}{2} - 2. \tag{75}$$

Finally, the power of the pulse has been normalized, yielding the constraint:

$$\sum_{n=0}^{N-1} g_n = \frac{N}{2}. \tag{76}$$

Therefore, the generic pulse shaping problem may be formulated as [69]:

$$\begin{aligned} \min_{0\le \boldsymbol{g}\le 1} \quad & \mathbb{E}(|\overline{\mathsf{R}}_k|^2), \quad \forall\ k \in \mathcal{K}_{\rm SL} \\ \text{s.t.} \quad & (74)-(76), \end{aligned} \tag{77}$$

which is a linearly constrained convex Pareto problem.

2) Iceberg Shaping: To further simplify the problem, note that the geometry of $\mathbb{E}(|\overline{\mathsf{R}}_k|^2)$ is primarily determined by the "iceberg" part when the coherent integration number M is sufficiently large. Based on this observation, one can focus on shaping the "iceberg", i.e., the squared ACF of the pulse shaping filter itself, rather than minimizing the sidelobes of both the "iceberg" and "sea level" components. In this case, the objective is to minimize either the sum of the sidelobes over the region $\mathcal{K}_{\rm SL}$ of the iceberg, or the maximum sidelobe within this region, yielding the following problem [66]:

$$\begin{aligned} \min_{0\le \boldsymbol{g}\le 1} \quad & \sum_{k\in\mathcal{K}_{\rm SL}} \left|\widetilde{\boldsymbol{f}}_{k+1}^H \widetilde{\boldsymbol{g}}_k\right|^2 \ \text{ or } \ \max_k \left|\widetilde{\boldsymbol{f}}_{k+1}^H \widetilde{\boldsymbol{g}}_k\right|^2 \\ \text{s.t.} \quad & (74)-(76), \end{aligned} \tag{78}$$

which is a linearly constrained convex quadratic program that can be efficiently solved via off-the-shelf numerical tools.

3) Example of ISAC Pulse Shaping Design: We present a design example of the ISAC pulse shaping filter with coherent integration in Fig. 12, where we apply the iceberg shaping technique in (78) to minimize the summation of the ranging sidelobes within the region $[23.74\text{m}, 31.24\text{m}]$. The ISAC signal adopts OFDM modulation, carrying $N = 128$ i.i.d. 16-QAM symbols, under an over-sampling ratio of $L = 10$. To demonstrate the performance improvement gained from sidelobe reduction in the "iceberg", we consider a two-target detection scenario, where one target is located at 20m and the other at 30m. The target at 20m has an amplitude $43 \sim 46$ dB higher than the one at 30m. The benchmark is the RRC pulse shaping, with a roll-off factor of $\alpha = 0.35$ set for both the RRC and iceberg shaping techniques.

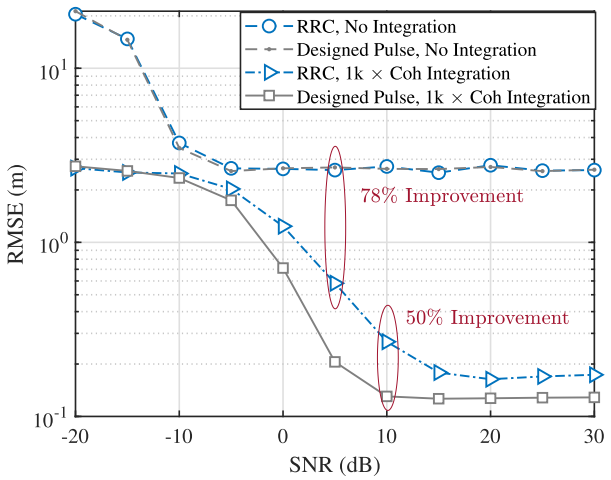

(a) Range estimation performance with/without coherent integration.

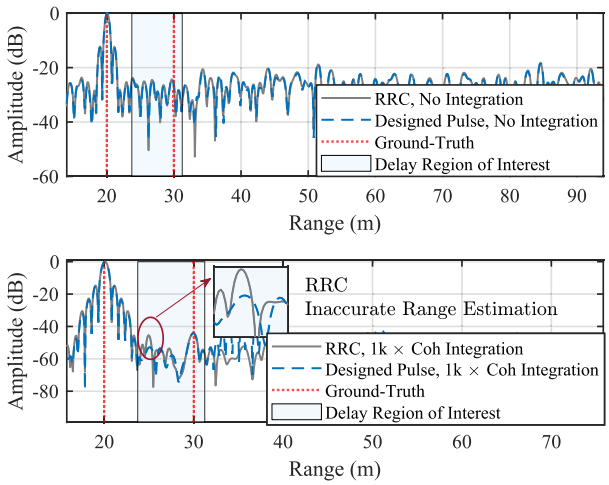

(b) Range profiles with/without coherent integration.

Fig. 12. The range estimation performance and profiles of two targets under OFDM with 16-QAM constellation, where $N = 128$, $\alpha = 0.35$, $L = 10$, $M = 1000$, and range region of interest is $[23.74\text{m}, 31.24\text{m}]$.

Fig. 12a shows the ranging root mean squared error (RMSE) curves with and without coherent integration. It can be observed that, before the coherent integration operation, both the RRC and iceberg shaping techniques suffer from poor ranging performance. However, after coherently integrating over $M = 1000$ i.i.d. MF output signals, the ranging RMSE is reduced by more than 78%. Additionally, the iceberg shaping method achieves an extra 50% improvement in ranging accuracy compared to its RRC counterpart. This improvement is also clearly visible in the corresponding range profiles shown in Fig. 12b. Without coherent integration, the weak target is obscured by the sidelobes generated by the "sea level" for both pulses, resulting in large range estimation errors. With 1000 times of coherent integration, the "sea level"

sidelobes are effectively reduced by 30 dB, after which the ranging performance is primarily determined by the sidelobes generated from pulses themselves. In this case, the peak corresponding to the weak target can be accurately detected for the ISAC signaling scheme with the designed pulse, thanks to the minimization of the sidelobes within the range region of interest. However, for the RRC pulse, the weak target may be inaccurately located due to the high sidelobe at 24.5m.

V. MIMO Precoding With Random ISAC Signals

Building on the insights from single-antenna systems in the previous sections, we now extend our analysis to multi-antenna ISAC systems, where spatial-domain precoding introduces an additional DoF for balancing S&C performance. While earlier sections focused on time-frequency waveform design aspects such as modulation, constellation, and pulse shaping under random signaling constraints, this section examines how spatial processing can be exploited to further enhance the sensing capabilities of communication-centric ISAC systems. The motivation for this section stems directly from the DRT discussed in Sec. II. In MIMO systems, the random nature of the transmitted symbols still limits the direct control over the signal pattern in time and frequency, but precoding enables structured control over the spatial distribution of signal energy, even when the symbols remain random. This opens up new research opportunities for shaping the spatial beampattern for sensing purposes without compromising the information-carrying role of the communication signals.

Specifically, we present the general MIMO ISAC signal model in Sec. V-A, and then introduce a pair of precoding strategies, namely, data-independent and data-dependent, which respectively offer long-term and symbol-level control of the sensing performance. Dedicated algorithms for designing such precoders under both sensing-only and ISAC scenarios are detailed in Sec. V-B and V-C, respectively. By doing so, we provide a unified signal-level framework for extending random ISAC waveform design into the spatial domain.

A. Signal Model and Ergodic LMMSE

Consider a P2P monostatic MIMO ISAC system, with a BS equipped with N_t transmit antennas and N_s receive antennas at its sensing Rx, serving a communication user (CU) with N_c receive antennas while simultaneously detecting one or multiple targets. Assume that target sensing is conducted over a coherent processing interval consisting of N time-domain snapshots. Following the vector Gaussian model in (13), the MIMO signal models for S&C are expressed as

$$\mathbf{Y}_c = \mathbf{H}_c\mathbf{X} + \mathbf{Z}_c, \tag{79a}$$

$$\mathbf{Y}_s = \mathbf{H}_s\mathbf{X} + \mathbf{Z}_s. \tag{79b}$$

In the above, $\mathbf{Y}_c \in \mathbb{C}^{N_c\times N}$ represents the received signal matrix at the CU receiver and $\mathbf{Y}_s \in \mathbb{C}^{N_s\times N}$ denotes the echoes at the BS sensing receiver, the matrix $\mathbf{H}_c \in \mathbb{C}^{N_c\times N_t}$ is the P2P MIMO channel and $\mathbf{H}_s \in \mathbb{C}^{N_s\times N_t}$ is the spatial-domain TIR matrix to be estimated, the matrices $\mathbf{Z}_c \in \mathbb{C}^{N_c\times N}$ and $\mathbf{Z}_s \in \mathbb{C}^{N_s\times N}$ represent additive noise, with each entry following $\mathcal{CN}(0,\sigma_c^2)$ and $\mathcal{CN}(0,\sigma_s^2)$, and $\mathbf{X} \in \mathbb{C}^{N_t\times N}$ denotes the ISAC signal matrix. Additionally, we assume that the TIR matrix $\mathbf{H}_s$ follows a wide-sense stationary random process, such that its statistical correlation matrix $\boldsymbol{R}_H = \mathbb{E}\{\mathbf{H}_s^H\mathbf{H}_s\}$ keeps unchanged.

We now make some remarks on the signal model in (79). First, the model in (79) aligns with the one in (40) in a MIMO-OFDM setting, which can be interpreted as narrowband S&C signals over a sub-channel. Accordingly, $\mathbf{H}_s$ and $\mathbf{H}_c$ are S&C channel matrices defined for each sub-carrier. Second, this model may be seen as a special case of the generic vector Gaussian model in (13), with the parameter to be estimated being the sensing channel matrix itself, namely, $\boldsymbol{\eta} = \mathrm{vec}\,(\mathbf{H}_s)$. As a special case, the TIR matrix may also be modeled as (14). For sensing purposes, this section focuses solely on estimating the TIR matrix $\mathbf{H}_s$ for each sub-carrier, which will then be collected across all sub-carriers for further processing to extract delay and angle parameters of the targets.

Let us provide more elaboration on the ISAC signal matrix $\mathbf{X}$ in (79), which is expressed as

$$\mathbf{X} = \boldsymbol{W}\mathbf{S}, \tag{80}$$

where $\boldsymbol{W} \in \mathbb{C}^{N_t\times N_t}$ is the precoding matrix to be optimized and $\mathbf{S} \in \mathbb{C}^{N_t\times N}$ represents the data payload matrix. Let $f(\boldsymbol{W};\mathbf{S})$ denote a generic sensing cost function, as described in (6). The objective of this section is to design the precoding matrix $\boldsymbol{W}$ to optimize the sensing cost function $f(\boldsymbol{W};\mathbf{S})$, given the (statistical) information of **S.**

Analyzing and exploring the structure of the cost function $f(\boldsymbol{W};\mathbf{S})$ often provides valuable insights into the solution of the corresponding optimization problem [99], [100]. To facilitate the discussion, we use the linear minimum mean squared error (LMMSE) precoder as a specific example of the sensing cost function $f(\boldsymbol{W};\mathbf{S})$ in this section. Given the ISAC signal $\mathbf{X}$ and the correlation matrix $\boldsymbol{R}_H$ for the sensing channel, the celebrated LMMSE estimator of $\mathbf{H}_s$ is given by:

$$\hat{\mathbf{H}}_s = \mathbf{Y}_s\left(\mathbf{X}^H\boldsymbol{R}_H\mathbf{X} + \sigma_s^2N_s\boldsymbol{I}_N\right)^{-1}\mathbf{X}^H\boldsymbol{R}_H, \tag{81}$$

which results in an MSE expressed as [101]

$$f(\boldsymbol{W};\mathbf{S}) = \mathrm{Tr}\left\{\left(\boldsymbol{R}_H^{-1} + \frac{1}{\sigma_s^2N_s}\boldsymbol{W}\mathbf{S}\mathbf{S}^H\boldsymbol{W}^H\right)^{-1}\right\}. \tag{82}$$

Based on this, the precoding design problem can be straightforwardly formulated as:

$$\begin{aligned}\min_{\boldsymbol{W}}\ & f(\boldsymbol{W};\mathbf{S})\\ \text{s.t.}\ & \|\boldsymbol{W}\|_F^2 \le P_T,\end{aligned} \tag{83}$$

where P_T is the transmit power budget.

In traditional MIMO radar systems, $\mathbf{S}$ in (80) is a deterministic orthogonal training signal satisfying $\frac{1}{N}\mathbf{S}\mathbf{S}^H = \boldsymbol{I}_{N_t}$ [102]. In this case, problem (83) simplifies into:

$$\min_{\boldsymbol{W}}\ \mathrm{Tr}\left\{\left(\boldsymbol{R}_H^{-1} + \frac{1}{\sigma_s^2N_s}\boldsymbol{W}\boldsymbol{W}^H\right)^{-1}\right\} \tag{84a}$$

$$\text{s.t.}\ \ \|\boldsymbol{W}\|_F^2 \le P_T. \tag{84b}$$

The above problem has a closed-form water-filling solution given by [101]:

$$\boldsymbol{W}_{\mathsf{WF}} = \sqrt{\frac{\sigma_s^2 N_s}{N}} \boldsymbol{Q} \left\{ \max\left(\mu_0 \boldsymbol{I}_{N_t} - \boldsymbol{\Lambda}^{-1}, \boldsymbol{0}\right) \right\}^{\frac{1}{2}}, \tag{85}$$

where $\boldsymbol{Q}\boldsymbol{\Lambda}\boldsymbol{Q}^H$ is the eigenvalue decomposition of $\boldsymbol{R}$ and μ_0 is a constant (i.e., the "water level") such that $\|\boldsymbol{W}_{\mathsf{WF}}\|_F^2 = P_T$.

In sharp contrast to traditional radar systems, ISAC systems must employ random signals for target sensing. Since Gaussian signals achieve the capacity of P2P Gaussian channels as shown in (79a), we consider Gaussian signaling for ISAC systems as an example. Let $\mathbf{S} = [\mathbf{s}_1, \mathbf{s}_2, \ldots, \mathbf{s}_N] \in \mathbb{C}^{N_t \times N}$ denote the transmitted random ISAC signal, where each column is i.i.d. and follows the complex Gaussian distribution with zero mean and covariance $\boldsymbol{I}_{N_t}$, i.e., $\mathbf{s}_\ell \sim \mathcal{CN}(\boldsymbol{0}, \boldsymbol{I}_{N_t})$. In this case, the objective function in problem (83) becomes a random variable (as it depends on the random variable $\mathbf{S}$). Therefore, it is natural to consider an ergodic LMMSE (ELMMSE) that accounts for the signal randomness, defined as [70]:

$$\begin{aligned} &f_{\mathsf{ELMMSE}}(\boldsymbol{W}) \\ &:= \mathbb{E}\left\{ \mathrm{Tr}\left[\left(\boldsymbol{R}_H^{-1} + \frac{1}{\sigma_s^2 N_s} \boldsymbol{W}\mathbf{S}\mathbf{S}^H\boldsymbol{W}^H \right)^{-1} \right] \right\}, \end{aligned} \tag{86}$$

where the expectation is performed over $\mathbf{S}$. The ELMMSE may be interpreted as a sensing analogy to the ergodic communication rate [103], which can be regarded as a time average of the MSE achieved by random ISAC signals.

B. Sensing-Only Precoding Design

In this part, we explore the sensing-only precoding designs under random signaling, which serves as a performance benchmark for the ISAC precoding that will be detailed later on. The corresponding optimization problem may be formulated as:

$$\begin{aligned} \min_{\boldsymbol{W}} \ & f_{\mathsf{ELMMSE}}(\boldsymbol{W}) \\ \text{s.t.} \ & \|\boldsymbol{W}\|_F^2 \le P_T. \end{aligned} \tag{87}$$

We present two precoding schemes tailored for problem (87): Data-dependent precoding (DDP) scheme and data-independent precoding (DIP) scheme.

1) Data-Dependent Precoding: Let $\{\boldsymbol{S}_m\}_{m=1}^M$ denote a set of M i.i.d. Gaussian data realizations. In the monostatic mode, each $\boldsymbol{S}_m$ is known to both the ISAC Tx and the sensing Rx. As a result, the precoding matrix $\boldsymbol{W}$ in problem (87) can be designed as a function of $\mathbf{S}$ across all data realizations, which we denote as $\boldsymbol{W}_m := \boldsymbol{W}(\boldsymbol{S}_m)$. The corresponding optimization problem then takes the following form:

$$\begin{aligned} \min_{\boldsymbol{W}_m} \ & \mathrm{Tr}\left\{ \left(\boldsymbol{R}_H^{-1} + \frac{1}{\sigma_s^2 N_s} \boldsymbol{W}_m \boldsymbol{S}_m \boldsymbol{S}_m^H \boldsymbol{W}_m^H \right)^{-1} \right\} \\ \text{s.t.} \ & \|\boldsymbol{W}_m\|_F^2 \le P_T. \end{aligned} \tag{88}$$

For each given data realization $\boldsymbol{S}_m$, problem (88) admits a closed-form solution, as shown in [70, Theorem 1]. Specifically, let $\boldsymbol{S}_m = \boldsymbol{U}_m \boldsymbol{\Sigma}_m \boldsymbol{V}_m^H$ denote the singular value decomposition (SVD) of $\boldsymbol{S}_m$ and define the matrix $\boldsymbol{\Pi}_0$ as

$$\boldsymbol{\Pi}_0 = \begin{bmatrix} 0 & 0 & \cdots & 1 \\ 0 & \cdots & 1 & 0 \\ \vdots & \vdots & \vdots & \vdots \\ 1 & 0 & \cdots & 0 \end{bmatrix}. \tag{89}$$

Then, the modified water-filling solution of problem (88) is expressed as [104]:

$$\boldsymbol{W}_m^{\mathsf{opt}} = \boldsymbol{Q} \left[\left(\mu_m \boldsymbol{\Theta}_m^{\frac{1}{2}} - \boldsymbol{B}_m \right)^+ \right]^{\frac{1}{2}} \boldsymbol{\Pi}_0 \boldsymbol{U}_m^H, \ m = 1, 2, \ldots, M, \tag{90}$$

where $\boldsymbol{\Theta}_m = \frac{1}{\sigma_s^2 N_s} \boldsymbol{\Pi}_0 \boldsymbol{\Sigma}_m \boldsymbol{\Sigma}_m^T \boldsymbol{\Pi}_0$, $\boldsymbol{B}_m = (\boldsymbol{\Lambda}\boldsymbol{\Theta}_m)^{-1}$, and μ_m is a parameter chosen to satisfy the transmit power constraint $\|\boldsymbol{W}_m^{\mathsf{opt}}\|_F^2 = P_T$.

It is evident from the expression of $\boldsymbol{W}_m^{\mathsf{opt}}$ in (90) that the precoding matrix $\boldsymbol{W}_m$ depends on the data realization $\boldsymbol{S}_m$. Therefore, this scheme is referred to as the data-dependent precoding (DDP). Since the DDP scheme is designed adaptively based on the instantaneous data realization, it generally achieves the minimum ELMMSE; however, this comes at the cost of high computational complexity.

2) Data-Independent Precoding: Different from the DDP scheme, the DIP scheme aims to find a precoder $\boldsymbol{W}$ that is independent of the signal realization. Given the fact that the closed-form expression of f_{ELMMSE} is non-obtainable, the data-independent precoder can be obtained by applying the stochastic gradient descent (SGD) algorithm to solve problem (87) offline, providing a favorable tradeoff between estimation performance and computational complexity. Below we present the SGD algorithm in detail.

Let $f(\boldsymbol{W}; \mathbf{S})$ be defined as in (82). The gradient of $f(\boldsymbol{W}; \mathbf{S})$ with respect to the variable $\boldsymbol{W}$ at a given point $\boldsymbol{W}_0$ is

$$\begin{aligned} &\nabla f(\boldsymbol{W}_0; \mathbf{S}) \\ &= \frac{-\left(\boldsymbol{R}_H^{-1} + \frac{1}{\sigma_s^2 N_s} \boldsymbol{W}_0 \mathbf{S}\mathbf{S}^H \boldsymbol{W}_0^H \right)^{-2} \boldsymbol{W}_0 \mathbf{S}\mathbf{S}^H}{\sigma_s^2 N_s}. \end{aligned} \tag{91}$$

Accordingly, the gradient of f_{ELMMSE} with respect to $\boldsymbol{W}$ at point $\boldsymbol{W}_0$ is given by

$$\nabla f_{\mathsf{ELMMSE}}(\boldsymbol{W}_0) = \mathbb{E}\left\{ \nabla f(\boldsymbol{W}_0; \mathbf{S}) \right\}, \tag{92}$$

which again has no closed-form expression. Towards that end, the key idea behind SGD is to approximate the true gradient in (92) by the gradient evaluated at a mini-batch of samples, given by

$$\hat{\nabla} f_{\mathsf{ELMMSE}}(\boldsymbol{W}_0) = \frac{1}{|\mathcal{D}|} \sum_{\boldsymbol{S} \in \mathcal{D}} \nabla f(\boldsymbol{W}_0; \boldsymbol{S}), \tag{93}$$

where $\mathcal{D}$ denotes number of Gaussian samples generated at point $\boldsymbol{W}_0$. At the r-th iteration of the projected SGD algorithm, the precoding matrix $\boldsymbol{W}$ is updated as

$$\boldsymbol{W}^{(r+1)} = \mathsf{Proj}\left\{ \boldsymbol{W}^{(r)} - \varepsilon^{(r)} \hat{\nabla} f_{\mathsf{ELMMSE}}(\boldsymbol{W}^{(r)}) \right\}, \tag{94}$$

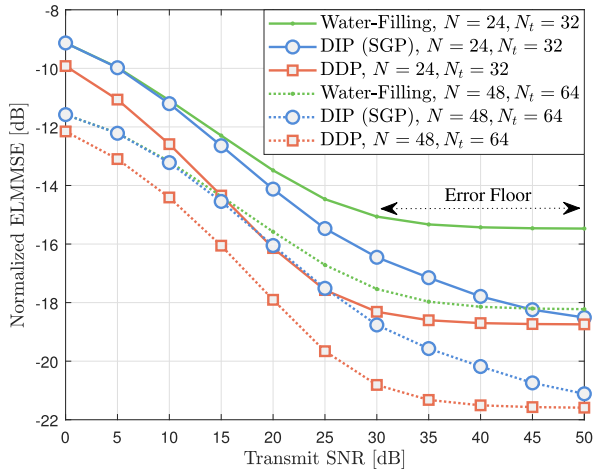

Fig. 13. Achievable sensing performance of the DDP and DIP schemes compared with the conventional water-filling approach under Gaussian signaling, where the $N_t = 32, N = 24$ and $N_t = 64, N = 48$ cases are illustrated.

where $\varepsilon^{(r)}$ is the stepsize (or "learning rate") and $\mathsf{Proj}\{\cdot\}$ is the projection operator onto the feasible set of problem (87), i.e., the ball constraint.

Some remarks regarding the above SGD algorithm are in order. First, to ensure the convergence of the (projected) SGD algorithm, the nonnegative stepsizes $\varepsilon^{(r)}$ in (94) must be chosen to satisfy the following conditions [105], [106]:

$$\sum_{r=1}^{\infty} \varepsilon^{(r)} = \infty \text{ and } \sum_{r=1}^{\infty} \left|\varepsilon^{(r)}\right|^2 < \infty. \tag{95}$$

Second, increasing the mini-batch size $|\mathcal{D}|$ can reduce the variance of the error in approximating the true gradient, thereby improving numerical performance in terms of computational efficiency and robustness. However, this comes at the cost of having to compute a larger number of local gradients. By the law of large numbers, as the mini-batch size tends to infinity, the gradient in (93) converges to the true gradient in (92), and the (projected) SGD algorithm effectively reduces to the (projected) GD algorithm. Finally, incorporating the moment information into the SGD algorithm can accelerate its convergence. In particular, a modified version of SGD with momentum was introduced in [70] to solve problem (87) in the presence of complex unknown variables.

3) Example of Sensing-Only Precoding Design: We provide an example in Fig. 13 to show the superiority of MIMO precoding designs dedicated to random signals under sensing-only scenarios, where we consider two parameter settings with $N_t = N_s = 32, N = 24$ and $N_t = N_s = 64, N = 48$, respectively. The attainable ELMMSE with varying SNR is shown for both DDP and DIP approaches, with the water-filling precoder (85) serving as the baseline scheme. The results for all the three methods are averaged over 1000 random realizations of i.i.d. Gaussian signal samples. As predicted by the theoretical analysis, the DDP scheme achieves the lowest ELMMSE in general, followed by its DIP counterpart. On the other hand, the water-filling precoder tailored for deterministic training signals suffers from a 3 dB performance loss as well as a severe error floor compared to the DDP and DIP designs, confirming the necessity of taking the data randomness into account.

C. ISAC Precoding Design

In this subsection, we extend the precoding design from the sensing-only scenario discussed in the previous subsection to the ISAC scenario. Throughout this subsection, we assume that the channel matrix $\boldsymbol{H}_c$ in (79a) is perfectly known. Then the achievable communication rate (in bps/Hz) of the P2P Gaussian channel in (79a) is [107]:

$$R(\boldsymbol{W}) = \log\det\left(\boldsymbol{I}_{N_c} + \sigma_c^{-2}\boldsymbol{H}_c\boldsymbol{W}\boldsymbol{W}^H\boldsymbol{H}_c^H\right). \tag{96}$$

The precoding design problem in the ISAC system is formulated as the minimization of ELMMSE, subject to communication performance and power budget constraints, as follows:

$$\begin{aligned} \min_{\boldsymbol{W}} \;& f_{\mathsf{ELMMSE}}(\boldsymbol{W}) \\ \text{s.t.} \;& R(\boldsymbol{W}) \geq R_0, \; \|\boldsymbol{W}\|_F^2 \leq P_T, \end{aligned} \tag{97}$$

where R_0 corresponds to the communication rate requirement. Again, we present two precoding schemes, namely, DDP and DIP, tailored for problem (97).

1) Data-Dependent Precoding: We follow the same approach and notation as in Sec. V-B. By introducing an auxiliary variable $\boldsymbol{\Omega}_m = \boldsymbol{W}_m\boldsymbol{W}_m^H$, we can rewrite the rate constraint in problem (97) as

$$\tilde{R}(\boldsymbol{\Omega}_m) := \log\det\left(\boldsymbol{I}_{N_c} + \sigma_c^{-2}\boldsymbol{H}_c\boldsymbol{\Omega}_m\boldsymbol{H}_c^H\right) \geq R_0. \tag{98}$$

The data-dependent precoder $\boldsymbol{W}$ can then be obtained by solving the following optimization problem with respect to $\boldsymbol{W}_n$ for a given data realization $\boldsymbol{S}_m$:

$$\begin{aligned} \min_{\boldsymbol{W}_m, \boldsymbol{\Omega}_m} \;& f(\boldsymbol{W}_m; \boldsymbol{S}_m) \\ \text{s.t.} \;& \tilde{R}(\boldsymbol{\Omega}_m) \geq R_0, \; \boldsymbol{\Omega}_m = \boldsymbol{W}_m\boldsymbol{W}_m^H, \; \|\boldsymbol{W}\|_F^2 \leq P_T. \end{aligned} \tag{99}$$

A penalty-based alternating optimization (AO) algorithm has been proposed in [70] for solving problem (99). The algorithm essentially applies the AO algorithm to solve the penalized version of problem (99) as follows:

$$\begin{aligned} \min_{\boldsymbol{W}_m, \boldsymbol{\Omega}_m} \;& f(\boldsymbol{W}_m; \boldsymbol{S}_m) + \frac{\rho}{2}\|\boldsymbol{\Omega}_m - \boldsymbol{W}_m\boldsymbol{W}_m^H\|_F^2 \\ \text{s.t.} \;& \tilde{R}(\boldsymbol{\Omega}_n) \geq R_0, \; \|\boldsymbol{W}\|_F^2 \leq P_T, \end{aligned} \tag{100}$$

where $\rho > 0$ is the penalty parameter. Specifically, problem (100) with respect to the variable $\boldsymbol{\Omega}_m$ is convex and can be solved efficiently; the corresponding subproblem with respect to the other variable $\boldsymbol{W}_m$ can be addressed using the projected gradient descent algorithm. For more details on the proposed penalty-based AO algorithm, please refer to [70, Sec. IV].

2) Data-Independent Precoding: By introducing the auxiliary variable $\boldsymbol{\Omega} = \boldsymbol{W}\boldsymbol{W}^H$ and adding a penalty term for this equality constraint to the objective function, we obtain the following penalized version of problem (97):

$$\begin{aligned} \min_{\boldsymbol{W}, \boldsymbol{\Omega}} \;& \mathbb{E}_{\mathbf{S}}\left\{f(\boldsymbol{W}; \mathbf{S})\right\} + \frac{\rho}{2}\|\boldsymbol{\Omega} - \boldsymbol{W}\boldsymbol{W}^H\|_F^2 \\ \text{s.t.} \;& \tilde{R}(\boldsymbol{\Omega}) \geq R_0, \; \|\boldsymbol{W}\|_F^2 \leq P_T. \end{aligned} \tag{101}$$

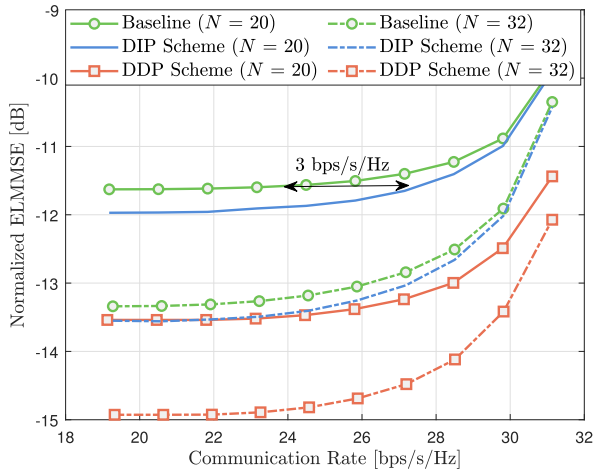

Fig. 14. The S&C performance tradeoff under different precoding designs, with the parameter setting $N_t = N_s = 32, N = 20$ and 32, and SNR $=$ 15 dB.

This problem can be solved in a similar manner to problem (100) using the AO algorithm. The only difference is that the projected SGD algorithm is employed to solve the subproblem with respect to the variable $\boldsymbol{W}$.

3) Example of ISAC Precoding Design: We illustrate the tradeoff between S&C performance of DDP and DIP schemes in Fig. 14, under $N_t = N_s = 32, N = 20$ and 32, and SNR $=$ 15 dB. The baseline technique here is the precoding design that minimizes the deterministic LMMSE (84a) subject to the communication rate and power constraints. It can be clearly observed that the DIP design acquires 3bps/Hz communication rate improvements over the baseline method for $N = 20$, while achieving the same ELMMSE for sensing. Moreover, DDP achieves more than 1.5 dB reduction in the ELMMSE compared to the DIP, while satisfying the required communication rate.

VI. Open Problems and Future Directions

In this section, we highlight the open problems in sensing with random communication signals, and identify promising directions for future research in this area.

A. Open Problems

1) 2D Ambiguity Function Characterization: While much of the current literature (including this tutorial) focuses on the ACF to assess the sensing performance of communication-centric ISAC signals, it is important to recognize that the ACF offers only a partial characterization of the sensing capability. In particular, the ACF corresponds to the zero-Doppler cut of the ambiguity function (AF) [84], and thus primarily captures performance in terms of multi-target ranging under static or low-Doppler conditions. This makes it well-suited for applications such as indoor positioning or vehicular sensing in slow-speed regimes. However, future 6G ISAC systems are expected to operate in dynamic environments with high-mobility users and targets, where both delay and Doppler resolution are critical. In such scenarios, the 2D AF, which jointly characterizes the resolution and multi-target interference properties in the delay-Doppler domain, becomes a more comprehensive and meaningful metric for analyzing the sensing performance of random ISAC signals. That said, extending the analysis from ACF to the full AF is highly non-trivial. The AF involves a two-dimensional correlation structure in the time-frequency domain. For random ISAC signals carrying modulated data symbols, the statistical behavior of the AF depends critically on the modulation scheme, pulse shaping, and data distribution of the signal. Deriving closed-form expressions or meaningful performance bounds under general signaling formats thus poses a significant theoretical and computational challenge. Despite this, the insights obtained from ACF-based analysis provide a solid first step toward understanding sensing with random signals.

2) Mismatched Filtering and Sparse Recovery Under Random ISAC Signaling: In this tutorial, as well as in most of the existing literature, sensing signal processing is performed using the MF framework. In this approach, the received echo signal is convolved with a replica of the transmitted ISAC signal to form a range profile, and target detection is based on localizing the resulting peaks. While MF is known to maximize the target's SNR at each peak, it may not be optimal for reducing sidelobe levels caused by the data payload. To address this, mismatched filtering (MMF) could be explored as a more general method to further enhance the sensing performance, which conceives the impulse response of the filter as a nonlinear function of the transmitted ISAC signal. One example of the MMF is the *Reciprocal Filtering* [108], which performs element-wise division of the echo signal in the frequency domain. While the Reciprocal Filter can effectively eliminate sidelobes generated by random data, resulting in a clean "iceberg" without any "sea level", it may suffer from the SNR reduction by amplifying the noise. Thus, it is essential to develop novel MMF techniques that balance sidelobe suppression and SNR loss under random ISAC signaling. Furthermore, sparse recovery techniques, such as matching pursuit algorithms and their variants, can be employed in this context to enhance sensing resolution by exploiting the inherent sparsity of radar targets [109]. However, a comprehensive investigation is required to address the challenges posed by the randomness of ISAC signals and its impact on the performance of these algorithms.

3) Adaptive Modulation: In Sec. IV-B it was shown that sensing favors signals with reduced power variability or even constant modulus signals, at the expense of communication rates. These signals however tend to have higher power efficiency and offer higher SNRs, as well as the opportunity to exploit wireless interference [110]. This avails the potential to recover some of the rate loss through adaptive modulation (AM) schemes [111], [112] and constructive interference (CI) exploitation [113]. On one hand, this offers the opportunity to shift the S&C tradeoffs from the ones showed above to more favorable communication performance, and in this way better secure the communication QoS in the communication-centric ISAC scenarios. On the other hand, such approaches would necessitate the development of new AM approaches, co-designed with the ISAC signaling overviewed in this paper, and ISAC-tailored CI approaches founded on the constellation shaping above.

4) Sensing With Channel-Coded Signals: Channel coding is a critical component of modern communication systems, which adds redundancy to information bits to reduce or correct decoding errors. Most current studies on communication-centric ISAC systems focus on uncoded signals, where constellation symbols are i.i.d. drawn from predefined codebooks. While the effects of modulation schemes, constellation designs, pulse shaping filters, and MIMO precoders on the sensing performance have been investigated in this tutorial, the impact of channel coding remains largely unexplored [114]. Therefore, it would be valuable to evaluate the sensing performance of random ISAC signals under various practical channel coding schemes, such as Turbo, LDPC, and Polar codes, and to optimize these codes for achieving a balanced S&C performance.

B. Future Directions

1) Networked Sensing and ISAC With Communication Signals: In addition to the point-to-point (P2P) ISAC setting considered in this work, networked sensing and ISAC represent a transformative direction toward enabling large-scale seamless S&C [115], [116], [117], [118], [119]. This necessitates a more comprehensive investigation of ISAC waveform design and processing in multi-user, multi-target, and multi-static environments, which are considerably more prevalent in practical systems. By leveraging collaboration among BSs and distributed mobile devices, networked ISAC is particularly promising for applications like UAV-enabled low-altitude economy and smart transportation systems [120], [121]. Unlike their conventional P2P monostatic and bistatic counterparts, networked sensing and ISAC encounter unique challenges, particularly in interference management. In particular, the simultaneous transmissions from distributed nodes can significantly degrade both S&C performance across the network, and the inherent randomness of communication signals further complicates the analysis and management of interference. To tackle this challenge, comprehensive research is needed on BSs' synchronization, adaptive BS clustering and scheduling, collaborative precoding, and network-level joint resource allocation. For instance, BSs can be dynamically grouped into clusters, where joint precoding within each cluster can leverage cross-link interference as beneficial signals, while interference coordination cross clusters is crucial to mitigate inter-cluster interference. Based on the availability of data information, multiple BSs can employ the DDP and DIP techniques to improve the sensing performance without compromising communication quality. In such cases, the joint optimization of data-dependent and data-independent precoders across multiple BSs becomes crucial, with distributed algorithm design playing a key role in achieving enhanced performance while minimizing signaling overheads.

2) Secure ISAC With Communication Signals: The move to pervasive sensing through the ISAC infrastructure opens the door to entirely new security vulnerabilities over the wireless network [122]: i) *Data-Security*: the inclusion of data into the probing ISAC signal makes it prone to eavesdropping from potentially malicious radar targets, and with high signal powers typically used for target illumination. Even if the data itself is encrypted, simply detecting the existence of a communication link can jeopardize communication privacy [123], [124]. ii) *Sensing-Privacy*: The sensing functionality introduced by the wireless network can be adversely exploited by malicious nodes to independently sense potentially sensitive information about the environment [125]. This is an entirely new vulnerability that one never had to worry about in a cellular network. As there is no data link—this is the ability of a malicious node to independently sense its environment—higher layer security approaches are inapplicable. The severity of threat necessitates a new generation of PHY security solutions tailored for ISAC. The constellation, pulse shaping, and precoding design overviewed in this paper needs to be tuned for PHY security and can play a key role in protecting against both data eavesdropping and adversary sensing. Their co-design with classical PHY security approaches such as artificial noise design, jamming, cooperative security remains virtually unexplored. Most importantly, while data security in ISAC is being explored theoretically [126], the realm of sensing privacy lacks an information theoretic framework with which to design metrics, signal processing solutions and transmission mechanisms.

3) Sensing and ISAC With Artificial Intelligence (AI): While this paper focuses on the information theory and signal processing aspects of sensing and ISAC, AI has recently emerged as a key enabler, particularly in processing sensing and ISAC signals for recognition tasks [127], [128]. Deep learning algorithms, for instance, are increasingly being utilized for applications such as posture and activity recognition. The integration of AI with sensing and ISAC introduces both new challenges and exciting opportunities. A key challenge arises when random communication signals are employed, as designing AI algorithms capable of effectively processing the resulting echo signals becomes complex. A promising approach to address this is to combine well-established model-driven radar signal processing methods with innovative data-driven AI techniques. Another significant challenge is defining new sensing performance metrics (e.g., recognition accuracy), and understanding their relationship with the design parameters like modulation types and covariance matrices of transmitted communication signals to guide system optimization. The incorporation of AI makes establishing quantitative connections between them especially difficult. Despite these challenges, AI also offers powerful tools to address these issues. AI techniques can model complex, nonlinear relationships between sensing performance metrics and signal parameters, providing insights that are difficult to obtain through traditional methods. Furthermore, AI can optimize a variety of functional blocks, e.g., input distribution of the constellation, through end-to-end learning [129], making it an invaluable asset in advancing sensing and ISAC technologies.

4) Integrated Sensing, Communication, and Powering (ISCAP) With Communication Signals: In addition to supporting S&C, radio signals can wirelessly deliver energy to power low-power devices such as sensors and IoT devices through wireless power transfer (WPT). With spectrum resources becoming more limited, future wireless networks are anticipated to combine sensing, communication, and

WPT, creating multi-functional ISCAP networks [130], [131]. ISCAP presents new challenges in designing signal waveforms and optimizing communication signals to balance the tradeoff among sensing, communication, and WPT. Unlike traditional ISAC systems, ISCAP must address the unique requirements of WPT, where the energy harvesting efficiency depends heavily on the characteristics of the transmitted waveform. Due to the non-linear radio frequency (RF)-to-direct current (DC) conversion process in energy harvesting devices, waveforms with high peak-to-average power ratio (PAPR) are typically favored to maximize power transfer efficiency. To overcome these challenges, optimizing modulation, waveform design, and beamforming is crucial. While some initial studies have explored waveform and beamforming designs in simplified ISCAP scenarios, a comprehensive system-level analysis and design remain underdeveloped. For instance, analyzing WPT performance under various waveforms, such as OFDM, CDMA, and OTFS, while accounting for practical energy harvesting constraints, offers a promising research direction. Similarly, extending data-dependent and data-independent precoding techniques for ISCAP is also interesting.

VII. Conclusion

This tutorial paper has examined recent developments in the field of communication-centric ISAC transmission, which maximizes the resource utilization efficiency by leveraging random data payload signals for both S&C tasks. We first discussed the information-theoretic foundation of ISAC, emphasizing the necessity of developing signal processing techniques tailored for random ISAC signals. Following this, we reviewed the core models and methodologies for communication-centric ISAC systems, with a particular focus on analyzing the statistical properties of the ACF of ISAC signals, which is critical for evaluating multi-target sensing performance. As a step further, a significant part of the discussion was dedicated to the design principles for key components of ISAC systems, including modulation schemes, constellation design, and pulse shaping filters. Here, we highlighted the importance of optimizing the sensing functionality without sacrificing the communication performance, or in some cases, developing a scalable tradeoff that supports both functionalities. On top of that, we also explored the advancements in MIMO systems, particularly in the context of dedicated sensing and ISAC precoding techniques conceived for random data payload signals. Finally, the paper concluded by identifying several open research challenges and outlining future directions in communication-centric ISAC transmission. It is our hope that this work will help guide the ongoing development of ISAC air interface technologies that are compatible with the current cellular networks, and contribute to the standardization and implementation of ISAC in future 6G wireless networks.

References

[1] M. Chafii, L. Bariah, S. Muhaidat, and M. Debbah, "Twelve scientific challenges for 6G: Rethinking the foundations of communications theory," *IEEE Commun. Surveys Tuts.*, vol. 25, no. 2, pp. 868–904, 2nd Quart., 2023.

[2] W. Saad, M. Bennis, and M. Chen, "A vision of 6G wireless systems: Applications, trends, technologies, and open research problems," *IEEE Netw.*, vol. 34, no. 3, pp. 134–142, May 2020.

[3] Draft New Recommendation ITU-R M.[IMT. Framework for 2030 and Beyond], Standard ITU-R M.2541, ITU-R, 2023.

[4] Y. Cui, F. Liu, X. Jing, and J. Mu, "Integrating sensing and communications for ubiquitous IoT: Applications, trends, and challenges," *IEEE Netw.*, vol. 35, no. 5, pp. 158–167, Sep. 2021.

[5] J.A. Zhang et al., "Enabling joint communication and radar sensing in mobile networks—A survey," *IEEE Commun. Surveys Tuts.*, vol. 24, no. 1, pp. 306–345, 1st Quart., 2022.

[6] F. Liu et al., "Integrated sensing and communications: Toward dual-functional wireless networks for 6G and beyond," *IEEE J. Sel. Areas Commun.*, vol. 40, no. 6, pp. 1728–1767, Jun. 2022.

[7] F. Liu et al., "Seventy years of radar and communications: The road from separation to integration," *IEEE Signal Process. Mag.*, vol. 40, no. 5, pp. 106–121, Jul. 2023.

[8] A. Hassanien, M.G. Amin, Y.D. Zhang, and F. Ahmad, "Signaling strategies for dual-function radar communications: An overview," *IEEE Aerosp. Electron. Syst. Mag.*, vol. 31, no. 10, pp. 36–45, Oct. 2016.

[9] M. Roberton and E.R. Brown, "Integrated radar and communications based on chirped spread-spectrum techniques," in *IEEE MTT-S Int. Microw. Symp. Dig.*, vol. 1, Aug. 2003, pp. 611–614.

[10] G.N. Saddik, R.S. Singh, and E.R. Brown, "Ultra-wideband multifunctional communications/radar system," *IEEE Trans. Microw. Theory Techn.*, vol. 55, no. 7, pp. 1431–1437, Jul. 2007.

[11] M. Temiz, C. Horne, N.J. Peters, M.A. Ritchie, and C. Masouros, "An experimental study of radar-centric transmission for integrated sensing and communications," *IEEE Trans. Microw. Theory Techn.*, vol. 71, no. 7, pp. 3203–3216, Jul. 2023.

[12] A. Hassanien, M.G. Amin, E. Aboutanios, and B. Himed, "Dual-function radar communication systems: A solution to the spectrum congestion problem," *IEEE Signal Process. Mag.*, vol. 36, no. 5, pp. 115–126, Sep. 2019.

[13] A. Hassanien, M.G. Amin, Y.D. Zhang, and F. Ahmad, "Dual-function radar-communications: Information embedding using sidelobe control and waveform diversity," *IEEE Trans. Signal Process.*, vol. 64, no. 8, pp. 2168–2181, Apr. 2016.

[14] A. Hassanien, M.G. Amin, Y.D. Zhang, F. Ahmad, and B. Himed, "Non-coherent PSK-based dual-function radar-communication systems," in *Proc. IEEE Radar Conf. (RadarConf)*, May 2016, pp. 1–6.

[15] E. BouDaher, A. Hassanien, E. Aboutanios, and M.G. Amin, "Towards a dual-function MIMO radar-communication system," in *Proc. IEEE Radar Conf. (RadarConf)*, May 2016, pp. 1–6.

[16] D. Ma, N. Shlezinger, T. Huang, Y. Liu, and Y.C. Eldar, "FRaC: FMCW-based joint radar-communications system via index modulation," *IEEE J. Sel. Topics Signal Process.*, vol. 15, no. 6, pp. 1348–1364, Nov. 2021.

[17] T. Huang, N. Shlezinger, X. Xu, D. Ma, Y. Liu, and Y.C. Eldar, "Multi-carrier agile phased array radar," *IEEE Trans. Signal Process.*, vol. 68, pp. 5706–5721, 2020.

[18] T. Huang, N. Shlezinger, X. Xu, Y. Liu, and Y.C. Eldar, "MAJoRCom: A dual-function radar communication system using index modulation," *IEEE Trans. Signal Process.*, vol. 68, pp. 3423–3438, 2020.

[19] L. Zheng, M. Lops, Y.C. Eldar, and X. Wang, "Radar and communication coexistence: An overview: A review of recent methods," *IEEE Signal Process. Mag.*, vol. 36, no. 5, pp. 85–99, Sep. 2019.

[20] Z. Wei et al., "Integrated sensing and communication signals toward 5G-A and 6G: A survey," *IEEE Internet Things J.*, vol. 10, no. 13, pp. 11068–11092, Jul. 2023.

[21] P. Kumari, J. Choi, N. González-Prelcic, and R.W. Heath, "IEEE 802.11ad-based radar: An approach to joint vehicular communication-radar system," *IEEE Trans. Veh. Technol.*, vol. 67, no. 4, pp. 3012–3027, Apr. 2018.

[22] M. Jamil, H. Zepernick, and M.I. Pettersson, "On integrated radar and communication systems using oppermann sequences," in *Proc. IEEE Mil. Commun. Conf.*, Apr. 2008, pp. 1–6.

[23] K. Wu, J.A. Zhang, X. Huang, and Y.J. Guo, "Integrating low-complexity and flexible sensing into communication systems," *IEEE J. Sel. Areas Commun.*, vol. 40, no. 6, pp. 1873–1889, Jun. 2022.

[24] K. Wu, J.A. Zhang, Z. Ni, X. Huang, Y.J. Guo, and S. Chen, "Joint communications and sensing employing optimized MIMO-OFDM signals," *IEEE Internet Things J.*, vol. 11, no. 6, pp. 10368–10383, Mar. 2024.

[25] C. Sturm and W. Wiesbeck, "Waveform design and signal processing aspects for fusion of wireless communications and radar sensing," *Proc. IEEE*, vol. 99, no. 7, pp. 1236–1259, Jul. 2011.

[26] L. Gaudio, M. Kobayashi, G. Caire, and G. Colavolpe, "On the effectiveness of OTFS for joint radar parameter estimation and communication," *IEEE Trans. Wireless Commun.*, vol. 19, no. 9, pp. 5951–5965, Sep. 2020.

[27] W. Yuan et al., "From OTFS to DD-ISAC: Integrating sensing and communications in the delay Doppler domain," *IEEE Wireless Commun.*, vol. 31, no. 6, pp. 152–160, Dec. 2024.

[28] M.F. Keskin, C. Marcus, O. Eriksson, A. Alvarado, J. Widmer, and H. Wymeersch, "Integrated sensing and communications with MIMO-OTFS: ISI/ICI exploitation and delay-Doppler multiplexing," *IEEE Trans. Wireless Commun.*, vol. 23, no. 8, pp. 10229–10246, Aug. 2024.

[29] L. Gaudio, G. Colavolpe, and G. Caire, "OTFS vs. OFDM in the presence of sparsity: A fair comparison," *IEEE Trans. Wireless Commun.*, vol. 21, no. 6, pp. 4410–4423, Jun. 2022.

[30] A. Bemani, N. Ksairi, and M. Kountouris, "Affine frequency division multiplexing for next generation wireless communications," *IEEE Trans. Wireless Commun.*, vol. 22, no. 11, pp. 8214–8229, Nov. 2023.

[31] A. Bemani, N. Ksairi, and M. Kountouris, "Integrated sensing and communications with affine frequency division multiplexing," *IEEE Wireless Commun. Lett.*, vol. 13, no. 5, pp. 1255–1259, May 2024.

[32] F. Liu, L. Zhou, C. Masouros, A. Li, W. Luo, and A. Petropulu, "Toward dual-functional radar-communication systems: Optimal waveform design," *IEEE Trans. Signal Process.*, vol. 66, no. 16, pp. 4264–4279, Aug. 2018.

[33] F. Liu, C. Masouros, A. Li, H. Sun, and L. Hanzo, "MU-MIMO communications with MIMO radar: From co-existence to joint transmission," *IEEE Trans. Wireless Commun.*, vol. 17, no. 4, pp. 2755–2770, Apr. 2018.

[34] X. Liu, T. Huang, and Y. Liu, "Transmit design for joint MIMO radar and multiuser communications with transmit covariance constraint," *IEEE J. Sel. Areas Commun.*, vol. 40, no. 6, pp. 1932–1950, Jun. 2022.

[35] X. Liu, T. Huang, N. Shlezinger, Y. Liu, J. Zhou, and Y.C. Eldar, "Joint transmit beamforming for multiuser MIMO communications and MIMO radar," *IEEE Trans. Signal Process.*, vol. 68, pp. 3929–3944, 2020.

[36] Z. Ren et al., "Fundamental CRB-rate tradeoff in multi-antenna ISAC systems with information multicasting and multi-target sensing," *IEEE Trans. Wireless Commun.*, vol. 23, no. 4, pp. 3870–3885, Apr. 2024.

[37] H. Hua, T.X. Han, and J. Xu, "MIMO integrated sensing and communication: CRB-rate tradeoff," *IEEE Trans. Wireless Commun.*, vol. 23, no. 4, pp. 2839–2854, Apr. 2024.

[38] J. A. Zhang, X. Huang, Y. J. Guo, J. Yuan, and R.W. Heath, "Multibeam for joint communication and radar sensing using steerable analog antenna arrays," *IEEE Trans. Veh. Technol.*, vol. 68, no. 1, pp. 671–685, Jan. 2019.

[39] C.B. Barneto, T. Riihonen, S.D. Liyanaarachchi, M. Heino, N. González-Prelcic, and M. Valkama, "Beamformer design and optimization for joint communication and full-duplex sensing at mm-waves," *IEEE Trans. Commun.*, vol. 70, no. 12, pp. 8298–8312, Dec. 2022.

[40] F. Liu, Y.-F. Liu, A. Li, C. Masouros, and Y.C. Eldar, "Cramér-rao bound optimization for joint radar-communication beamforming," *IEEE Trans. Signal Process.*, vol. 70, pp. 240–253, 2022.

[41] J.M. Mateos-Ramos, C. Häger, M.F. Keskin, L. Le Magoarou, and H. Wymeersch, "Model-based end-to-end learning for multi-target integrated sensing and communication under hardware impairments," *IEEE Trans. Wireless Commun.*, vol. 24, no. 3, pp. 2574–2589, Mar. 2025.

[42] N. González-Prelcic et al., "The integrated sensing and communication revolution for 6G: Vision, techniques, and applications," *Proc. IEEE*, vol. 112, no. 7, pp. 676–723, Jul. 2024.

[43] P. Pulkkinen and V. Koivunen, "Model-based online learning for active ISAC waveform optimization," *IEEE J. Sel. Topics Signal Process.*, vol. 18, no. 5, pp. 1–15, Jul. 2024.

[44] V. Koivunen, M.F. Keskin, H. Wymeersch, M. Valkama, and N. González-Prelcic, "Multicarrier ISAC: Advances in waveform design, signal processing, and learning under nonidealities," *IEEE Signal Process. Mag.*, vol. 41, no. 5, pp. 17–30, Sep. 2024.

[45] J. Zhang, C. Masouros, F. Liu, Y. Huang, and A.L. Swindlehurst, "Low-complexity joint radar-communication beamforming: From optimization to deep unfolding," *IEEE J. Sel. Topics Signal Process.*, early access, Jan. 13, 2025, doi: 10.1109/JSTSP.2024.3522787.

[46] Z. Wu, Y.-F. Liu, W.-K. Chen, and C. Masouros, "Quantized constant-envelope waveform design for massive MIMO DFRC systems," *IEEE J. Sel. Areas Commun.*, vol. 43, no. 4, pp. 1056–1073, Apr. 2025.

[47] H.-S. Cha, G. Lee, A. Ghosh, M. Baker, S. Kelley, and J. Hofmann, "5G NR positioning enhancements in 3GPP release-18," 2024, *arXiv:2401.17594*.

[48] *Feasibility Study on Integrated Sensing and Communication (Release 19)*, document TR 22.837 v19.4.0, 3GPP, Apr. 2022.

[49] *Service Requirements for Integrated Sensing and Communication; Stage 1 (Release 19)*, document TS22.137 v19.1.0, 3GPP, Aug. 2023.

[50] *Summary #1 on ISAC Channel Modelling*, document TSG RAN WG1, 3GPP, Apr. 2024.

[51] *Study on 6G Radio*, document RP-251809, 3GPP, Jun. 2025.

[52] R. Du et al., "An overview on IEEE 802.11bf: WLAN sensing," *IEEE Commun. Surveys Tuts.*, vol. 27, no. 1, pp. 184–217, Feb. 2025.

[53] X. Lin, "The bridge toward 6G: 5G-advanced evolution in 3GPP release 19," 2023, *arXiv:2312.15174*.

[54] Z. Wei et al., "5G PRS-based sensing: A sensing reference signal approach for joint sensing and communication system," *IEEE Trans. Veh. Technol.*, vol. 72, no. 3, pp. 3250–3263, Mar. 2023.

[55] Z. Wei et al., "Multiple reference signals collaborative sensing for integrated sensing and communication system towards 5G-A and 6G," *IEEE Trans. Veh. Technol.*, vol. 73, no. 10, pp. 15185–15199, Oct. 2024.

[56] Q. Zhang, K. Ji, Z. Wei, Z. Feng, and P. Zhang, "Joint communication and sensing system performance evaluation and testbed: A communication-centric approach," *IEEE Netw.*, vol. 38, no. 5, pp. 286–294, Sep. 2024.

[57] Y. Cui, X. Jing, and J. Mu, "Integrated sensing and communications via 5G NR waveform: Performance analysis," in *Proc. ICASSP*, 2022, pp. 8747–8751.

[58] Wireless LAN Medium Access Control (MAC) and Physical Layer (PHY) Specifications Amendment 3: Enhancements for Very High Throughput in the 60 GHz Band, Standard IEEE Std. 802.11ad, 2012, pp. 1–628.

[59] T.M. Cover and J.A. Thomas, *Elements of Information Theory*. Hoboken, NJ, USA: Wiley, 1999.

[60] F. Liu, Y. Xiong, K. Wan, T.X. Han, and G. Caire, "Deterministic-random tradeoff of integrated sensing and communications in Gaussian channels: A rate-distortion perspective," in *Proc. IEEE ISIT*, Apr. 2023, pp. 2326–2331.

[61] Y. Xiong, F. Liu, Y. Cui, W. Yuan, T.X. Han, and G. Caire, "On the fundamental tradeoff of integrated sensing and communications under Gaussian channels," *IEEE Trans. Inf. Theory*, vol. 69, no. 9, pp. 5723–5751, Sep. 2023.

[62] Y. Xiong, F. Liu, K. Wan, W. Yuan, Y. Cui, and G. Caire, "From torch to projector: Fundamental tradeoff of integrated sensing and communications," *IEEE BITS Inf. Theory Mag.*, vol. 4, no. 1, pp. 73–90, Mar. 2024.

[63] M. Ahmadipour, M. Kobayashi, M. Wigger, and G. Caire, "An information-theoretic approach to joint sensing and communication," *IEEE Trans. Inf. Theory*, vol. 70, no. 2, pp. 1124–1146, Feb. 2024.

[64] Y. Zhang, S. Aditya, and B. Clerckx, "Input distribution optimization in OFDM dual-function radar-communication systems," *IEEE Trans. Signal Process.*, vol. 72, pp. 5258–5273, 2024.

[65] J.G. Proakis and M. Salehi, *Digital Communications*. New York, NY, USA: McGraw-Hill, 2008.

[66] F. Liu et al., "Uncovering the iceberg in the sea: Fundamentals of pulse shaping and modulation design for random ISAC signals," *IEEE Trans. Signal Process.*, vol. 73, pp. 2511–2526, 2025.

[67] F. Liu et al., "CP-OFDM achieves the lowest average ranging sidelobe under QAM/PSK constellations," *IEEE Trans. Inf. Theory*, vol. 71, no. 9, pp. 6950–6967, Sep. 2025.

[68] Z. Du, F. Liu, Y. Xiong, T.X. Han, Y.C. Eldar, and S. Jin, "Reshaping the ISAC tradeoff under OFDM signaling: A probabilistic constellation shaping approach," *IEEE Trans. Signal Process.*, vol. 72, pp. 4782–4797, 2024.

[69] Z. Liao et al., "Pulse shaping for random ISAC signals: The ambiguity function between symbols matters," *IEEE Trans. Wireless Commun.*, vol. 24, no. 4, pp. 2832–2846, Apr. 2025.

[70] S. Lu et al., "Random ISAC signals deserve dedicated precoding," *IEEE Trans. Signal Process.*, vol. 72, pp. 3453–3469, 2024.

[71] M. Kobayashi, G. Caire, and G. Kramer, "Joint state sensing and communication: Optimal tradeoff for a memoryless case," in *Proc. IEEE Int. Symp. Inf. Theory (ISIT)*, Jun. 2018, pp. 111–115.

[72] M. Kobayashi, H. Hamad, G. Kramer, and G. Caire, "Joint state sensing and communication over memoryless multiple access channels," in *Proc. IEEE Int. Symp. Inf. Theory (ISIT)*, Jul. 2019, pp. 270–274.

[73] M. Ahmadipour, M. Wigger, and M. Kobayashi, "Joint sensing and communication over memoryless broadcast channels," in *Proc. IEEE Inf. Theory Workshop (ITW)*, Apr. 2021, pp. 1–5.

[74] S.M. Kay, *Fundamentals of Statistical Signal Processing, Volume. I: Estimation Theory*. Englewood Cliffs, NJ, USA: Prentice-Hall, 1998.

[75] S.M. Kay, *Fundamentals of Statistical Signal Processing, Volume. II: Detection Theory*. Englewood Cliffs, NJ, USA: Prentice-Hall, 1998.

[76] A. Liu et al., "A survey on fundamental limits of integrated sensing and communication," *IEEE Commun. Surveys Tuts.*, vol. 24, no. 2, pp. 994–1034, 2nd Quart., 2022.

[77] S. Arimoto, "An algorithm for computing the capacity of arbitrary discrete memoryless channels," *IEEE Trans. Inf. Theory*, vol. IT-18, no. 1, pp. 14–20, Jan. 1972.

[78] R. Blahut, "Computation of channel capacity and rate-distortion functions," *IEEE Trans. Inf. Theory*, vol. IT-18, no. 4, pp. 460–473, Jul. 1972.

[79] R. Miller and C. Chang, "A modified Cramér-rao bound and its applications (Corresp.)," *IEEE Trans. Inf. Theory*, vol. IT-24, no. 3, pp. 398–400, May 1978.

[80] H.L. Van Trees, *Detection, Estimation, and Modulation Theory, Part I: Detection, Estimation, and Linear Modulation Theory*. Hoboken, NJ, USA: Wiley, 2004.

[81] R.T. Derryberry, S.D. Gray, D. M. Ionescu, G. Mandyam, and B. Raghothaman, "Transmit diversity in 3G CDMA systems," *IEEE Commun. Mag.*, vol. 40, no. 4, pp. 68–75, Apr. 2002.

[82] R. Hadani et al., "Orthogonal time frequency space modulation," in *Proc. IEEE Wireless Commun. Netw. Conf. (WCNC)*, Apr. 2017, pp. 1–6.

[83] B. Bamieh, "Discovering transforms: A tutorial on circulant matrices, circular convolution, and the discrete Fourier transform," 2018, *arXiv:1805.05533*.

[84] N. Levanon and E. Mozeson, *Radar Signals*. Hoboken, NJ, USA: Wiley, 2004.

[85] D. Cohen and Y.C. Eldar, "Sub-nyquist radar systems: Temporal, spectral, and spatial compression," *IEEE Signal Process. Mag.*, vol. 35, no. 6, pp. 35–58, Nov. 2018.

[86] M.A. Richards, *Fundamentals of Radar Signal Processing*. New York, NY, USA: McGraw-Hill, 2005.

[87] P. Stoica, H. He, and J. Li, "On designing sequences with impulse-like periodic correlation," *IEEE Signal Process. Lett.*, vol. 16, no. 8, pp. 703–706, Aug. 2009.

[88] O. Chterental and D.Ž. Doković, "On orthostochastic, unistochastic and qustochastic matrices," *Linear Algebra its Appl.*, vol. 428, no. 4, pp. 1178–1201, Feb. 2008.

[89] L.T. DeCarlo, "On the meaning and use of kurtosis," *Psychol. Methods*, vol. 2, no. 3, pp. 292–307, 1997.

[90] I.C. Abou-Faycal, M.D. Trott, and S. Shamai (Shitz), "The capacity of discrete-time memoryless Rayleigh-fading channels," *IEEE Trans. Inf. Theory*, vol. 47, no. 4, pp. 1290–1301, May 2001.

[91] M.C. Gursoy, H.V. Poor, and S. Verdu, "The noncoherent Rician fading channel-part I: Structure of the capacity-achieving input," *IEEE Trans. Wireless Commun.*, vol. 4, no. 5, pp. 2193–2206, Sep. 2005.

[92] M.C. Gursoy, H.V. Poor, and S. Verdu, "Noncoherent Rician fading channel-part II: Spectral efficiency in the low-power regime," *IEEE Trans. Wireless Commun.*, vol. 4, no. 5, pp. 2207–2221, Sep. 2005.

[93] C. Xing, S. Wang, S. Chen, S. Ma, H.V. Poor, and L. Hanzo, "Matrix-monotonic optimization—Part I: Single-variable optimization," *IEEE Trans. Signal Process.*, vol. 69, pp. 738–754, 2021.

[94] C. Xing, S. Wang, S. Chen, S. Ma, H.V. Poor, and L. Hanzo, "Matrix-monotonic optimization—Part II: Multi-variable optimization," *IEEE Trans. Signal Process.*, vol. 69, pp. 179–194, 2021.

[95] C. Xing, S. Ma, and Y. Zhou, "Matrix-monotonic optimization for MIMO systems," *IEEE Trans. Signal Process.*, vol. 63, no. 2, pp. 334–348, Jan. 2015.

[96] J. Barrueco, J. Montalban, E. Iradier, and P. Angueira, "Constellation design for future communication systems: A comprehensive survey," *IEEE Access*, vol. 9, pp. 89778–89797, 2021.

[97] J. Cho and P. J.Winzer, "Probabilistic constellation shaping for optical fiber communications," *J. Lightw. Technol.*, vol. 37, no. 6, pp. 1590–1607, Mar. 15, 2019.

[98] R.W. Yeung, *Information Theory and Network Coding*. Cham, Switzerland: Springer, 2008.

[99] S.P. Boyd and L. Vandenberghe, *Convex Optimization*. Cambridge, U.K.: Cambridge Univ. Press, 2004.

[100] Y.-F. Liu et al., "A survey of recent advances in optimization methods for wireless communications," *IEEE J. Sel. Areas Commun.*, vol. 42, no. 11, pp. 2992–3031, Nov. 2024.

[101] M. Biguesh and A.B. Gershman, "Training-based MIMO channel estimation: A study of estimator tradeoffs and optimal training signals," *IEEE Trans. Signal Process.*, vol. 54, no. 3, pp. 884–893, Mar. 2006.

[102] J. Li and P. Stoica, "MIMO radar with colocated antennas," *IEEE Signal Process. Mag.*, vol. 24, no. 5, pp. 106–114, Sep. 2007.

[103] D. Tse and P. Viswanath, *Fundamentals of Wireless Communication*. Cambridge, U.K.: Cambridge Univ. Press, 2005.

[104] B. Tang, J. Tang, and Y. Peng, "Waveform optimization for MIMO radar in colored noise: Further results for estimation-oriented criteria," *IEEE Trans. Signal Process.*, vol. 60, no. 3, pp. 1517–1522, Mar. 2012.

[105] L. Bottou, "Online learning and stochastic approximations," *Online Learn. Neural Netw.*, vol. 17, no. 9, p. 142, 1998.

[106] A. Liu, V.K.N. Lau, and B. Kananian, "Stochastic successive convex approximation for non-convex constrained stochastic optimization," *IEEE Trans. Signal Process.*, vol. 67, no. 16, pp. 4189–4203, Aug. 2019.

[107] A. Goldsmith, *Wireless Communications*. Cambridge, U.K.: Cambridge Univ. Press, 2005.

[108] M. Furkan Keskin et al., "Fundamental trade-offs in monostatic ISAC: A holistic investigation towards 6G," 2024, *arXiv:2401.18011*.

[109] Y.C. Eldar and G. Kutyniok, *Compressed Sensing: Theory and Applications*. Cambridge, U.K.: Cambridge Univ. Press, 2012.

[110] A. Li et al., "A tutorial on interference exploitation via symbol-level precoding: Overview, state-of-the-art and future directions," *IEEE Commun. Surveys Tuts.*, vol. 22, no. 2, pp. 796–839, 2nd Quart., 2020.

[111] S. Taek Chung and A.J. Goldsmith, "Degrees of freedom in adaptive modulation: A unified view," *IEEE Trans. Commun.*, vol. 49, no. 9, pp. 1561–1571, Sep. 2001.

[112] A. Li and C. Masouros, "A two-stage vector perturbation scheme for adaptive modulation in downlink MU-MIMO," *IEEE Trans. Veh. Technol.*, vol. 65, no. 9, pp. 7785–7791, Sep. 2016.

[113] C. Masouros and G. Zheng, "Exploiting known interference as green signal power for downlink beamforming optimization," *IEEE Trans. Signal Process.*, vol. 63, no. 14, pp. 3628–3640, Jul. 2015.

[114] M. Ahmadipour, M. Wigger, and M. Kobayashi, "Coding for sensing: An improved scheme for integrated sensing and communication over MACs," in *Proc. IEEE Int. Symp. Inf. Theory (ISIT)*, Jun. 2022, pp. 3025–3030.

[115] K. Meng, C. Masouros, G. Chen, and F. Liu, "Network-level integrated sensing and communication: Interference management and BS coordination using stochastic geometry," *IEEE Trans. Wireless Commun.*, vol. 23, no. 12, pp. 19365–19381, Dec. 2024.

[116] K. Meng, C. Masouros, A.P. Petropulu, and L. Hanzo, "Cooperative ISAC networks: Opportunities and challenges," *IEEE Wireless Commun.*, vol. 32, no. 3, pp. 1–8, Jun. 2025.

[117] K. Meng, C. Masouros, A.P. Petropulu, and L. Hanzo, "Cooperative ISAC networks: Performance analysis, scaling laws, and optimization," *IEEE Trans. Wireless Commun.*, vol. 24, no. 2, pp. 877–892, Feb. 2025.

[118] G. Cheng, Y. Fang, J. Xu, and D.W.K. Ng, "Optimal coordinated transmit beamforming for networked integrated sensing and communications," *IEEE Trans. Wireless Commun.*, vol. 23, no. 8, pp. 8200–8214, Aug. 2024.

[119] Y. Huang, Y. Fang, X. Li, and J. Xu, "Coordinated power control for network integrated sensing and communication," *IEEE Trans. Veh. Technol.*, vol. 71, no. 12, pp. 13361–13365, Dec. 2022.

[120] Z. Lyu, G. Zhu, and J. Xu, "Joint maneuver and beamforming design for UAV-enabled integrated sensing and communication," *IEEE Trans. Wireless Commun.*, vol. 22, no. 4, pp. 2424–2440, Apr. 2023.

[121] G. Cheng, X. Song, Z. Lyu, and J. Xu, "Networked ISAC for low-altitude economy: Coordinated transmit beamforming and UAV trajectory design," *IEEE Trans. Commun.*, vol. 73, no. 8, pp. 5832–5847, Aug. 2025.

[122] Z. Wei, F. Liu, C. Masouros, N. Su, and A.P. Petropulu, "Toward multifunctional 6G wireless networks: Integrating sensing, communication, and security," *IEEE Commun. Mag.*, vol. 60, no. 4, pp. 65–71, Apr. 2022.

[123] N. Su, F. Liu, Z. Wei, Y.-F. Liu, and C. Masouros, "Secure dual-functional radar-communication transmission: Exploiting interference for resilience against target eavesdropping," *IEEE Trans. Wireless Commun.*, vol. 21, no. 9, pp. 7238–7252, Sep. 2022.

[124] N. Su, F. Liu, and C. Masouros, "Secure radar-communication systems with malicious targets: Integrating radar, communications and jamming functionalities," *IEEE Trans. Wireless Commun.*, vol. 20, no. 1, pp. 83–95, Jan. 2021.
[125] J. Zou, C. Masouros, F. Liu, and S. Sun, "Securing the sensing functionality in ISAC networks: An artificial noise design," *IEEE Trans. Veh. Technol.*, vol. 73, no. 11, pp. 17800–17805, Nov. 2024.
[126] O. Günlü, M.R. Bloch, R. F. Schaefer, and A. Yener, "Secure integrated sensing and communication," *IEEE J. Sel. Areas Inf. Theory*, vol. 4, pp. 40–53, 2023.
[127] Y. Cui, X. Cao, G. Zhu, J. Nie, and J. Xu, "Edge perception: Intelligent wireless sensing at network edge," *IEEE Commun. Mag.*, vol. 63, no. 3, pp. 166–173, Mar. 2024.
[128] G. Zhu et al., "Pushing AI to wireless network edge: An overview on integrated sensing, communication, and computation towards 6G," *Sci. China Inf. Sci.*, vol. 66, no. 3, Mar. 2023, Art. no. 130301.
[129] B. Geiger, F. Liu, S. Lu, A. Rode, and L. Schmalen, "Joint optimization of geometric and probabilistic constellation shaping for OFDM-ISAC systems," 2025, *arXiv:2501.11583*.
[130] Y. Chen, H. Hua, J. Xu, and D.W.K. Ng, "ISAC meets SWIPT: Multi-functional wireless systems integrating sensing, communication, and powering," *IEEE Trans. Wireless Commun.*, vol. 23, no. 8, pp. 8264–8280, Aug. 2024.
[131] Y. Chen, Z. Ren, J. Xu, Y. Zeng, D.W.K. Ng, and S. Cui, "Integrated sensing, communication, and powering: Toward multi-functional 6G wireless networks," *IEEE Commun. Mag.*, vol. 63, no. 8, pp. 146–153, Aug. 2025.

Fan Liu (Senior Member, IEEE) received the B.Eng. and Ph.D. degrees from Beijing Institute of Technology (BIT), Beijing, China, in 2013 and 2018, respectively.

He is currently a Professor with the National Mobile Communications Research Laboratory, School of Information Science and Engineering, Southeast University, Nanjing, China. Prior to that, he was an Assistant Professor with the Southern University of Science and Technology, Shenzhen, China, from 2020 to 2024. He has previously held academic positions at University College London (UCL), London, U.K., as a Visiting Researcher, from 2016 to 2018, and a Marie Curie Research Fellow, from 2018 to 2020. His research interests include the general area of signal processing and wireless communications, and in particular in the area of integrated sensing and communications (ISAC). He is a member of the IMT-2030 (6G) ISAC Task Group. He was a recipient of numerous best paper awards, including the 2025 IEEE Communications Society and Information Theory Society Joint Paper Award, the 2024 IEEE Signal Processing Society Best Paper Award, the 2024 IEEE Signal Processing Society Donald G. Fink Overview Paper Award, the 2024 IEEE Communications Society Asia–Pacific Outstanding Paper Award, the 2023 IEEE Communications Society Stephan O. Rice Prize, and the 2021 IEEE Signal Processing Society Young Author Best Paper Award. He is the founding Academic Chair of the IEEE ComSoc ISAC Emerging Technology Initiative (ISAC-ETI), the Vice Chair and a founding member of the IEEE SPS ISAC Technical Working Group (ISAC-TWG), an elected member of the IEEE SPS Sensor Array and Multichannel Technical Committee (SAM-TC), an Associate Editor of IEEE TRANSACTIONS ON COMMUNICATIONS, IEEE TRANSACTIONS ON MOBILE COMPUTING, and IEEE OPEN JOURNAL OF SIGNAL PROCESSING, and a Guest Editor of IEEE JOURNAL ON SELECTED AREAS IN COMMUNICATIONS, IEEE WIRELESS COMMUNICATIONS, and *IEEE Vehicular Technology Magazine*. He was the TPC Co-Chair of the 2nd–4th IEEE Joint Communication and Sensing (JC&S) Symposium, the Symposium Co-Chair of the IEEE ICC 2026 and IEEE GLOBECOM 2023, and the Track Co-Chair of the IEEE WCNC 2024. He was listed among the Clarivate Highly Cited Researchers in 2025 and among the Elsevier Highly-Cited Chinese Researchers from 2023 to 2024.

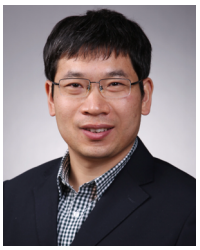

Ya-Feng Liu (Senior Member, IEEE) is currently a Professor at the School of Mathematical Sciences, Beijing University of Posts and Telecommunications. His research interests include nonlinear optimization and its applications to signal processing, wireless communications, and machine learning. He is an elected member of the Signal Processing for Communications and Networking Technical Committee (SPCOM-TC) of the IEEE Signal Processing Society (2020–2022 and 2023–2025). He received the Best Paper Award from the IEEE International Conference on Communications (ICC) in 2011, the Science and Technology Award for Young Scholars from the Operations Research Society of China in 2018, the 15th IEEE ComSoc Asia–Pacific Outstanding Young Researcher Award in 2020, the Youth Science Award of Applied Mathematics from the China Society for Industrial and Applied Mathematics in 2022, and the IEEE Signal Processing Society Best Paper Award in 2024. Students supervised and co-supervised by him won the Best Student Paper Award from the International Symposium on Modeling and Optimization in Mobile, Ad Hoc, and Wireless Networks (WiOpt) in 2015 and the Best Student Paper Award of the IEEE International Conference on Acoustics, Speech, and Signal Processing (ICASSP) in 2022. He serves as an Associate Editor for IEEE TRANSACTIONS ON SIGNAL PROCESSING and *Journal of Global Optimization*. He served as an Editor for IEEE TRANSACTIONS ON WIRELESS COMMUNICATIONS (2019–2022), an Associate Editor for IEEE SIGNAL PROCESSING LETTERS (2019–2023), and a Lead Guest Editor for IEEE JOURNAL ON SELECTED AREAS IN COMMUNICATIONS special issue on "Advanced Optimization Theory and Algorithms for Next-Generation Wireless Communication Networks."

Yuanhao Cui (Member, IEEE) is currently an Assistant Professor with the School of Information Science and Engineering, Beijing University of Posts and Telecommunications, Beijing, China. His research interests include the general area of signal processing and wireless communications, and in particular in the area of integrated sensing and communications (ISACs) and low-altitude wireless network (LAWN). He is a member of the IMT-2030 (6G) ISAC Task Group. He is the Founding Chair of the IEEE ComSoc Special Interest Group on Low-Altitude Wireless Networks (LAWN-SIG), the founding Secretary of the IEEE ComSoc ISAC Emerging Technology Initiative (ISAC-ETI), and the founding Secretary of the CCF Scientific Communication Standing Committee. He was the Symposium Co-Chair of IEEE GLOBECOM 2024 and an Organizer/the Chair of several workshops and special sessions on ISAC in flagship IEEE and ACM conferences, including IEEE ICC, IEEE/CIC ICCC, IEEE SPAWC, IEEE VTC, IEEE WCNC, IEEE ICASSP, and ACM MobiCom. He was listed among the World's Top 2% Scientists by Stanford University for citation impact from 2023 to 2024. He was a recipient of numerous best paper awards, including the 2025 IEEE Communications Society and Information Theory Society Joint Paper Award, the 2024 IEEE Communications Society Asia–Pacific Outstanding Paper Award, the 2024 IEEE Globecom Best Paper Award, the 2024 IEEE JC&S Symposium Best Paper Award, the 2023 ACM MobiCom Best Paper Award in ISAC, and the 2023 IEEE/CIC ICCC 2023 Best Paper Award. He serves on the editorial board for IEEE TRANSACTIONS ON MOBILE COMPUTING, *IEEE Vehicular Technology Magazine*, IEEE JOURNAL OF INTERNET OF THINGS, and IEEE JOURNAL OF BIOMEDICAL AND HEALTH INFORMATICS.

Christos Masouros (Fellow, IEEE) received the Diploma degree in electrical and computer engineering from the University of Patras, Greece, in 2004, and the M.Sc. and Ph.D. degrees in electrical and electronic engineering from The University of Manchester, U.K., in 2006 and 2009, respectively.

In 2008, he was a Research Intern at Philips Research Labs, U.K., working on the LTE standards. From 2009 to 2010, he was a Research Associate at The University of Manchester and a Research Fellow at Queen's University Belfast, from 2010 to 2012. In 2012, he joined University College London, as a Lecturer. He has held a Royal Academy of Engineering Research Fellowship from 2011 to 2016. Since 2019, he has been a Full Professor of signal processing and wireless communications at the Information and Communication Engineering Research Group, Department of Electrical and Electronic Engineering, and with the Institute for Communications and Connected Systems, University College London. From 2018 to 2022, he was the Project Coordinator of the €4.2m EU H2020 ITN project PAINLESS, involving 12 EU partner universities and industries, and toward energy-autonomous networks. From 2024 to 2028, he will be the Scientific Coordinator of the €2.7m EU H2020 DN project ISLANDS, involving 19 EU partner universities and industries, and toward next generation vehicular networks. His research interests include the field of wireless communications and signal processing with particular focus on green communications, large scale antenna systems, integrated sensing and communications, and interference mitigation techniques for MIMO and multicarrier communications. He is a fellow of the Institute of Electronics Engineers (IET), the Artificial Intelligence Industry Alliance (AIIA), and Asia–Pacific Artificial Intelligence Association (AAIA). He is a member of the IEEE Standards Association Working Group on ISAC performance metrics and a founding member of the ETSI ISG on ISAC. He was a recipient of the 2024 IEEE SPS Best Paper Award, the 2024 IEEE SPS Donald G. Fink Overview Paper Award, the 2023 IEEE ComSoc Stephen O. Rice Prize, and a co-recipient of the 2021 IEEE SPS Young Author Best Paper Award and a recipient of the Best Paper Awards in the IEEE GlobeCom 2015 and IEEE WCNC 2019 conferences. He is a founding member and the Vice-Chair of the IEEE Emerging Technology Initiative on Integrated Sensing and Communications (SAC), the Chair of the IEEE SPS ISAC Technical Working Group, and the Chair of the IEEE Green Communications and Computing Technical Committee, Special Interest Group on Green ISAC. He is the TPC Chair for the IEEE ICC 2024 Selected Areas in Communications (SAC) Track on ISAC, the Chair of the IEEE PIMRC2024 Track 1 on PHY and Fundamentals, the Chair of the "Integrated Imaging and Communications" stream in IEEE CISA 2024, and the TPC Co-Chair of IEEE VTC 2025. He is an IEEE ComSoc Distinguished Lecturer (2024–2025), and his work on ISAC has been featured in the World Economic Forum's report on the top 10 emerging technologies. He has been recognized as an Exemplary Editor of IEEE COMMUNICATIONS LETTERS and an Exemplary Reviewer of IEEE TRANSACTIONS ON COMMUNICATIONS. He is an Area Editor of IEEE TRANSACTIONS ON WIRELESS COMMUNICATIONS and the Editor-at-Large of IEEE OPEN JOURNAL OF THE COMMUNICATIONS SOCIETY. He has been an Editor of IEEE TRANSACTIONS ON COMMUNICATIONS, IEEE TRANSACTIONS ON WIRELESS COMMUNICATIONS, and IEEE OPEN JOURNAL OF SIGNAL PROCESSING, an Associate Editor of IEEE COMMUNICATIONS LETTERS, and a Guest Editor of a number of IEEE JOURNAL ON SELECTED TOPICS IN SIGNAL PROCESSING issues.

Jie Xu (Fellow, IEEE) received the B.E. and Ph.D. degrees from the University of Science and Technology of China. He is currently an Associate Professor (Tenured) with the School of Science and Engineering, Shenzhen Future Network of Intelligence Institute (FNii-Shenzhen), and Guangdong Provincial Key Laboratory of Future Networks of Intelligence, The Chinese University of Hong Kong (Shenzhen). His research interests include wireless communications, wireless information and power transfer, UAV communications, edge computing and intelligence, and integrated sensing and communication (ISAC). He was a recipient of the 2017 IEEE Signal Processing Society Young Author BestPaper Award, the IEEE/CIC ICCC 2019 Best Paper Award, the 2019 IEEE Communications Society Asia–Pacific Outstanding Young Researcher Award, and the 2019 Wireless Communications Technical Committee Outstanding Young Researcher Award. He is the Symposium Co-Chair of the IEEE GLOBECOM 2019 Wireless Communications Symposium and the IEEE ICC 2025 Communication Theory Symposium, the Workshop Co-Chair of several IEEE ICC and GLOBECOM workshops, the Tutorial Co-Chair of the IEEE/CIC ICCC 2019/2022, the Chair of the IEEE Wireless Communications Technical Committee (WTC), and the Vice Co-Chair of the IEEE Emerging Technology Initiative (ETI) on ISAC. He served or is serving as the Associate Editor-in-Chief for IEEE TRANSACTIONS ON MOBILE COMPUTING; an Editor for IEEE TRANSACTIONS ON WIRELESS COMMUNICATIONS, IEEE TRANSACTIONS ON COMMUNICATIONS, IEEE WIRELESS COMMUNICATIONS LETTERS, and *Journal of Communications and Information Networks*; an Associate Editor of IEEE ACCESS; and a Guest Editor of the IEEE WIRELESS COMMUNICATIONS, IEEE JOURNAL ON SELECTED AREAS IN COMMUNICATIONS, *IEEE Internet of Things Magazine*, *Science China Information Sciences*, and *China Communications*. He is a Distinguished Lecturer of the IEEE Communications Society.

Tony Xiao Han (Senior Member, IEEE) received the B.E. degree in electrical engineering from Sichuan University and the Ph.D. degree in communications engineering from Zhejiang University, Hangzhou, China. He was a Post-Doctoral Research Fellow with the National University of Singapore, Singapore. He is currently a Research Expert and the Project Leader of Huawei Technologies Company Ltd. His research interests include wireless communications, signal processing, integrated sensing and communication (ISAC), and standardization of wireless communication. He was the Chair of the IEEE 802.11 WLAN Sensing Topic Interest Group (TIG) and the 802.11 WLAN Sensing Study Group (SG). He is also serving as the Chair for the IEEE 802.11bf WLAN Sensing Task Group (TG) and the Sensing Task Group in Wi-Fi Alliance. He is the founding Industry Chair of the IEEE ComSoc ISAC Emerging Technology Initiative (ISAC-ETI), the Vice Chair of the IEEE WTC Special Interest Group (SIG) on ISAC, a Guest Editor of the IEEE JOURNAL ON SELECTED AREAS IN COMMUNICATIONS special issue on "Integrated Sensing and Communications (ISAC)." He served as the Co-Chair for many workshops, e.g., IEEE GLOBECOM 2020 Workshop on ISAC.

Stefano Buzzi (Senior Member, IEEE) received the M.Sc. degree (summa cum laude) in electronic engineering and the Ph.D. degree in electrical and computer engineering from the University of Naples Federico II in 1994 and 1999, respectively. He had short-term research appointments with Princeton University, Princeton, NJ, USA, in 1999, 2000, 2001, and 2006. He joined the University of Cassino and Southern Lazio, Italy, in 2000, where he was an Assistant Professor and has been an Associate Professor since 2002 and a Full Professor since 2018. Since 2022, he has been with the Politecnico di Milano, Italy. He is the General Coordinator of the EU-Funded Innovative Training Network Project METAWIRELESS, on the application of metasurfaces to wireless communications, and the EU-Funded Doctoral Network ISLANDS, on integrated sensing and communications for the vehicular environment. He has co-authored about 200 technical peer-reviewed journals and conference papers, and among these, the highly cited paper "What will 5G be?," IEEE JOURNAL ON SELECTED AREAS IN COMMUNICATIONS in June 2014. His current research interests include communications and signal processing, with an emphasis on wireless communications and 6G systems. He serves regularly as a TPC member for several international conferences. He is a former Associate Editor of IEEE SIGNAL PROCESSING LETTERS and IEEE COMMUNICATIONS LETTERS and has been a Guest Editor of five IEEE JOURNAL ON SELECTED AREAS IN COMMUNICATIONS special issues. From 2014 to 2020, he was an Editor of IEEE TRANSACTIONS ON WIRELESS COMMUNICATIONS. He is also an Associate Editor of IEEE TRANSACTIONS ON COMMUNICATIONS.

Yonina C. Eldar (Fellow, IEEE) received the B.Sc. degree in physics and the B.Sc. degree in electrical engineering from Tel Aviv University, Tel Aviv-Yafo, Israel, in 1995 and 1996, respectively, and the Ph.D. degree in electrical engineering and computer science from Massachusetts Institute of Technology (MIT), Cambridge, MA, USA, in 2002. She was a Visiting Professor with Stanford University. She is currently a Professor with the Department of Mathematics and Computer Science, Weizmann Institute of Science, Rehovot, Israel, where she heads the Center for Biomedical Engineering and Signal Processing, and holds the Dorothy and Patrick Gorman Professorial Chair. She is also a Visiting Professor with MIT, a Visiting Scientist with the Broad Institute, and an Adjunct Professor with Duke University. She is a member with Israel Academy of Sciences and Humanities and an EURASIP Fellow. She was a Horev Fellow of the Leaders in Science and Technology Program at the Technion and an Alon Fellow. She received many awards for excellence in research and teaching, including the IEEE Signal Processing Society Technical Achievement Award (2013), the IEEE/AESS Fred Nathanson Memorial Radar Award (2014), and the IEEE Kiyo Tomiyasu Award (2016). She received the Michael Bruno Memorial Award from the Rothschild Foundation, the Weizmann Prize for Exact Sciences, the Wolf Foundation Krill Prize for Excellence in Scientific Research, the Henry Taub Prize for Excellence in Research (twice), the Hershel Rich Innovation Award (three times), and the Award for Women with Distinguished Contributions. She received several best paper awards and best demo awards together with her research students and colleagues, was selected as one of the 50 most influential women in Israel, and was a member of Israel Committee for Higher Education. She is the Editor-in-Chief of *Foundations and Trends in Signal Processing*, a member of several IEEE Technical Committees and Award Committees, and heads the Committee for Promoting Gender Fairness in Higher Education Institutions in Israel.

Shi Jin (Fellow, IEEE) received the B.S. degree in communications engineering from Guilin University of Electronic Technology, Guilin, China, in 1996, the M.S. degree from Nanjing University of Posts and Telecommunications, Nanjing, China, in 2003, and the Ph.D. degree in information and communications engineering from Southeast University, Nanjing, in 2007. From June 2007 to October 2009, he was a Research Fellow with University College London, Adastral Park Research Campus, London, U.K. He is currently a Chair Professor with the National Mobile Communications Research Laboratory, Southeast University. His research interests include wireless communications, random matrix theory, and information theory. He and his co-authors have been awarded the IEEE Communications Society Stephen O. Rice Prize Paper Award in 2011, the IEEE Jack Neubauer Memorial Award in 2023, the IEEE Marconi Prize Paper Award in Wireless Communications in 2024, the IEEE Signal Processing Society Young Author Best Paper Award in 2010, and the Best Paper Award in 2022. He is serving as an Area Editor for IEEE TRANSACTIONS ON COMMUNICATIONS and *Electronics Letters* (IET). He was an Associate Editor for IEEE TRANSACTIONS ON WIRELESS COMMUNICATIONS, IEEE COMMUNICATIONS LETTERS, and *IET Communications*.